The development of new molecular tools to investigate epidermal Ca^{2+} homeostasis

William James Talbot

UoL Institute of Translational Medicine

Thesis submitted in accordance with the requirements of the University of Liverpool for the degree of Doctor in Philosophy

January 2018

Declaration

I, **William James Talbot** confirm that the work presented in this thesis is my own. Where information has been derived from other sources, I confirm that this has been indicated in the thesis.

Acknowledgements

I would like to thank all the individuals that without whom, this thesis would not have been possible. First and foremost, my supervisor Alec Simpson. Thank you for not only giving me the amazing opportunity to undertake this PhD, to travel and experience Italy but also for your continued support. I have thoroughly enjoyed the beers, coffees, and bacon sandwiches. Learning from you has been an absolute pleasure.

Nicholas Harper, whose knowledge, guidance, time and effort helped shape Chapter 5 in this thesis. You taught and gave me a great deal and I thank you for that.

I am eternally grateful to Rosario Rizzuto for agreeing to let me travel and work in Padova, it was an experience I will never forget. To Diego De Stefani and Anna Raffaello, two of the greatest scientific minds I have had the pleasure of working with, thank you for your patience and assistance.

Thank you to Victoria Burchell, whose molecular biology expertise helped make the probe a reality. The coffees and the tears were all part of the experience!

On a more personal level, I would first like to extend thanks to Helen Burrell, for not only having confidence in me and introducing me to Alec but being an amazing listener when I needed it the most! A special thanks to Marco Pacifici, Annetta Tosatto and Lauren Wright for making me feel instantly welcome in Padova and helping me find my way in the early months. I have made so many friends whilst undertaking this PhD, both at home and abroad. Many of which I continue to have the pleasure of spending time with. To Antonio Marusic, Alec Drean, Michael Warwick, Giulio Vecchia, and more - thank you!

To all the PhD, Masters, and undergraduate students I have had the pleasure of teaching and sharing this time with both in Liverpool and Padova, thank you and I wish you all the best of luck in whatever you go on to do.

To my family, it has been a long and difficult road but the love and support has always been there. To my parents and my sister, whose confidence in me never wavered, especially when I needed it the most. Uncle Norman, thank you, your support has meant the world to me. Auntie Chris and Eddie, you were always there when I needed a shoulder to lean on. To my nan, I wish you were here to celebrate with me but I know that you have been with me every step of the way and I hope that I continue to make you proud.

Finally, to my incredible fiancèe, Jiff. Your constant support and patience through the highs and lows kept me on a steady path to where I am today. Experiencing this journey with you has made it all the more special.

Abstract

The calcium ion (Ca^{2+}) is a ubiquitous second messenger with well-established roles across many tissue systems. In the epidermis, Ca^{2+} has long been identified as a primary regulator of proliferation, differentiation, and barrier homeostasis. A gradient in Ca^{2+} has been observed with the general view that both intracellular and extracellular Ca^{2+} concentrations are lowest in the basal layer and peaking in the upper granular layer. Work *in vitro* has identified that modifications of extracellular Ca^{2+} dictate the proliferation state of keratinocytes. However, this extracellular switch has not been elucidated *in vivo*. In addition, despite defective Ca^{2+} uptake into organelles such as ER and golgi being shown to disrupt barrier homeostasis, only now is it emerging that mitochondria may play a significant role in epidermal homeostasis on regulation and differentiation as well as apoptosis.

In this thesis, a bi-fold approach was taken in order to develop new molecular tools in order to allow the investigation into the role of extracellular Ca^{2+} in epidermis *in vivo* and the role of mitochondrial Ca^{2+} in proliferating and differentiating HaCaT keratinocytes.

Firstly, two extracellular genetically encoded Ca^{2+} indicators targeted to the extracellular surface were designed and generated. The first CatchER, was unsuccessful despite protein production being confirmed. The second, green and red (G/R)-CEPIA1pm, was successfully targeted to the plasma membrane and using live cell imaging, Ca^{2+} sensitivity of the probe was confirmed. Incorporation of this novel probe into 3D-culture systems has the potential to throw new light on the role of extracellular Ca^{2+} in tissues.

In order to investigate the role of mitochondrial Ca^{2+} on keratinocyte homeostasis, the recently described mitochondrial Ca^{2+} uniporter was knocked out using the CRISPR/Cas9 gene editing system. Using qPCR and Western blotting, the relative expression of some MCU family proteins was investigated. Mitochondrial aequorin was used to investigate Ca^{2+} handling in keratinocytes in proliferating or differentiating conditions. In addition, in the same conditions, proliferation studies were used in order to assess the effect of reduced mitochondrial Ca^{2+} uptake on keratinocyte homeostasis.

HaCaT keratinocytes grown in low Ca^{2+} proliferate at a higher rate than those in high Ca^{2+} conditions. This increased growth rate is accompanied by an increase in agonist-evoked mitochondrial Ca^{2+} uptake and also a decrease in the gene expression of the MCU inhibitor, MICU2. HaCaT keratinocytes devoid of the MCU protein struggle to proliferate in high Ca^{2+} conditions, with cell death and cell senescence appearing to occur. This reduction in proliferation rate of MCU -/- HaCaT keratinocytes is partly rescued when grown in low Ca^{2+} conditions. These results indicate an important role for mitochondrial Ca^{2+} in keratinocyte and in turn, epidermal homeostasis.

.

Table of Contents

Table of Figures

Table of Tables

Abbreviations

Ca^{2+}	Ionised calcium
$[Ca^{2+}]$	Ca^{2+} concentration
$[Ca^{2+}]_c$	Cytosolic Ca^{2+} concentration
$[Ca^{2+}]_{er}$	ER Ca^{2+} concentration
$[Ca^{2+}]_i$	Intracellular Ca^{2+} concentration
$[Ca^{2+}]_m$	Mitochondrial Ca^{2+} concentration
$[Ca^{2+}]_o$	Extracellular Ca^{2+} concentration
CEPIA	Ca^{2+}-measuring organelle-entrapped protein indicators
CRISPR	Clustered-regularly interspaced protospacer motifs
DMEM	Dulbecco's modified Eagle medium
DMSO	Dimethyl sulfoxide
DNA	Deoxyribonucleic acid
EGFP	Enhanced green fluorescent protein
EDTA	Ethylenediaminetetraacetic acid
EGTA	Ethylene glycol tetraacetic acid
ER	Endoplasmic reticulum
FBS	Foetal bovine serum
FLIM	Fluorescence lifetime imaging

GECI	Genetically encoded Ca^{2+} indicator
GFP	Green fluorescent protein
GPCR	G-protein-coupled receptor
HBS	HEPES buffered saline
HEPES	4-(2-hydroxyethyl)-1-piperazineethanesulfonic acid
IFE	Interfollicular epidermis
KO	Knockout
MCU	Mitochondrial Ca^{2+} uniporter
MICU	Mitochondrial Ca^{2+} uptake
mRNA	Messenger RNA
PBS	Phosphate buffered saline
PCR	Polymerase chain reaction
PIXE	Proton-induced X-ray emission
qPCR	Quantitative PCR
RNA	Ribonucleic acid
SERCA	Sarcoplasmic/endoplasmic reticulum Ca^{2+} ATPase
STIM1	Stromal interacting molecule 1
TCA cycle	Tricarboxylic acid cycle

1 Introduction

1.1 Structure of the epidermis

The epidermis is the outermost, superficial layer of the skin. It provides the primary physical and chemical barrier against foreign objects, toxic agents, and other various insults. A stratified squamous epithelium, the epidermis mainly consists of keratinocytes (90 %). However, melanocytes, Merkel cells, and Langerhans' cells are also present (Haake et al., 2001). Mammalian epidermis consists of hair follicles that interject interfollicular epidermis (IFE). This IFE is characterised by the organisation of cells into four layers, stratum basale or basal layer, stratum spinosum (spinous layer), stratum granulosum (granular layer), and the stratum corneum (corneocyte or horny layer). These layers are defined by the morphology of keratinocytes within that layer and will be discussed in more detail below.

The stratum basale, is the innermost layer of the epidermis and the only one in which cells are mitotically active (Blanpain and Fuchs, 2006). The IFE is constantly renewing and repairing, and there are two main ideas that surround the mechanism of this renewal. The notion of renewal would implicate the presence of stem cells. Early work on this hypothesis found discrete columns of cells from basal to differentiated. This was consistent with previous histological work that identified differentiated cells lying over a bed of basal cells (Mackenzie, 1970, Potten, 1974). This structure was termed the epidermal proliferative unit (EPU) whereby proliferative and differentiating cells surround a putative stem cell (SC). The proliferating daughter cells were termed transient amplifying cells (TA cells) and were characterised by their asymmetric division to the basement membrane, producing a proliferative daughter and also a differentiating cell on top (Lechler and Fuchs, 2005). After a

limited number of divisions however, these TA cells simply symmetrically divide into differentiating cells (Potten, 1981). As work continued, the identification of epidermal undulations (rete ridges) thought to aid the anchoring of epidermis to the dermis contained cells in various stages of proliferation rate. Stem cells, used infrequently, were located at the base of these ridges (Lavker and Sun, 1982). It was later identified that expression of β1-integrin was proportional to the rate of proliferation *in vitro* (Jones and Watt, 1993). In line with this, cells expressing the most β1-integrin were found in these rete ridges, with expression deepening into the ridge in line with the thickness of the total epidermis (Jones et al., 1995).

The presence of an EPU containing a single stem cell and TA cells with a limited life time would reach a steady state peak where colony size would not change, which has been shown mathematically (Clayton et al., 2007). This is in contrast with work that labelled basal cells with enhanced yellow fluorescent protein (EYFP) and observed that over time, colony size progressively increased (Clayton et al., 2007). Again in contrast with the EPU hypothesis, it has been observed that only 3 % of mitotic cells contain spindles that are perpendicular to the basal membrane, yet 84 % of divisions generate both one 'cycling' and one 'non-cycling' daughter cell (Clayton et al., 2007). Clayton *et al* (2007) termed these mitotic cells epidermal progenitor cells (EPC), stating their potential to be capable of an unlimited number of divisions, unlike the limited divisions proposed for TA cells previously (Potten, 1981).

As mitotic spindles are mostly parallel to the membrane, it is proposed that post-mitotic cells are transferred to the suprabasal layers as opposed to division driving their upward momentum (Clayton et al., 2007). This study is analogous with previous work that states as keratinocytes begin to differentiate and committed cells

are formed, they increase in size and lose their adhesiveness to the basement membrane (Adams and Watt, 1990, Watt, 1987). As cells begin to move away (Potten, 1974), they undergo phenotypic and proteomic changes, rather than are moved away from the membrane prior to these changes.

In addition to keratinocytes, melanocytes are located in the basal layer at a ratio of 1:36 with keratinocytes (Quevedo et al., 1975). These cells migrate early in embryogenesis and are characterised by dendritic processes that extend and surround neighbouring keratinocytes. Melanocytes generate and secrete melanosomes, a pigment capsule that is accumulated by keratinocytes (Ando et al., 2012) and provides ultraviolet radiation (UV) protection to the nucleus (Cichorek et al., 2013). Merkel cells, constitute the nerve component of the skin mainly for touch, contain dense-granules of neuropeptides that may act as neurotransmitters (Moll et al., 2005). Langerhans' cells are involved in the skins immune system, with a part to play in antimicrobial immunity and inflammation (Chomiczewska et al., 2009).

Keratinocytes primarily synthesize keratin (Eckert, 1989), an α-type fibrous protein that has the ability to form coiled-coil α-helices (Fraser et al., 1964). The expression of keratin is commonly used to indicate the differentiation state of keratinocytes as the expression profile of its various isoforms changes with differentiation (Fuchs and Green, 1980). The basal layer is often identified by the expression of keratin-5 (K5) and K14 in keratinocytes. Typically, as keratinocytes exit this layer and begin to differentiate, cytokeratins K5/K14 are downregulated and K1/K10 are upregulated (Fuchs and Green, 1980). Work expressing K10 under the K5 promoter, has shown that K10 arrests the cell cycle (Santos et al., 2002) therefore inhibiting proliferation. In addition, it has been shown that the K1/K10 partnership mediates the implantation

of desmosomes into the cell membrane, giving the cells a spiny-like structure, hence the term stratum spinosum. The synthesising of key proteins such as involucrin and transglutaminases initiates in the stratum spinosum (Thacher and Rice, 1985, Banks-Schlegel and Green, 1980) and these proteins are crosslinked at the membrane (Rice and Green, 1978). The stratum granulosum draws its name from the granular-like appearance of cells in this layer. This appearance is due to the presence of keratohyalin granules in the cytoplasm. These granules are tightly packed amorphous particles that contain amino acids rich in proline and sulfur. The association of these keratohyalin granules with the keratin filaments, is responsible for the high structural rigidity of cells, chemical resistance, and elasticity found in the stratum corneum (Matoltsy and Matoltsy, 1970).

In the granular layer, keratinocytes contain a large number of ovoid secretory vesicles called lamellar bodies (LBs) (Feingold, 2007). These vesicles contain phospholipids, glucosylceramides, sphingomyelin, and cholesterol. There are numerous enzymes also located in the LBs, including lipid hydrolases such as β-glucocerebrosidase, acidicsphingomyelinase, secretory phospholipase A2, and neutral lipases. As well as these, proteases such as chemotryptic enzymes (kallikreins) and cathepsins have been identified (Feingold, 2007). Lamellar bodies are secreted upon terminal differentiation and the lipids described are metabolised in the extracellular space by the co-secreted enzymes. This mix of ceramides, cholesterol and free fatty acids are vital to the formation of the permeability layer found in the corneum (Grayson et al., 1985, Wertz et al., 1984, Freinkel and Traczyk, 1985). The stratum corneum is the outermost layer of the epidermis and is characterised by denucleation of the differentiating keratinocytes to leave an elastic, yet rigid permeability barrier against damage.

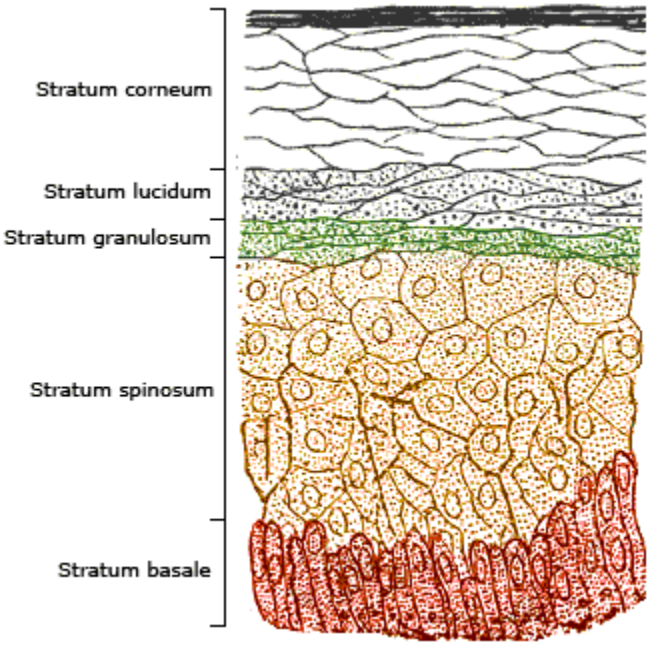

Figure 1.1. Structure of the epidermis.

Image taken from (Wikipedia, 2018)

1.2 Ca^{2+} signalling

Since the somewhat serendipitous discovery of its role in cardiac cell function in 1883 (Ringer, 1883), and the work of Heilbrunn and Wiercinski (1947), who identified that injection of the Ca^{2+} ion, and only the Ca^{2+} ion, resulted in contraction of frog leg muscle (Heilbrunn and Wiercinski, 1947) a plethora of work has ensued, attempting to elucidate the action of this common second messenger (Berridge et al., 2003). A large number of channels, pumps and exchangers have been identified in a range of cell and tissue types, which act to regulate $[Ca^{2+}]$ in the cell, typically maintaining a resting ~ 10,000-fold gradient between intracellular and extracellular concentrations in mammalian cells. Some of these channels, pumps and exchangers will be reviewed here, in order to understand the mechanism of Ca^{2+} movement across the membrane and within the cell.

The versatility of Ca^{2+} signalling requires a complex 'signalling toolkit' that can be grouped into four general processes (Berridge et al., 2000). Firstly, a stimulus triggers Ca^{2+} mobilising signals such as inositol trisphosphate (IP_3). This stimulus activates mechanisms that drive Ca^{2+} into the cytoplasm, either from the extracellular environment or from intracellular stores. This increase in $[Ca^{2+}]$ activates ON mechanisms leading to the stimulation of a wide range of Ca^{2+} sensitive processes including protein activation and gene expression. OFF mechanisms such as Ca^{2+} buffers then act in order to sequester and remove Ca^{2+} from the cytoplasm.

The triggers that induce influx or release of Ca^{2+} most commonly begin in the extracellular environment. In non-excitable cells, $[Ca^{2+}]_c$ elevation is often induced via the activation of cell surface receptors. These receptors are bound by a variety of agonists such as hormones, paracrine agents and growth factors. Most common

amongst these receptors are G-protein-coupled receptors (GPCRs), receptor tyrosine kinases (RTKs) and store-operated channels (SOCs). Activation of GPCRs leads to a downstream signalling cascade and the production of IP_3, which in turn, binds the IP_3-receptor (IP_3R) on the endoplasmic reticulum. Other receptors such as RTKs can also lead to downstream activation of IP_3 (Cheng et al., 2010). Binding of IP_3 to its receptor stimulates a transient release of Ca^{2+} into the cytoplasm. Stromal interacting molecule 1 (STIM1), a Ca^{2+} binding protein located in the endoplasmic reticulum (ER) membrane, forms puncta when Ca^{2+} is not bound to its ER lumen facing EF-hand. This puncta, binds to the plasma membrane located ORAI which forms a channel allowing Ca^{2+} influx into the cell. This influx is termed store-operated Ca^{2+} entry (SOCE). Once the $[Ca^{2+}]_c$ begins to increase, the ER located Ca^{2+} pumps sarco/endoplasmic reticulum Ca^{2+}-ATPase (SERCA) begin to pump Ca^{2+} into the ER lumen, refilling the store. As the ER store refills, Ca^{2+} binds to STIM1 which then dissociates from ORAI, providing a negative feedback for SOCE.

An example of GPCR stimulated $[Ca^{2+}]_c$ increase is the Ca^{2+} sensitive receptor (CaSR or CaR). This receptor is sensitive to Ca^{2+} in the 0.5 – 5 mM range and when stimulated, elicits an increase in $[Ca^{2+}]_i$ (Breitwieser and Gama, 2001, Rey et al., 2010). Pharmacological inhibition or knock-down of the CaR, other GPCRs and/or other SOCE entry proteins leads to an inhibition of cellular proliferation in a range of cell types from endothelial to cancer cells (Borowiec et al., 2014). Highlighting the importance of the role of $[Ca^{2+}]_o$ and its relationship with $[Ca^{2+}]_i$ transients on cellular processes.

Intracellular Ca^{2+} transients are not only seen in the cytosol and ER, but also in other organelles such as mitochondria (Rizzuto et al., 1992) and the nucleus (Brini et al., 1993).

1.3 Measuring Ca^{2+}

Ca^{2+} is a highly versatile intracellular signal. The ability to measure signals generated by Ca^{2+} ion movement are invaluable in understanding its role. Therefore, methods previously and currently used to measure Ca^{2+} changes will be discussed below.

The Ca^{2+}-sensitive bioluminescent protein aequorin (Shimomura et al., 1962) was the first ever used to identify intracellular Ca^{2+} changes (Ridgway and Ashley, 1967). Aequorin was employed before a method was identified to use exogenous DNA in cells (Hsiung et al., 1980) and was therefore injected into cells for use. Aequorin requires apo-aequorin and coelentrazine, a light emitting prosthetic group to luminesce (Shimomura and Johnson, 1978). Both apo-aequorin and coelentrazine can be modified in order to improve and fine-tune the probes response to Ca^{2+} (Shimomura et al., 1989).

In 1980, the late Roger Tsien began the process of generating Ca^{2+} sensitive compounds, based on the Ca^{2+} chelating properties of EGTA. Initially removing the pH sensitivity of EGTA to generate BAPTA, and later using BAPTA to create the acidic, fluorescent compound Quin-2. Quin-2, upon binding Ca^{2+} would undergo a large spectral shift, which could be measured and equated to Ca^{2+} levels (Tsien, 1980). Tsien's work continued with the generation of Quin2-AM., a free-acid ester that could pass freely into cells, hydrolysed once in the cell the Ca^{2+} sensor was then 'trapped' within the cell membrane. Despite its pitfalls with regards to fluorescence intensity and slight tendency to buffer Ca^{2+} transients, its ability to freely diffuse into the cell made it extremely desirable against other Ca^{2+} sensors at the time such as ion-selective electrodes, injectable aequorin, and arsenazo III (Tsien, 1981, Tsien and Pozzan, 1989).

Since its discovery in 1979 (Shimomura, 1979) and the isolation of its cDNA (Prasher et al., 1992), GFP has become increasingly useful as a genetically encoded Ca^{2+} indicator (GECI). The mutations made to GFP in order increase its brightness, useable wavelengths and modify the colour for use in fluorescence energy transfer (Heim and Tsien, 1996) were benefited by the earlier identification of the Ca^{2+} binding protein calmodulin (CaM) (Babu et al., 1988). These studies allowed the development of GFP bound CaM sensors that were able to measure Ca^{2+} in real time (Miyawaki et al., 1997). In addition, it was later identified that the GFP beta-can structure could be modified to directly bind Ca^{2+} without a loss of function (Baird et al., 1999) and subsequently led to a second family of Ca^{2+} sensors based on the fluorescence of a single GFP molecule.

Combinations of dyes and GECIs have been used to measure Ca^{2+} in a variety of systems, tissues and subcellular locations, some of which will be discussed below.

1.3.1 Cytoplasmic Ca^{2+}

As mentioned briefly, the first cytoplasmic Ca^{2+} recording took place in muscle fibers of the acorn barnacle (Ridgway and Ashley, 1967). Purified aequorin was injected into the fibre and upon stimulation, an increase in light emitted was recorded in a transient wave. The generation of Quin-2AM led to work in a range of cell types identifying resting Ca^{2+} at around 120 nM (Tsien et al., 1982, Rink and Tsien, 1982). The limitations of Quin-2 were always recognised and this led to the generation of a range of new Ca^{2+} dyes. These new dyes showed much stronger fluorescence, shifting wavelengths upon Ca^{2+} binding, and a weaker affinity for Ca^{2+} yet a better selectivity against other divalent cations (Grynkiewicz et al., 1985). One of these

dyes was called Fura-2 and quickly became one of the most widely used Ca^{2+} indicators available.

Unfortunately, a number of studies identified localisation of these indicators in organelles (Almers and Neher, 1985, Steinberg et al., 1987, Roe et al., 1990, Cobbold and Rink, 1987). Although they quickly saturated, early work was somewhat hindered by an increased background and slight misrepresentations of $[Ca^{2+}]_c$ quantification. Despite this, Fura-2 and other small-molecule Ca^{2+} indicators like it are the go to compounds for cytoplasmic Ca^{2+} measurements.

1.3.2 Organelle Ca^{2+}

The resolution of true organelle Ca^{2+} came with the work of Rizzuto *et al* (1992) whereby apo-aequorin was targeted directly to mitochondria using a targeting fragment of human cytochrome c (Rizzuto et al., 1992). Work followed allowing targeting of other GECIs to organelles such as the endoplasmic reticulum (Miyawaki et al., 1997) and mitochondria (Palmer et al., 2006) in order to quantify resting and stimulated Ca^{2+} concentrations.

1.3.3 Endoplasmic reticulum

Indicators such as Mag-Fura2 (Hofer and Machen, 1993) were used due to a proclivity to accumulate in subcellular stores such as the ER, by use of a buffer to wash away excess cytoplasmic dye it was possible to measure fluorescence changes following store depletion. This method was quick and simple, however small amounts of dye leakage into the cytoplasm have been shown to have a large effect on Ca^{2+} estimation (Hofer and Schulz, 1996). In addition, dye reporting from regions of low Ca^{2+} outside the Mag-Fura2 range (< 5μM) also leads to an underestimation of Ca^{2+} levels.

Aequorin was later developed as an ER-targeted probe (Kendall et al., 1992). The use of an N-terminal ER retention sequence and its high dynamic range 10^{-7} to 10^{-3} M (Alvarez and Montero, 2002) made this probe highly desirable. Nevertheless this technique required total depletion of the ER store prior to measurements which in some cell types may cause cell stress and apoptosis. Additionally, the aequorin probe released only a small amount of light that was consumed incredibly fast and therefore $[Ca^{2+}]_{er}$ concentrations could only be measured as > 100 μM as the probe saturated (Montero et al., 1995).

Following on from generating GFP colour variants and linking them to CaM, Tsiens group identified that the binding of Ca^{2+} to the M13 peptide of CaM would cause it to shorten and wrap itself around CaM. When this peptide was placed in between GFP variants, they would be bought in close enough proximity to allow fluorescence resonance energy transfer (FRET) to occur (Miyawaki et al., 1997). These probes, termed cameleons' were used to quantify endoplasmic reticulum Ca^{2+} to between 60 – 400 μM at rest and 1 – 50 μM following stimulation. The sensitivity and accuracy of these probes made them highly desirable, however the real-time application and simplicity of calibration, meant these probes were a real step forward in the investigation into the role of Ca^{2+} as a second messenger.

In 2007, Zou *et al* generated a plethora of single-GFP molecule Ca^{2+} sensors that had similar Ca^{2+} binding sensitivity as previous sensors but with negligible Ca^{2+} buffering due to the lack of mirocmolar levels of proteins such as CaM. Using these probes, they too identified an $[Ca^{2+}]_{er}$ of 0.4 – 2 mM in resting – stimulated cells (Zou et al., 2007).

1.3.4 Mitochondria

The first work on mitochondrial Ca^{2+} using genetically encoded indicators was that of Rizzuto *et al* (1992), targeting apo-aequorin directly to the mitochondria. This work demonstrated that agonist-evoked cytosolic increases in Ca^{2+} were followed by an increase in $[Ca^{2+}]_m$. Despite this, due to the inherent limitations of aequorin, true quantitative measurements of $[Ca^{2+}]_m$ were limited. It wasn't until later that cameleon probes were successfully and accurately targeted to the mitochondria and $[Ca^{2+}]_m$ was observed to be around 100 μM following stimulation (Arnaudeau et al., 2001). Work continued to improve the localisation and sensitivity of mitochondrial targeted cameleon probes and the generation of D*cpv probes (* indicating the number 2,3 or 4) (Palmer et al., 2006) took mitochondrial Ca^{2+} work forward. Using these probes resting $[Ca^{2+}]_m$ was observed to be ~ 50 – 300 nM at rest and stimulated between 1.5 – 200 μM, consistent with previous cameleon based work.

Fluorescent organic-based dyes such as Rhod-2 and Rhod-FF have also been used to measure mitochondrial Ca^{2+} fluxes. Although these dyes are very useful for measuring single stimulation driven peaks, they struggle when it comes to multiple stimulations compared to aequorin and cameleon. In addition, accurate measurements of $[Ca^{2+}]_m$ were limited due a large tendency to buffer intramitochondrial Ca^{2+} (Fonteriz et al., 2010).

1.3.5 Extracellular

There is a plethora of information regarding the role of extracellular Ca^{2+}. Techniques and tools mentioned previously such as small molecule dyes and GECIs have made measuring influx and steady-state Ca^{2+} very simple. Measuring efflux and general extracellular Ca^{2+} has however, proved more difficult. Early work used Ca^{2+}-

45 ($^{45}Ca^{2+}$), a β-emitting radioactive isotope of Ca^{2+}. This method of measuring efflux using $^{45}Ca^{2+}$ has its weaknesses, as it requires removal of the extracellular fluid from the cells to measure the radioactivity, meaning the results are not in real time (Bloomquist and Curtis, 1972, Huddart and West, 1975).

With the generation of small molecule dyes such as Fura-2, came the ability to load the extracellular space with dye and measure fluorescence modulation. The ratiometric dye Fura-2 was used to identify Ca^{2+} efflux of a few hundred nanomolar (Zolle et al., 2000) with concurrent work in single cells using Fura-2 in the cytoplasm and Fluo-3 in the extracellular space (Tepikin et al., 1994).

Another method less commonly used is Ca^{2+}-sensitive microelectrodes, this measures an electrical current stimulated by the movement of charged ions. Although the dynamic range of sensitivity is better with microelectrodes, the response time of measurements is extremely slow (Takahashi et al., 1999).

1.4 Ca^{2+} and the epidermis

1.4.1 The Ca^{2+} gradient

It was first described in 1980, that isolated primary mouse keratinocytes proliferated in < 0.1 mM extracellular Ca^{2+}, much lower than that previously seen for other cell types (Hennings et al., 1980). In addition to this, switching the Ca^{2+} to > 1 mM induced apparent differentiation, with a reduction in DNA production, protein production, and an induction of desmosome formation. Work followed that confirmed the role of extracellular Ca^{2+} in determining the proliferation state of keratinocytes (Dykes et al., 1982, Hennings et al., 1981). As work continued to elucidate the 'Ca^{2+} switch' involved with epidermal cells, proteins required for epithelial stratification were shown to be induced by an increase in extracellular Ca^{2+} as small as 0.1 mM (Stanley and Yuspa, 1983), hypothesising that this switch occurs *in vivo* too. It wasn't until 1985 that Menon *et al* were able to describe a gradient of Ca^{2+} in neonatal mouse epidermis (Menon et al., 1985). Using ion-capture chemistry, a gradient in total (bound + free) Ca^{2+} was observed, with lowest concentrations at the basal layer, increasing to the late granular layer and falling rapidly at the cornified layer. Low Ca^{2+} was observed surrounding the basal cells and also low intracellular Ca^{2+}, some Ca^{2+} deposits were observed in the mitochondria and nuclear chromatin, possibly playing a role in the cell cycle. Early granular cells appeared to have more mitochondrial and some lamellar body Ca^{2+} whereas late granular cells had high cytoplasmic Ca^{2+} and also dense extracellular deposits. Through the cornified layer, very low amounts of Ca^{2+} were observed in the lower layer with the cells in the upper layer completely devoid of Ca^{2+} (Menon et al., 1985). Later work with ion-capture chemistry on isolated neonatal human keratinocytes grown in high

Ca^{2+} (1.2 mM) and allowed to stratify, observed Ca^{2+} precipitates in organelles in the basal layers and more heterogeneous precipitates were observed in the stratified layers (Pillai et al., 1993). The small molecule, ratiometric Ca^{2+} indicator Indo-1 was used to quantify cytoplasmic Ca^{2+} in cells grown in low (0.07 mM) and high (1.2 mM) Ca^{2+}. As expected, $[Ca^{2+}]_i$ was increased in cells grown in high Ca^{2+}. In addition, in both conditions, $[Ca^{2+}]_i$ increased upon post-confluent growth. The Ca^{2+} ionophore ionomycin induced a transient rise in cytoplasmic Ca^{2+} with peaks higher in differentiated then proliferating keratinocytes in the presence of extracellular EGTA. Confirming that, differentiated keratinocytes maintain a higher $[Ca^{2+}]_i$ (Pillai et al., 1993).

The use of proton-induced X-ray emission (PIXE) followed ion-capture chemistry, sections of murine epidermis were frozen and Ca^{2+} concentrations were quantified and recorded along with their distance from the epidermal surface (Mauro et al., 1998). Starting very low in the corneum, Ca^{2+} concentrations sharply increased in the granular layer before falling gradually towards the basal layer, concurrent with the ion-capture studies.

The work carried out in these early studies was invaluable, showing for the first time the presence of an epidermal Ca^{2+} gradient. However, Ca^{2+} precipitation and PIXE studies measure total Ca^{2+}, not free Ca^{2+}, and they require dehydrated and/or fixed tissue, therefore molar Ca^{2+} concentrations cannot be measured in the tissue. Furthermore, spatial resolution is limited, meaning new techniques were needed in order to accurately quantify epidermal Ca^{2+} with resolution between organelles, cytoplasm and extracellular space.

Ca^{2+} green 5N is a very sensitive Ca^{2+} probe that has been shown to have two species of fluorescence, Ca^{2+} bound and Ca^{2+} free, which decay at different rates (Yoshiki et al., 2005). These properties make CG5N very useful for fluorescence lifetime imaging (FLIM). In addition, FLIM does not require dehydration or fixing of tissue and can resolve morphology of tissue to much greater deal than Ca^{2+} precipitation or PIXE studies, therefore this technique was promising for further investigation into the epidermal Ca^{2+} gradient. Using a standard loading protocol with CG5N and two-photon imaging, Celli *et al* (2010) observed in intact epidermis, the variation in cell morphology throughout the layers along with the Ca^{2+} gradient and subcellular localisation of Ca^{2+} hotspots. The basal and spinous layers contained more cuboidal cells with easily visible nuclei, alluding to their viability. The granular layer appeared as much larger cells with obvious granules throughout the cytoplasm, large anuclear cells could be observed at the corneum with little intracellular staining of CG5N.

Using the FLIM technique, four sets of concentrations of Ca^{2+} were used, 0 μM < $[Ca^{2+}]$ < 3 μM, 3 μM < $[Ca^{2+}]$ < 7 μM, 7 μM < $[Ca^{2+}]$ < 15 μM, and $[Ca^{2+}]$ > 20 μM, images were taken calibrated to each of these concentrations in four layers, dermis, SB, SG, and SC. Unfortunately, no distinction was made between the SB and SS. The SC was characterised by the lowest Ca^{2+} of < 3 μM with mostly extracellular-like fluorescence. The SG had the highest Ca^{2+}, saturating in the > 20 μM range. Due to this, no discernible structures could be seen and therefore no resolution of the dyes location. In the SB, heterogeneous Ca^{2+} concentrations across the cells have been reported, with $[Ca^{2+}]$ varying from 3 μM to 20 μM (saturation) (Celli et al., 2010). This may be explained by the asymmetric mitosis of keratinocytes previously explained. However, this technique measures only free Ca^{2+}, if free Ca^{2+} is high in

the SB organelles, as alluded to in earlier studies, saturation of late SB organelles at 20 μM may not be unexpected. As the signal saturates completely in the SG, further quantification organelle/store Ca^{2+} is needed to really determine the peak $[Ca^{2+}]$.

It has already been shown that differentiated cells have a higher $[Ca^{2+}]_i$, however, a study directly investigating $[Ca^{2+}]_{er}$ using the Ca^{2+} dye Fura-2, identified that thapsigargin induced a Ca^{2+} release from the ER. This release had a larger peak (~ 1 μM) in differentiated cells than in basal cells (~ 600 μM). In the presence of extracellular Ca^{2+}, Ca^{2+} uptake into the cytoplasm (probably by SOCE) by differentiated cells (~ 1.8 μM) was almost double that of the basal cells (1 μM). Using the ER based dye Mag-Fluo4, the release was observed almost immediately after thapsigargin addition, interestingly, addition of ionomycin and EGTA to investigate the Ca^{2+} store size, reduced ER fluorescence by almost ~ 35 % more in the differentiated cells. These data, along with western blotting of a 3-fold increase in the ER protein calreticulin and a 10-fold increase in SERCA2b expression, leads to the notion of an increase in the size of the ER Ca^{2+} store and also its ability to sequester Ca^{2+} (Beck et al., 2008).

Early work showed that disruption of the barrier led to lamellar body secretion, these lamellar bodes replenished lipids and restored the permeability gradient (Feingold et al., 1990, Holleran et al., 1991, Grubauer et al., 1987). Interestingly, ion-capture chemistry performed on acetone treated and tape-stripped epidermis identified a marked decrease in total Ca^{2+} across the epidermis (Menon et al., 1992). This suggests that exocytosis is driven by a decrease in Ca^{2+}, paradoxical to that seen in many other systems (Burgoyne and Morgan, 2003).

Topical solvent treatment (acetone) in intact mice led to an increase in trans-epidermal water loss (TEWL), however, experiments in hypertonic and hypotonic solutions identified that water transit, was not the signal necessary for repair (Lee et al., 1992). Addition of as little as 10 μM Ca^{2+} inhibited repair (Lee et al., 1992), confirming that the lamellar body exocytosis is driven by a loss of Ca^{2+}.

The study mentioned previously using FLIM, identified that immediately after tape-stripping, a large release of Ca^{2+} is observed from the stores, filling the extracellular space with Ca^{2+} (Behne et al., 2011). Later work, using numerical modelling, postulated the same whereby barrier disruption (defined as removal of the corneum with air exposure), leads to an increase in Ca^{2+} throughout the epidermis (Kobayashi et al., 2016) rather than a decrease observed by (Menon et al., 1992). Kobayashi *et al* (2016) hypothesised that the focus is to restore the permeability barrier and afterwards, the basal layer can recover its thickness. These contradictory hypotheses highlight the notion that temporal regulation may be as important as spatial regulation in the recovery and maintenance of the epidermis.

1.4.2 Receptors, pumps, and channels

As discussed above, a gradient involving organelle, cytoplasmic and extracellular Ca^{2+} has been observed in the epidermis. This gradient in total Ca^{2+} is largely accepted to be lowest in the basal layer rising towards the granular layer and falling sharply at the cornified layer. As cells begin to differentiate and move upwards towards terminal differentiation, they appear to accumulate Ca^{2+}, before releasing their contents at the granular layer allowing Ca^{2+} to diffuse back down the layers as depicted in Figure 1.2. Tight junctions (TJs) in the granular layer regulate trans-epidermal water loss (TEWL) and therefore ensure the Ca^{2+} is retained. This cycle of Ca^{2+} is maintained by a range of receptors, pumps and channels. Some of which will be described below.

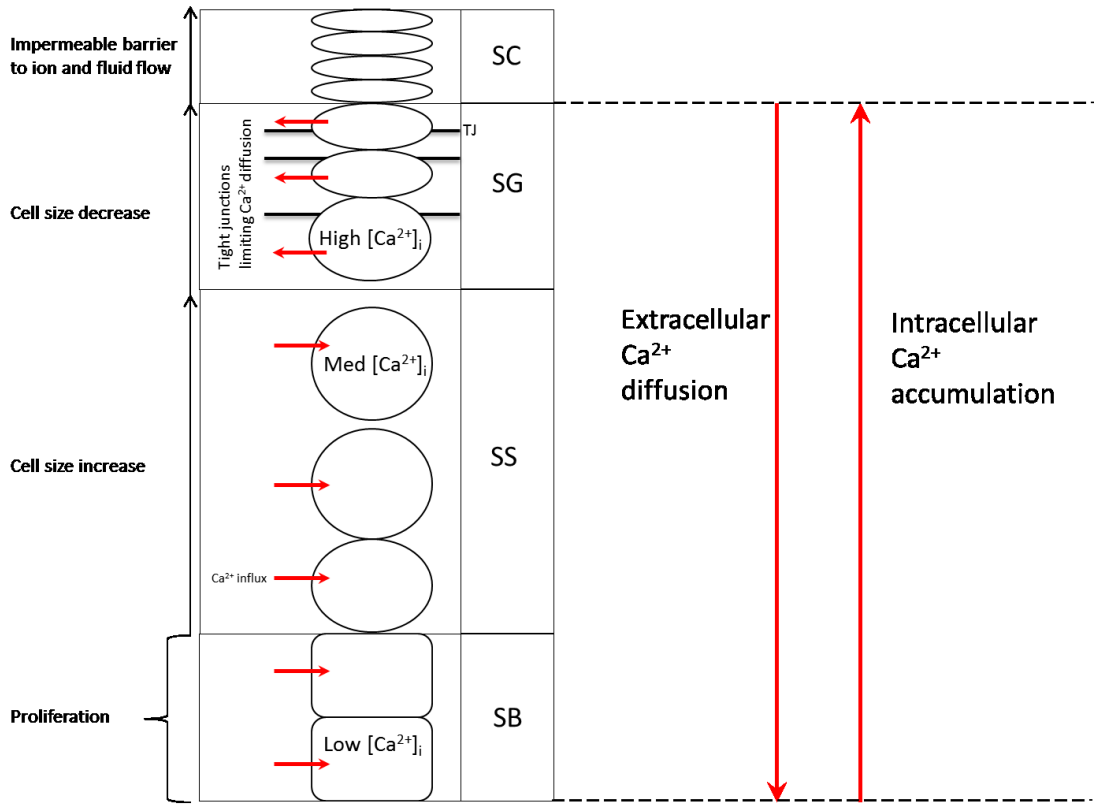

Figure 1.2. Schematic diagram of the epidermal Ca^{2+} gradient.

Adapted from (Adams et al., 2015).

The basal and suprabasal layers are often characterised by low $[Ca^{2+}]_o$ and generally low $[Ca^{2+}]_i$ with some organelles retaining Ca^{2+} (Mauro et al., 1998, Behne et al., 2011). Sarco/endoplasmic reticulum Ca^{2+}-ATPase (SERCA2b) is expressed evenly throughout the epidermis (Tavadia et al., 2004) but notably, the basal layer has very high expression of secretory pathway Ca^{2+}-ATPase 1 (SPCA1) (Tu et al., 2007) suggesting an enhanced capacity to accumulate Ca^{2+}. In addition, STIM1 and Orai1, proteins involved in SOCE are necessary for keratinocyte proliferation in the basal layer (Numaga-Tomita and Putney, 2013). This further indicates a key role for Ca^{2+} uptake in the basal layer.

Several studies have long indicated that cells in the granular layer maintain high $[Ca^{2+}]_c$ (Hennings et al., 1980, Kumamoto et al., 2017). Voltage-gated Ca^{2+} channels (VGCC) have been identified in the epidermis with expression almost solely in the granular layer where they act to supress LB release (Denda et al., 2006). VGCC are known to elevate $[Ca^{2+}]_c$ in keratinocytes (Denda et al., 2006). Ryanodine receptors are activated by local variations in $[Ca^{2+}]_c$ (Nabauer et al., 1989, Cannell et al., 1987) and it has been identified that RyR subtypes RyR1 and RyR2 are increasingly expressed in the differentiating layers (Denda et al., 2012). Therefore indicating that Ca^{2+} influx and Ca^{2+}-induced Ca^{2+} release from the stores may play a role in maintaining the elevated $[Ca^{2+}]_c$.

Interestingly, as discussed in Section 1.4.1, loss of $[Ca^{2+}]_e$ leads to lamellar body secretion, possibly in an IP_3 mediated manner. In cells that maintain high circulating IP_3, a reduction in $[Ca^{2+}]_o$ leads to an IP_3-mediated release from the intracellular stores. This LB secretion could be triggered by a reduction in $[Ca^{2+}]_o$ that may occur during the initial stages of a wound when the Ca^{2+} gradient collapses. The CaR has

been identified in epidermis with expression increasing as the cells differentiate (Oda et al., 2000, Bikle et al., 1996, Komuves et al., 2002). Activity of the CaR in the presence of $[Ca^{2+}]_o$ would continuously generate IP_3, albeit largely inactivated by $[Ca^{2+}]_c$. In addition, the TRP/EGFR relationship identified by Cheng *et al* (2010) whereby activation EGFR by TNF-α of these receptors leads to the production of IP_3, Ca^{2+} influx through TRPV3 and also the generation of new TNF-α providing a continuous loop of activation.

Overall, this information identifies that there is a cycling of Ca^{2+} both within the cell and across the epidermis. The elevated $[Ca^{2+}]$ in the differentiating cells is likely to be key to their differentiation, playing a role in gene expression and protein production. In addition, it may be involved in driving apoptosis with intracellular Ca^{2+} overload a key element of death, in particular mitochondrial Ca^{2+} overload. In addition elevated $[Ca^{2+}]_m$ can lead to an increase in ROS and this ROS is known to be a key regulator of keratinocyte differentiation (Hamanaka et al., 2013).

1.5 Mitochondria

Mitochondria are reported to have been around for roughly two billion years following the engulfment of an α-proteobacterium by a precursor of the eukaryotic cell that we know currently (Lane and Martin, 2010). These organelles, often termed the powerhouses of the cell due to their adenosine triphosphate (ATP) production, are vital to the cells life cycle. Mitochondria are rod-shaped organelles that are known to form a network across the cytoplasm of the cell, this network is regulated by the dynamic cytoskeletal proteins, the interaction of mitochondria with other organelles (i.e. the ER and plasma membrane), and the interactions of mitochondria with each other (Friedman et al., 2011, Anesti and Scorrano, 2006).

Mitochondria are composed of two membranes: an outer mitochondrial membrane (OMM) containing pores permeable to solutes and proteins, 5 kDa in size. The inner membrane is much more selective, containing proteins, pumps and channels all of which generate ionic gradients across the membrane. This IMM, much larger in surface area than the OMM, folds into cristae and surrounds the mitochondrial matrix. Here, lie the bulk of the mitochondrial metabolic enzymes and also the mitochondrial DNA (mtDNA), a 16 kDa circle of DNA that encodes for 37 mitochondrial genes not coded for by the nuclear DNA (Figure 1.3).

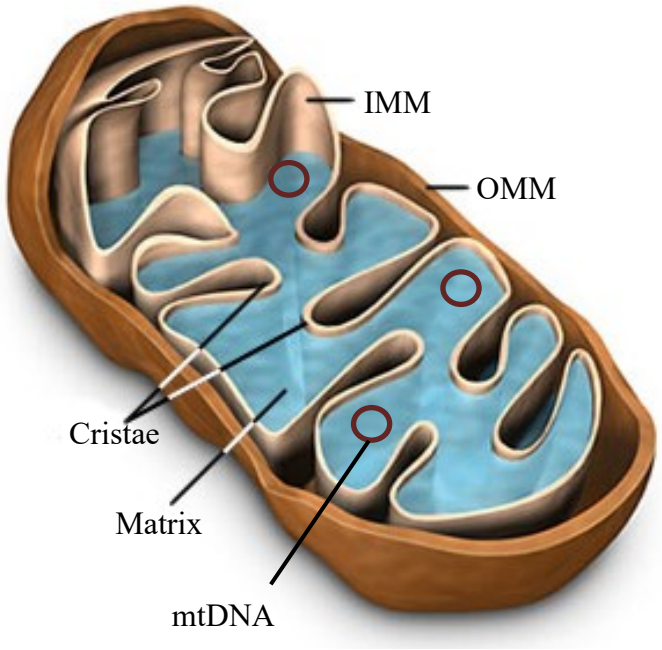

Figure 1.3. Mitochondrial structure

1.5.1 Mitochondrial Ca^{2+}

Since 1961, it has long been known, although only elucidated more recently, that mitochondria can accumulate large amounts of Ca^{2+} (Deluca and Engstrom, 1961). Continuing studies identified that mitochondrial Ca^{2+} was maintained by a balance of influx and efflux (Drahota et al., 1965), in a cycling mechanism (Carafoli, 1979). Isolated mitochondria were observed to preferentially uptake Ca^{2+} before carrying out other cellular processes (Rossi and Lehninger, 1964). This uptake was inhibited by ruthenium red, characteristic of a Ca^{2+} specific uniporter (Moore, 1971). As work slowed, confusion ensued regarding the relatively low affinity of the uniporter for Ca^{2+} as it implied that mitochondria could not take up useful amounts of Ca^{2+}. In 1992 however, mitochondrial Ca^{2+} dynamics were brought back to the forefront thanks to the development of a targeted, genetically encoded Ca^{2+} indicator based on the fluorescent protein aequorin (Rizzuto et al., 1992). Using this probe, Rizzuto *et al* (1992) were able to show that changes in $[Ca^{2+}]_c$ were mirrored by changes in $[Ca^{2+}]_m$.

As work continued, mitochondria were shown to both sense (Rizzuto et al., 1993) and later gradually accumulate (Rizzuto et al., 1998, Csordás et al., 1999) Ca^{2+} after an IP_3-mediated Ca^{2+} increase. Additionally, mitochondria were shown to buffer Ca^{2+} overload, similar to the ER, by taking up Ca^{2+} in a $\Delta\Psi_m$-dependent manner through a Ca^{2+} uniporter when cytosolic levels are high, then releasing it via ion exchangers when the wave has passed (Werth and Thayer, 1994).

In 2011, the search for the elusive Ca^{2+} uniporter came to an end, when two independent laboratories discovered the, now termed, mitochondrial Ca^{2+} uniporter (MCU) (Baughman et al., 2011, De Stefani et al., 2011).

1.5.2 The mitochondrial Ca^{2+} uniporter (MCU)

This 40 KDa protein was originally shown to be sufficient alone to mediate Ca^{2+} entry into mitochondria (De Stefani et al., 2011), this was confirmed *in vivo* when MCU was silenced in mouse liver (Baughman et al., 2011). This was further confirmed in neonatal rat cardiomyocytes (Drago et al., 2012), heart (Joiner et al., 2012), pancreatic β cells (Tarasov et al., 2012), and neurons (Qiu et al., 2013). Following the generation of an MCU knockout mouse model, analysis of mitochondria from various tissues showed a lack of Ca^{2+} uptake and therefore the need for MCU (Pan et al., 2013). However, as shown previously (Csordás et al., 1999), mitochondrial Ca^{2+} uptake is not an all-or-nothing process rather it is fine tuned. The identification of other proteins and regulators that interact with MCU and are able to affect the rate and amount of Ca^{2+} uptake followed.

1.5.3 The MICU family

The first protein to be discovered was MICU1 (Perocchi et al., 2010), a protein later found to be a member of the mitochondrial Ca^{2+} uptake (MICU) family, which includes MICU2 and MICU3. The true function of MICU1 was much debated during early studies, with one hypothesising that it resided in the IMM (Perocchi et al., 2010). As work progressed it became clear that MICU1 was in fact a soluble protein, localised to the intermembrane space of mitochondria (Lam et al., 2015, Patron et al., 2014, Hung et al., 2014). MICU1 has been shown to have various effects on mitochondrial Ca^{2+}, by maintaining MCU in a closed state when Ca^{2+} is low outside (Mallilankaraman et al., 2012) the mitochondria and vice versa (Csordás et al., 2013). Additionally, works showed that in MICU1 silenced cells, mitochondria were constitutively overloaded (Csordás et al., 2013) yet uptake was much less efficient

(Mallilankaraman et al., 2012). Together it is clear to see that although MCU alone is sufficient to allow movement of Ca^{2+} into mitochondria, the sigmoidal property of this influx is regulated largely by MICU1. MICU1 has two reported isoforms, MICU2 and MICU3. MICU2 shares 42 % similarity with MICU1 at the protein level (Patron et al., 2014) and has been observed to interact with MICU1 on mitochondria (Plovanich et al., 2013, Patron et al., 2014), with the complex observed in the intermembrane space (Csordás et al., 2013).

It was later found that following silencing of MICU1, there was a reduction in MICU2 protein, but not of mRNA (Patron et al., 2014). MICU2 has been deemed a genuine MCU inhibitor thanks to work carried out in intact HeLa cells where silencing of MICU2, and subsequent dimerisation of MICU1 protein, led to a significant increase in mitochondrial Ca^{2+} following histamine stimulation (Patron et al., 2014). Concurrently, overexpression of MICU2 led to a reduced histamine response peak.

It has been shown that at low micromolar $[Ca^{2+}]_c$ (< 2.5 uM) MICU1 inhibits Ca^{2+} influx via MCU (de la Fuente et al., 2014). Interestingly, it has also been observed that silencing of MICU2 will only increase agonist-evoked Ca^{2+} uptake below 5 μM $[Ca^{2+}]_c$. At $[Ca^{2+}]_c$ of around 7 – 10 μM, MICU2 silencing does not affect mitochondrial uptake, however, at all these concentrations, once the transient $[Ca^{2+}]_m$ increase had occurred, resting levels all returned to the same baseline (Matesanz-Isabel et al., 2016). These studies are in line with early work that suggested MICU1 and MICU2 cooperatively inhibit MCU (Baughman et al., 2011).

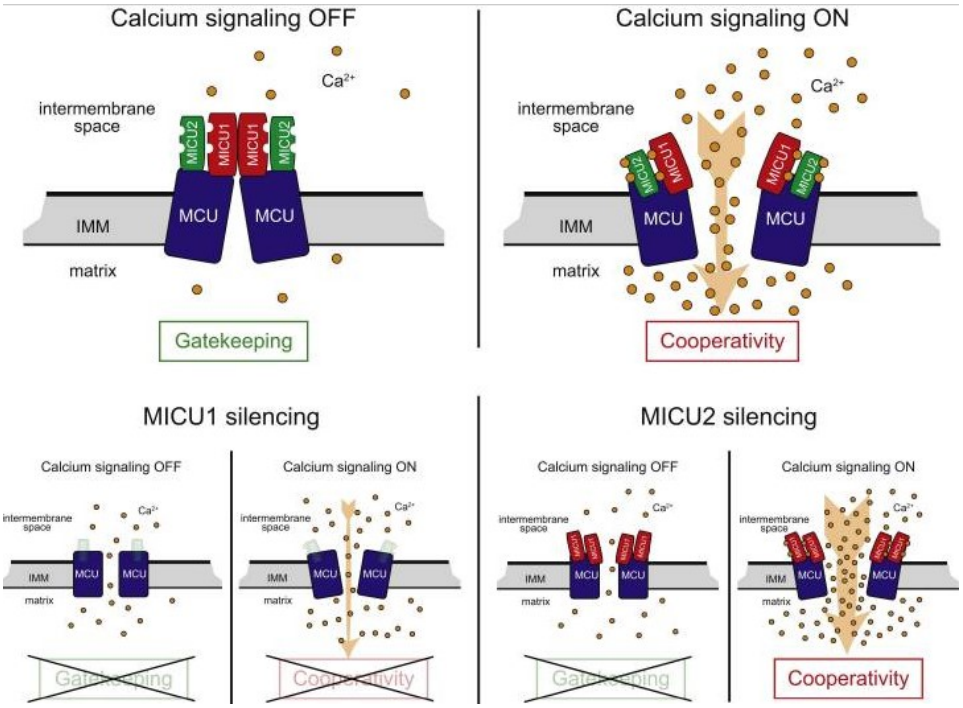

Figure 1.4. Fine tuning of mitochondrial influx through MCU by MICU1 and MICU2.

Taken from (Patron et al., 2014)

1.5.4 EMRE

Another protein identified to play a role in the MCU complex is the essential MCU regulator protein (EMRE), a membrane-bound 10 kDa protein (Sancak et al., 2013). Early work on this protein postulated that EMRE was required as a complex stabilising protein, bridging and maintaining the interaction of the MICU1-MICU2 Ca^{2+} sensing heterodimer with the Ca^{2+} conducting MCU protein. In line with this, increased protein levels of MCU, MICU1 and MICU2 are followed by an increase in EMRE. Additionally, using immunoprecipitation, it was shown that the interaction of MICU1-MICU2 with MCU was lost when EMRE was silenced (Sancak et al., 2013). Notably however, this data goes against observations made in a planar lipid bilayer where Ca^{2+} fluxes are increased when MICU1 and MCU are expressed together, independent of EMRE. This protein is clearly involved in Ca^{2+} movement into mitochondria *in vivo* and in the post-translational production of the MCU complex, although further work is needed to prove, indisputably, the true role of EMRE.

1.5.5 MCUb

Another protein discovered and thought to play a role in mitochondrial Ca^{2+} accumulation is MCUb, a dominant negative isoform of MCU. With 50% protein sequence similarity to MCU, it has been observed to hetero-oligomerise with MCU, possibly in a tetramer (Raffaello et al., 2013). An amino acid substitution identified in the loop region of MCUb leads to a negative charge removal. Concurrently, MCUb does not form a Ca^{2+}-permeable channel *in vitro* alone and drastically reduces agonist induced Ca^{2+} accumulation when co-expressed with MCU (Raffaello et al., 2013).

1.5.6 Mitochondrial Ca^{2+} and the epidermis

As discussed, topical increases in $[Ca^{2+}]_o$ led to an increase in $[Ca^{2+}]_m$ as reported previously in the literature (Rizzuto et al., 1992) and Ca^{2+} influx into keratinocyte mitochondria leads to mitochondrial depolarisation (Savignan et al., 2004). Interestingly, the depolarisation was more pronounced in the low Ca^{2+} cultured (proliferating) cells when compared to the high Ca^{2+} cultured (differentiating) cells

The role of mitochondria during the initiation and regulation of differentiation remains largely elusive. Savignan *et al* (2004) reported a causal relationship between mitochondrial membrane depolarisation and HaCaT keratinocyte differentiation (Savignan et al., 2004). Using JC-1, a ratiometric fluorescent probe, to measure mitochondrial membrane potential (DeltaPsi), they found that mitochondria of cells grown in low Ca^{2+} media (< 0.1 mM) were hyperpolarised in comparison to those of cells grown in high Ca^{2+} media (> 1.5 mM) (Savignan et al., 2004) which were slightly depolarised.

1.5.7 Mitochondria in cell death

Uptake of Ca^{2+} into the mitochondria stimulates the production of ATP, by activity of three key rate-limiting TCA cycle enzymes (McCormack et al., 1988, Denton et al., 1980). This increase in ATP availability allows the cells to deal with the increased demand due to the Ca^{2+} stimulus (Jouaville et al., 1999). However, excessive uptake into the mitochondria triggers the permeability transition pore to open, thus releasing Ca^{2+} into the cytoplasm. This high cytosolic Ca^{2+} can then stimulate and activate cell death mechanisms (Rasola and Bernardi, 2011).

Cell death occurs through two major pathways: apoptosis and necrosis. Apoptosis is characterised by membrane blebbing and cell shrinkage (Kerr et al., 1972) whereas

in necrosis, cell swelling is observed before the cell ruptures and subsequently releases its contents into the extracellular environment (Golstein and Kroemer, 2007). Defective mitochondrial Ca^{2+} homeostasis has been shown to lead to cell death, by either of these mechanisms (Krieger and Duchen, 2002).

1.5.8 Mitochondria and ROS

In addition to direct Ca^{2+} signalling, reactive oxygen species (ROS) have been identified as key mitochondrial regulators. ROS were originally classified as cell damaging agents early on, being identified to have a causal role in various diseases and pathologies. However, more recently, there is convincing evidence that ROS are a critical factor in the regulation of many cellular functions including proliferation, differentiation, and immunity (Schieber and Chandel, 2014). To test the role of ROS on epidermal differentiation *in vivo*, Hamanaka *et al* (2014) generated a mitochondrial transcription factor A (TFAM) knock-out, under the control of the keratin 14 promoter. TFAM is well documented to be necessary for the replication of the mitochondrial genome, playing a role in encoding for the electron transport chain, production of adenosine triphosphate (ATP), and also ROS (Hamanaka et al., 2013). The TFAMfl/fl/KRT14-Cre+ mice was characterised by an increased proliferation in the basal layer of murine epidermis. Similarly, *in vitro,* differentiation was reduced, along with a suppression of Notch signalling. All of which was restored using galactose and galactose oxidase to induce ROS, exogenous H_2O_2, or by the introduction of Notch intracellular domain (NICD). This work is consistent with later works that confirmed superoxide production (Bidaux et al., 2015) and more generally ROS production (Kennedy et al., 2013), play a key role in keratinocyte differentiation.

1.5.9 Mitochondria and cell senescence

Cellular senescence is a state of irreversible growth arrest (Hayflick and Moorhead, 1961) often seen in aging (Jeyapalan et al., 2007) and excessive cell culture (Campisi and d'Adda di Fagagna, 2007). Amongst a number of genotypic changes including decreased nuclear expression of lamins (Freund et al., 2012) and high presence of nuclear damage (Rodier et al., 2009), it is also associated with an increase in cell size (Hayflick and Moorhead, 1961).

Defective mitochondrial homeostasis has been heavily linked with cell senescence, both as a cause and a consequence. One line of studies that conflict over the cause or consequence surrounds ROS. Induction of ROS following mitochondrial damage is required for DNA damage to maintain the DNA damage response. However as this feedback loop continues, and the cell cycle arrest continues, senescence is achieved. A mathematical model by Lawless *et al* (2012), proposed that as senescent cells have more mitochondria (Passos et al., 2007), they will inevitably produce more ROS and therefore ROS production is a consequence of cell senescence and not a cause.

Studies often correlate cellular senescence with elongation of mitochondria, with some studies stating that mitochondrial elongation, due to decreased fission and increased fusion, was followed by a decrease in damaged mtDNA but also an increase in cellular ROS (Yoon et al., 2006). This elongation was followed by a down-regulation of the Fis1 gene and was rectified with subsequent overexpression (Yoon et al., 2006). In addition to the increased ROS, a decrease in mitochondrial respiration was observed in cells with elongated mitochondria. Other work has confirmed that elongation follows cellular stress on the way to senescence, yet describes this process as protective rather than detrimental as fusion allows recovery

of cristae and healthy mitochondria, increasing ATP production and therefore driving recovery (Gomes et al., 2011).

1.6 Protein translation and the UPR

In eukaryotic cells, most secreted and transmembrane proteins fold and mature in the lumen of the endoplasmic reticulum (ER) (Ron and Walter, 2007). The ER is able to modify the influx of these unfolded polypeptide chains in order to maintain high fidelity of the protein output. However, in such a case that the amount of unfolded protein entering the ER outweighs the capacity of the processing machinery, a complex process takes place to restore the balance, this process is termed the unfolded protein response (UPR). The UPR has been indicated to play a role in diseases including neurodegeneration, metabolic disorders, and inflammatory disorders (Wang and Kaufman, 2012). Generally, it is accepted that following the activation of the UPR, the amount of protein allowed to enter into the ER is reduced, superseded by an increase in the capacity of the ER to deal with the unfolded chains (Ron and Walter, 2007). The UPR has been largely elucidated with the identification of three major pathways leading to the upregulation of UPR genes. These pathways are IRE1α (endoribonuclease inositol-requiring enzyme 1-alpha) (Tirasophon et al., 1998), PERK (protein kinase RNA-like endoplasmic reticulum kinase) (Harding et al., 1999), and ATF6α (activating transcription factor 6) (Haze et al., 1999). In normal conditions b*inding immunoglobulin protein* (*BiP*), also known as glucose-regulated *protein 78* (GRP78), is an ER localised protein that is bound to the luminal domains of IRE1, PERK, and ATF6α. However, BiP is reported to bind the exposed hydrophobic domains of misfolded proteins with a higher affinity (Bertolotti et al., 2000), therefore dissociating from these proteins and allowing auto-

transphosporylation (IRE1 and PERK), oligomerization (IRE1 and PERK) and ER exporting (ATF6α) (Shen et al., 2002) of the proteins. These, now free, proteins lead to a signal cascade resulting in the upregulation of UPR genes. Downstream of PERK, genes that control protein folding, antioxidation, autophagy, amino acid metabolism, and apoptosis are all upregulated (Harding et al., 2003, Ye and Koumenis, 2009). ATf6α leads to upregulation of ER-associated degradation (ERAD) components (Yamamoto et al., 2007) and IRE1α to genes for protein folding, secretion, ERAD components, and lipid synthesis (Lee et al., 2003, Acosta-Alvear et al., 2007, Hetz et al., 2011). If the processes described is unsuccessful in restoring the normal working order of the ER and chronic stress persists, then apoptosis is set in motion (Tabas and Ron, 2011). If PERK signalling preservers, the transcription factor CHOP is generated, leading to the inhibition of BCL-2 expression, an anti-apoptotic protein (Marciniak et al., 2004, McCullough et al., 2001). In addition, it is reported that the UPR response can lead to the upregulation of four distinct BH3-only proteins (Shore et al., 2011). However, not all UPR occurrences are fatal to the cell, in fact the UPR varies depending on the level of stress encountered by the cell (Rutkowski et al., 2006). Pancreatic β cells and B lymphocytes are in a state of consistently low ER stress and function normally (Cornejo et al., 2013). Concurrently, previous studies have also observed that during differentiation, NHK undergo the UPR in order to facilitate secretory processes (Sugiura et al., 2009) such as LB exocytosis.

Protein folding is a highly regulated yet efficient process. Beginning with a strand of mRNA, a linear amino acid protein is translated which is then folded, quite rapidly, into its native confirmation. A process that is mainly driven by the proteins desire to reach its lowest state of entropy and therefore highest state of thermostability.

However, this process can be affected by external factors including pH, temperature, and mechanical stress. It can also be affected by mutations in the amino acid sequence and in turn problems forming bonds such as hydrogen (Cieplak and Niewieczerzał, 2009) and disulphide bonds (Kadokura et al., 2003). Due to their thermoinstability, misfolded or partly folded proteins tend to unfold and at low concentrations are stable enough to be degraded. However, at high concentrations the unfolded proteins aggregate as a nucleus of aggregated proteins becoming an almost irreversible reaction for the cell (Nelson et al., 2005).

Early work identified a level of correlation between codon usage and subsequent gene expression (Gouy and Gautier, 1982, Bennetzen and Hall, 1982). This coined the codon adaptation index (CAI), a measure of the codon usage bias, a method for predicting the expression of a gene due to its synonymous codon usage bias (CUB) (Sharp and Li, 1987). It was generally accepted that an increased CUB or CAI leads to faster and in turn more efficient translation (Powell and Moriyama, 1997).

1.7 Objectives of this thesis

The information in this chapter implies that the epidermis is a complex Ca^{2+} cycling system that involves extracellular, organelle and cytoplasmic Ca^{2+}. Work has identified a Ca^{2+} gradient in the epidermis, with the general view of lowest total $[Ca^{2+}]$ in the basal layer and peaking in the granular layer. Despite the plethora of studies discussed, there are still some questions that remain unanswered. This thesis aims to build on those studies and begin answering the following questions:

Extracellular Ca^{2+}, the missing link regulating epidermal differentiation *in vivo*?

The identification of genetically-encoded Ca^{2+} sensors has vastly improved and simplified the investigation into the role of Ca^{2+} as a second messenger. These sensors have been targeted to and effectively used in organelles such as mitochondria and the ER. However, as discussed, the accepted view is that an increase in $[Ca^{2+}]_o$ initiates differentiation of keratinocytes both *in vitro* and *in vivo*. Despite this, there is a lack of tools that allow the investigation into extracellular Ca^{2+} both in real time and *in vivo*. Therefore in this thesis, a genetically-encoded GFP-CaM-based Ca^{2+} sensor will be generated.

Does mitochondrial Ca^{2+} regulate keratinocyte differentiation?

Despite some work investigating the role of mitochondrial depolarisation and ROS production on epidermal differentiation, it seems mitochondrial Ca^{2+} handling is largely overlooked, particularly as an initiator and regulator of differentiation. The identification of MCU and its family of regulators, has allowed further investigation into the role of Ca^{2+} on mitochondrial function and in turn, mitochondria's role on

proliferation and differentiation. However, in addition to mitochondrial Ca^{2+} handling, the role of MCU is yet to be investigated in the epidermis.

In this thesis, the CRISPR/Cas9 system will be used in order to knockout MCU from the HaCaT keratinocyte cell line and investigate the effect this has on proliferation rate and morphology. In addition, mitochondrial Ca^{2+} handling and MCU family gene expression will be investigated in proliferating and differentiating wild type HaCaT keratinocytes

2 Methods

2.1 Cell culture

2.1.1 Media

2.1.1.1 Cell growth medium

Unless stated otherwise, cells were cultured in Dulbecco's Modified Eagle medium (ThermoFisher #31966-021) containing 10 % Foetal Bovine Serum (FBS) (ThermoFisher #10270-106) and 1 % penicillin/streptomycin (100 units/ mL and 100 µg/ mL respectively; ThermoFisher #15140-122).

2.1.1.2 Conditioned medium

For recovery post-puromycin treatment, cells were grown in condition medium. To make this, cell growth medium was aspirated off cultured cells, collected into a 50 mL tube and stored at + 4 °C. Once 50 mL had been collected, the medium was filtered using a 0.22 µm filter. The medium was then frozen in 10-15 mL aliquots for use at a 1:4 ratio with cell growth medium.

2.1.1.3 Cell freezing solution

Freezing medium contained 90 % FBS with 10 % sterile filtered dimethyl sulfoxide (DMSO)

2.1.2 Cell passaging

Culture medium was aspirated off the cells before washing with PBS (ThermoFisher #14200-075). HaCaT keratinocytes needed incubation in 0.05 mM EDTA/PBS for 10 minutes at 37°C, 5 % CO_2, all other adherent cells did not require this step.

Following this, cells were incubated at 37°c with 3-5 ml 0.025%/0.01% trypsin/EDTA in PBS (ThermoFisher #15400-054) for 3-5 minutes. Culture flasks were tapped gently to release cells into suspension. New medium was added to clean culture flasks before addition of appropriate amount of cell suspension, at dilutions between 1:2 and 1:8. HaCaT keratinocytes, HeLa cells and Swiss 3T3 fibroblasts were split commonly at a ratio of 1:5 where as HEK293 cells were passaged at 1:8 to 1:10 due to their faster growth rate.

2.1.3 Cell freezing

All adherent cells were frozen down using the same, standard protocol. Cell growth medium was aspirated and the cells were washed with PBS to remove remaining medium and debris. As with the passaging procedure above, the cells were trypsinised and added to equal amounts of supplemented growth media. The cell suspension was then pelleted using a table top centrifuge at 800 rpm. The cell pellet was resuspended in pre-warmed freezing medium (10 % DMSO/FBS) at ~ 5 million cells/ ml and 0.5 ml was transferred into a 2 ml cryovial. Cryovials were then allowed to freeze down overnight at – 80 °C in a 'Mr Frostie' freezing container (ThermoFisher #5100-0001). Following this, cryovials were transferred into liquid nitrogen for long-term storage.

2.1.4 Cell thawing

Cryovials were transferred directly from liquid nitrogen to a 37°C water bath, where the vial was agitated until fully thawed. The cell suspension was added directly to prewarmed, supplemented growth media in a 75 cm^2 flask (Corning #430725U). The cells were incubated (37°C, 5 % CO_2) and left to adhere overnight before medium was replaced.

2.1.5 Cell counting

Where necessary, cells were counted using a haemocytometer. Dead cells were detected using 0.4% trypan blue solution at a 1:1 ratio with the cell suspension. Trypan blue is excluded from intact cells, therefore any stained cells were disregarded from the count.

2.2 Transfection

Mammalian cell transfection is the process of delivering foreign nucleic acids into cells and in turn, generating genetically modified cells. Common transfection methods are classified into three subgroups, biological, physical and chemical. Biological transfection is often virus-mediated, integrating directly into the host genome. Physical methods include direct micro injection and electroporation. Often, physical transfection is very expensive and can cause lasting, physical damage to the cell. B far the most widely used transfection method is chemical. Often, reagents are used that form positively charged complexes with the negatively charged DNA and are attracted to the also negatively charged membrane. Following this, it is hypothesised that these complexes are endocytosed and translocated to the nucleus, where the DNA is transcribed. The plethora of reagents commercially available for chemical transfection identifies both the usefulness and importance of this technique.

Chemical transfection of cells with nucleic acid is termed a transient transfection, referring to the subsequent loss of the genetic materials by mitosis, degradation or other environmental factors. By introducing an antibiotic resistant marker gene, it is possible to select against that cells that have not incorporated the material into their genome. The major disadvantage with this method is that the integration into the genome is random and often rare.

2.2.1 Transient transfection of DNA

Cells were transfected between 60 – 80 % confluency using JetPrime^{TM} transfection reagent (PolyPlus, Illkirch-Graggenstaden, France) unless otherwise stated. Briefly, for one well of a 6 well plate, 1 µg plasmid DNA and 4 µl JetPrime reagent was diluted in 200 µl JetPrime buffer and incubated at room temperature for 20 minutes. The solution was then added to existing growth medium (fresh growth medium was not necessary for overnight transfections).

This protocol was optimised by myself previously during an MRes project whereby cells were transfected with Ca^{2+} phosphate, Gene Juice, JetPrime and HappyFect. Each reagent was tested with 0.5 and 1 µg per well for 4 hours, 8 hours and overnight.

2.2.2 Stable transfection of DNA

Cells were transfected as described above. Following 24-72 hours, 1 – 2 µg/ml Puromycin was added to fresh culture medium. Puromycin/medium was replaced every ~3 days and following passaging. It was maintained for at least 2 weeks before cells were placed in standard growth medium or conditioned medium and allowed to recover.

2.3 Molecular Biology

2.3.1 Transformation of competent E.coli

Escherichia coli (E.coli) strains used are listed in Table 2-1. For transformation, 50 ng of plasmid DNA was added to a vial of chemically competent E. coli (15 - 50 µL). The cell/ DNA suspension was incubated on ice for 30 minutes followed by a brief "heat-shock", in order to open holes within the cell membrane and allow subsequent entry of the plasmid DNA into the cells. "Heat-shock" requires 20-40 second incubation at exactly 42 °C before recovery on ice, for 2-10 mins. 200 µL of SOC media was then added and the bacteria incubated, with shaking for 45 mins - 1 h at 37 °C. This initial growth is required to allow the bacteria to begin expression of the plasmid's antibiotic resistance This mixture was then placed on a pre-warmed LB Agar plate containing the appropriate antibiotic (0.1 mg/ml Ampicillin or Kanamycin), and placed upside down overnight to form colonies.

Strain	Description
DH5α (ThermoFisher #18265017)	Chemically competent cells for routine cloning.
XL10-Gold (NEB # C2992I)	Chemically ultra-competent, cell line for large and/or complex plasmids.
One Shot™ TOP10™ (Invitrogen)	Chemically competent E. Coli for high-efficiency cloning with high-copy number plasmids.
One Shot™ Stbl3™ # C737303	Chemically competent E. Coli for cloning of direct repeats commonly found in lentiviral or transposon-based expression vectors

Table 2-1. Competent *E. Coli* used.

2.3.2 Plasmid extraction

For the preparation of small quantities of DNA, single bacterial colonies were selected using an autoclaved, sterile pipette tip and placed into ~ 5 ml LB broth containing appropriate antibiotic before incubation at 37 °C with shaking at 220 rpm overnight. The following day the bacterial suspension was aliquoted into a 2 mL Eppendorf tube and pelleted (5,000 rpm for 5 minutes), this process was repeated meaning 4 ml of suspension was pelleted and 1 mL remained. DNA was extracted from the pellet using the Qiagen Spin Miniprep kit (Qiagen, Crawley, UK). For larger quantities, following confirmation of DNA sequence, the remaining 1 ml of bacterial suspension was added to ~4 ml LB broth containing antibiotic and incubated 37 °C at 220 rpm for ~ 8 hr.1 ml of this culture was then used to inoculate

~ 200 ml LB broth containing antibiotic and incubated overnight at 37°C with shaking. DNA was extracted using the QiaFilter Maxiprep kit (Qiagen, Crawley, UK) following manufacturer's instructions. DNA was resuspended in nuclease-free water and stored at -20 °C. Plasmid concentration was measured using a NanoDrop 2000 spectrophotometer.

2.3.3 DNA purification

For constructs extracted from agarose gels or for ligations following digestion, DNA was purified using QiaQuick PCR purification column (Qiagen #28104) as per manufacturers' instructions. However, for constructs smaller than 100 basepairs, sodium acetate precipitation was used rather than a column. Briefly, precipitated DNA was resuspended in 100 µl deionised water and transferred to an eppendorf containing 1 ml 100% ethanol and 40 µl 3 M NaAc (pH 5.2). The eppendorf was kept at -80°C overnight to facilitate precipitation of DNA, then the DNA was pelleted by centrifugation at 16,000 g for 30 min in a cooled benchtop centrifuge. The supernatant was aspirated and the pellet allowed to air dry before resuspension in an appropriate volume of sterile deionised water.

2.3.4 Plasmid construction

In this thesis, CatchER and G-CEPIA1er constructs were retargeted to the plasma membrane using a combination of GeneART strings and PCR. Especially with G-CEPIA1er, the new constructs were transferred into a number of plasmid backbones. PCR was again used to add a linker into the CEPIA construct, in addition to generating a number of CRISPR guides found in the BROAD library (Addgene).

2.3.5 Golden Gate cloning

Engler and Marillonnet (Engler and Marillonnet, 2013) recently described a form of cloning termed Golden Gate cloning. This method uses the innate ability of type IIS enzymes to cleave DNA in a region downstream of its recognition site. Due to this, each overhang produced by the digestion is individual and specific only to the overhang designed into the insert using PCR. This ability to design individual restriction sites for an almost unlimited number of overhangs allows not only a high specificity of ligation but also a defined linear order, all within a single reaction. Additionally, this leads to the almost complete integration of insert into plasmid without reclosing of the plasmid. As each one is specific, the reaction can be cycled to ensure complete annealing of all products containing the IIS recognition site. Golden gate cloning requires a number of steps prior to the all-in-one reaction, the first is to design a set of independent fusion sites, flanked by IIS recognition sites of choice. Using PCR, add these sites to the gene of interest and finally set up a one-step restriction-ligation containing backbone of choice and genes of interest.

2.3.6 Ligation

DNA fragments and vector DNA with compatibly digested restriction sites were ligated in a 3:1 molar ratio insert:vector using T4 DNA ligase in a 10 µl reaction volume. Ligations were performed overnight at 16°C. As a negative control, an additional reaction was performed including the digested and dephosphorylated vector but not the DNA fragments to be inserted, in order to confirm that the vector was unable to re-ligate. Ligated DNA was transformed into chemically competent Top10 *E.coli* or Stbl3.

2.3.7 Polymerase chain reaction

Polymerase chain reaction (PCR) was performed with NEB Q5 High-Fidelity Master Mix or OneTaq as per manufacturer's instructions. Briefly, 25 ng template DNA and ~ 0.5 µM of each primer (forward and reverse) were added to a total volume of 12.5 µl, this was added to 12.5 µl of Q5 MasterMix. Reactions were carried out in a thermal cycler according to the conditions in Table 2-2 Primer sequences are listed in Table 2-3.

Step	Temp	Time	Cycles
Initialisation	95 °C	5 minutes	1
Denaturing	95 °C	15 seconds	
Annealing	50 - 72 °C*	30 seconds	25 - 35
	72 °C	20 – 30 seconds /kb	
Extension	72 °C	2 minutes	

Table 2-2. PCR thermal cycling conditions.

* Annealing temperature was usually 5°C lower than primer melting temperature

2.3.8 Agarose gel electrophoresis

Digested plasmids and PCR products were separated on a 1-2% (w/v) agarose gel made by dissolving 1 g agarose powder in 100 mL 1X TAE buffer and heated in a microwave. Ethidium bromide or GelRed was added at dilutions of 1:10,000 to allow visualisation of DNA under UV light. Once set, the gel was submerged in TAE buffer and DNA samples loaded. DNA was electrophoresed at 50 – 150 V for enough time to attain good separation of bands. If necessary, following visualisation under UV light, bands were excised and purified using QIAquick Gel Extraction kit (Qiagen) as per manufacturer's instructions.

2.3.9 DNA digestion

Purified PCR products and plasmid DNA were digested using restriction enzymes (NEB, Hitchin UK), commonly for 1-2 hours at 37°C. 1 µg DNA was digested with 10 U enzyme in a total reaction volume of 10 – 20 µl, using CutSmart buffer. Where restriction enzymes were compatible, double digests were performed. Digested DNA was separated on a 1% (w/v) agarose gel and appropriate bands excised and purified using a QIAquick Gel Extraction kit.

2.3.10 Sequencing

For each construct, a number of colonies were selected for PCR screening using insert and vector-specific primers. Positive clones were then picked for overnight culture then plasmid DNA purified by miniprep (Qiagen). All constructs were sequence verified prior to use (Source Bioscience, Rochdale UK). Sequencing primers were either supplied by Source Bioscience or custom designed and synthesised (IDT, Leuven Belgium). The programmes Ape Plasmid Editor and SnapGene were used to align chromatograms with expected sequences.

2.4 Quantitative PCR

2.4.1 RNA extraction

Cells were harvested for RNA extraction by scraping down in PBS (see section 2.4.1), transferred to an eppendorf and pelleted by centrifugation at 400 g for 5 min in a benchtop centrifuge. The supernatant was removed and the cell pellet either stored at -80°C, or immediately lysed for RNA extraction by resuspension in lysis buffer provided with the Qiagen RNeasy mini RNA extraction kit. Lysates were

homogenised using Qiagen QIAshredder columns, then RNA was extracted using the RNA extraction kit, according to the manufacturer's protocol.

2.4.2 Reverse transcription

For production of cDNA, 1 µg extracted RNA was reverse transcribed using Superscript III reverse transcriptase, according to the manufacturer's protocol. Briefly, RNA was combined with random hexamer primers (final concentration 2.5 µM) and dNTP mix (final concentration 0.5 mM) in an initial volume of 13 µl and incubated at 65°C for 5 min. The mixture was then incubated on ice for 1 min before addition of the provided First-Strand 5x buffer, 5 mM DTT and 200 U reverse transcriptase enzyme, bringing the total reaction volume to 20 µl. The reaction was incubated at 25°C for 5 min, then at 50°C for 50 min and finally the enzyme was inactivated at 70°C for 15 min.

2.4.3 Quantitative PCR

Quantitative polymerase chain reaction (qPCR) was used to assess the relative changes in gene expression of some MCU complex proteins in HaCaT keratinocytes following growth in basal or differentiating conditions.

Each reaction comprised of 7.5 µl of SYBR® Green Jumpstart™ Taq readymix™ (S4438, Sigma), 1.5 µl of the forward primer (250 nM final concentration), 1.5 µl of the reverse primer (250 nM final concentration) and the diluted cDNA (4.5 ng/ µl final concentration). Samples were vortexed and plated into hard shell white-coated 96 well plates (HSP-9645, BioRad). The qPCR was run on the CFX Connect Real-Time PCR (BioRad), using 2 step amplification settings. A melt curve was generated at the end of the amplification. All samples were run as triplicates for each gene per

reaction plate. Target experimental values were normalized to GAPDH housekeeping genes using the relative quantification method.

2.5 Primers

The primers used in this study were designed in-house either for cloning or detection of sequences in genomic DNA. The oligonucleotides were purchased from Sigma-Aldrich or Integrated DNA Technologies (IDT) as a lyophilized product and reconstituted in nuclease-free water to a stock concentration of 100 μM.

Primer Name	Sequence
Cloning	
CepiaEcoF	cacgtgatgacaaaccttgg
CepiaNotR	gatggctggcaactagaagg
CEPIA1pmFw	gaatcaagcttgccaccatgggtgacaatgacatcc
CEPIA1pmRev	cgagcttctagactaacgtg
CEPIA1erFw	gaatcaagcttgccaccatgggtgacaatgacatcc
CEPIA1erRev	gagcttctagactacagctcg
CepiamtFw	gaatcaagcttgccaccatgggcggtaggcg
CepiamtRev	gagcttctagactatgcgg
GFPFwEcoRV	aagcagatatcgatggagaagg
GFPRevSac	gccacattgcggccccattca
SacFwGFP	ggccgcaatgtggcacgagggac
SacRevPM	cccacagcattgctattcaggatggcccc

PMRevXbaI	gaattctagactaacgtggcttcttc
PMFwSac	ctgaatagcaatgctgtgggccagg
SacFwSac	tgaatagcatgtggcacgagggac
SacRevSac	tcgtgccacatgctattcaggatggcccc
EcoRIFw	gtaccgaattcacattgattattgagtagt
BamHIRev	attaatggatccatatatgtccagacctcaagcct
EcoRVFw	aagcttgcgatatcgatggagaaggtcagg
SacFwGFP	ccgcaatgtggcacgagggac
SacRevPM	cacagcattgctattcaggatggcccc
Xba1Rev	gaattctagactaacgtggcttcttcaagcttgc
SacRevSac	gccacatgctattcaggatggcccc
EcoRvFwGibson	aggttgatgaaatgatcagggaagcagatatcgatgga
Xba1RevGibson	gggtttaaacgggccctctagactaacgt
TGo-Fw1	gaatggatccgccaccatgattcacacc
TGo-Rev1	gtcgaccatctgggtgctgcttgaga
TGo-Fw2	agcacccagatggtcgactcttcacgtc
TGo-Rev2	gctatctagactatgcggccccattca
CGo-Fw1	gaatggatccgccaccatgctgagga
CGo-Rev1	agtcgaccattaaaacggagaaggtgattaggg
CGo-Fw2	tctccgttttaatggtcgactcttcacgtc
TGo-Rev2	gctatctagactatgcggccccattca
G-Cepia1 Sfil1 Fw	agctggcctctgaggccgccaccatgggtgacaatg

G-CEPIA1 Sfil1 Rev	aagcttggcctgacaggccctaacgtggcttcttctgcc
CEPIA Age1 Fw	accggtaccggtaccatgggtgacaatgacatccac
CEPIA EcoR1 Rev	ccggaattcctaacgtggcttcttctgccaaag
hPGK Prom Screen Rev	aagatccgggtgacgctgc
G-CEPIA1er screen For	tttgtacaaatgatgacagcgaagg
MCUG1Fw	caccgagagttgctatctattcacc
MCUG1Rev	cacttgactgtcgcaagtgcgcaaa
MCUG2	cacc gagagttgctatctattcacc
MCUG2	ctctcaacgatagataagtggcaaa
MCUG5	caccgaacagctcccaaattctgcc
MCUG5	cttgtcgagggtttaagacggcaaa
MCUG6	caccgatcgcttcctggcagaattt
MCUG6	ctagcgaaggaccgtcttaaa caaa
MCUGN1	caccgcaggagcgatctacctgcgg
MCUGN1	ctagcgaaggaccgtcttaacaaa
MCUGW1	caccgtggcggctgacgcccagccc
MCUGW1	caccgccgactgcgggtcgggcaaa
MCUGW2	cacc gatcgcttcctggcagaatt
MCUGW2	cgtcctcgctagatggacgcc caaa
MCU genomic identification	
MCU Exon 1 Fw	tcaagggctttagttggcccg
MCU Exon 1 Rev	gagaggttcaagtcccgtgc

MCU Exon 2 Fw	acttgaggcctggtagcacc
MCU Exon 2 Rev	ctctctctgacccctaagcc
MCU Exon 3 Fw	aatagacccccatgcaagaatgg
MCU Exon3 Rev	gtgcatacacatttgctaaaaccg

Table 2-3. List of primers used

.

2.6 Protein biochemistry

2.6.1 Cell lysis

Cells were washed multiple times with PBS and scraped into a 1.5 mL centrifuge tube before centrifugation at < 2000 rpm for 3 minutes. Supernatant was removed and the cell pellet was re-suspended in 100 – 200 µl lysis buffer (Section 2.8.1). The lysate was agitated at 4 °C for 30 minutes before centrifugation at max speed (~13,000 rpm) for 10 mins. Subsequently, the supernatant was removed and transferred to a new 1.5 ml Eppendorf tube for protein quantification.

2.6.2 Protein quantification

Protein concentration was measured using the Pierce™ BCA Protein Assay Kit (23225, ThermoFisher Scientific), following manufacturer's instructions. Briefly, a standard curve was generated by serially diluting a stock of 1 mg/ ml BSA solution with distilled water to concentrations between 0 and 1000 µg/ ml. A small amount of lysate was diluted in water and added, in duplicate to a 96 well plate. BCS solution was made by adding a 50:1 ratio of Reagent A (Bicinchoninic acid solution) and Reagent B (copper sulfate solution). The samples were incubated at 37 °C for 30 mins before absorbance (OD 562nm) was measured. Protein concentrations were calculated from a curve generated from the standards using Excel and used to normalise protein loading across the samples.

2.6.3 Western blotting

SDS-PAGE sample buffer was added to the lysates which were then denatured at 70 °C for 10 minutes before 20 µg of total protein was loaded on a 4-12% Bis-Tris gel (NP0335BOX, NuPAGE®, ThermoFisher Scientific). Gels were ran in MOPs

running buffer (section 2.16.2) at 150 V for 1.5 hours, at which point the blue running dye had reached the base of the gel. Following this, the gel was placed on a 0.45 µm nitrocellulose membrane (162-0112 BioRad) and both were sandwiched between Blotting Filter Paper (1703932, Bio Rad). Transfer of proteins was carried out using a semi-dry transfer apparatus (Trans-Blot® SD Semi-Dry Transfer Cell, Bio Rad) at 23 V for 1 hour. The membranes were blocked for 1 hour at RT Using Western Blocking solution (#1706404) before incubation with primary antibody solution overnight at 4 °C with agitation. The next day, membranes were washed with Tris-buffered saline containing 0.1% Tween-20 (TBST) for 30 minutes before addition of secondary antibody, for 1 hour at RT with agitation. Following further washing in TBST, proteins were imaged using Pierce ECL (32109, ThermoFisher Scientific).

2.6.4 Primary antibodies

Antibody	Type	Ab dilution	Supplier
Anti-HA Tag	Mouse monoclonal	1:1000	Abcam (ab18181)
Anti-GFP	Mouse	1:5000	Santa Cruz (sc-9996)
Anti-MCU	Rabbit	1:5000	Sigma (HPA016480)

Table 2-4. Primary antibodies used for Western blotting.

2.6.5 Secondary antibodies

Antibody	Type	2 Ab concentration	Supplier
HRP Conjugate	Goat anti-mouse IgG	1:10000	Bio Rad (1706516)
HRP Conjugate	Goat anti-rabbit IgG	1:10000	Bio Rad (1706515)

Table 2-5. Secondary antibodies used for Western blotting.

2.7 Materials

2.7.1 Constructs

Name of construct	Vector backbone/ promotor (if changed)	Obtained from
pcDNA3.1+	-	Alexei Tepikin (UoL)
G-CEPIA1er	pCMV	Rosario Rizzuto (UdP)
R-CEPIA1er	pCMV	Rosario Rizzuto (UdP)
G-CEPIA1pm	pcDNA3.1+	This thesis
R-CEPIA1pm	pcDNA3.1+	This thesis
G-CEPIA1pmSL	pcDNA3.1+	This thesis
G-CEPIA1pmSL2	pcDNA3.1+	This thesis
G-CEPIA1pm	pSBi/ SFFV	This thesis
G-CEPIA1pmSL	pSBi /SFFV	This thesis
G-CEPIA1pmSL2	pSBi /SFFV	This thesis
G-CEPIA1pm	pLJM1 /CMV	This thesis
G-CEPIA1pmSL	pLJM1 /CMV	This thesis
G-CEPIA1pmSL2	pLJM1 /CMV	This thesis
G-CEPIA1pm	pLJM1 /SFFV	This thesis
G-CEPIA1pmSL	pLJM1 /SFFV	This thesis
G-CEPIA1pmSL2	pLJM1 /SFFV	This thesis
Lenticrispr v2	-	Nicholas Harper (UoL)
MCU G#1	Lenticrispr /SFFV	This thesis
MCU G#2	Lenticrispr /SFFV	This thesis
MCU G#5	Lenticrispr /SFFV	This thesis
MCU G#6	Lenticrispr /SFFV	This thesis

MCU G#N1	Lenticrispr /SFFV	This thesis
MCU G#W1	Lenticrispr /SFFV	This thesis
MCU G#W2	Lenticrispr /SFFV	This thesis
MCU G#1+2	Lenticrispr /SFFV	This thesis
MCU G#$^{2+}$1	Lenticrispr /SFFV	This thesis

Table 2-6. List of constructs used.

2.8 Buffers, solutions, and dyes

2.8.1 Cell lysis buffer

(RIPA buffer + cOmplete™ + PhosSTOP™)

50 mM Tris-Cl pH 7.4 (2.5 mL 1M)

1 % Triton X-100 (0.5 mL Triton X-100)

0.1 % SDS 100 x (0.5 mL 10 %)

150 mM NaCl (7.5 mL 1M)

38.5 mL dH20 (total volume 50 mL)

5 tablets PhosSTOP (Sigma #4906845001)

1 tablet cOmplete Protease Inhibitor Cocktail (Sigma #4906845001)

2.8.2 MOPS buffer

95 % dH20 (950 mL)

5 % NuPAGE® MOPS SDS Running Buffer (20X) (ThermoFisher Scientific #NP0001; 50 mL)

2.8.3 Transfer buffer

5 % NuPAGE® MOPS SDS Running Buffer (20X) (ThermoFisher Scientific #NP0001; 50 mL)

0.1 % NuPAGE® antioxidant (ThermoFisher Scientific #NP0005; 1 mL)

10 % analytical grade methanol (100 mL)

In ddH2O

2.8.4 TBST

5% Pierce™ 20X TBS Tween™ 20 Buffer (ThermoFisher Scientific #28360; 50 mL)

0.1 % Tween-20 (1 mL)

In ddH2O

2.8.5 Blocking/Antibody buffer

5 % Blocking Grade buffer (10 g)

TBS-Tween (200 mL)

5 % Milk (10 mL)

2.8.6 Paraformaldehyde for fixation

4 % PFA (20 g)

PBS (500 mL)

0.05% NaOH (250 µL)

PFA powder was heated to 37 °C and regularly stirred until dissolved. The pH was adjusted to ~ 7.4 and aliquotted for use.

2.8.7 Tris-Borate-EDTA

45 mM Tris-Borate (54 g Tris Base and 27.5 g Boric acid)

1 mM EDTA (4.6875 g disodium EDTA)

Tris base, boric acid and EDTA were dissolved in 750 mL of deionised water. Once dissolved, solution was adjusted to pH 8.3 before addition of more deionised water to a total volume of 1 L. TBE was used at 1 X concentration.

2.8.8 Tail Lysis buffer/ SDS

50 mM Tris pH 7.6

2.5 mM EDTA

100 nM NaCl

0.2 % SDS

3 Design and generation of an extracellular calcium sensor, CatchPM

3.1 Introduction

As discussed in Chapter 1, there is a broad range of evidence to suggest the presence of a complex Ca^{2+} gradient in skin (Menon et al., 1985, Pillai et al., 1993, Mauro et al., 1998, Celli et al., 2010). The lowest [Ca^{2+}] was found in the basal layer, peaking in the late granular layer and falling sharply in the cornified layer. *In vitro*, topical addition of Ca^{2+} has been observed as a pivotal driver of keratinocyte differentiation (Hennings et al., 1980). However to date, the potential role of extracellular Ca^{2+} to regulate epidermal differentiation and homeostasis has not been elucidated *in vivo*. The main reason for this, is a lack of tools available to accurately, quantitatively and temporally, measure extracellular Ca^{2+} changes in the epidermis.

As described previously, current methods are limited in their ability to measure Ca^{2+} in real time in an epidermal model or *in vivo*. Although the generation of cell-permeant small molecule Ca^{2+} indicators made the measurements of Ca^{2+} signals more practical (Tsien, 1980), they were limited in their localisation and use in tissue models. The generation of genetically-encoded Ca^{2+} probes (Miyawaki et al., 1997, Rizzuto et al., 1992) allowed selective targeting of a range of probes with various properties, lending to a more accurate measurement of localised Ca^{2+}.

More recently, Tang *et al* (2011) generated a Ca^{2+} binding variant of enhanced GFP (EGFP). Making use of EGFPs inherent qualities of high fluorescence intensity, folding efficiency and thermostability (Wang et al., 2008), Tang *et al* (2011)

identified five residues, that when replaced with charged residues, would act, and appear like, a claw that would be in close enough proximity to the chromophore to affect proton interaction and therefore modulate fluorescence, this new variant was termed CatchER. Investigations into the metal binding properties of CatchER, the ER targeted Catch sensor, identified a 1:1 binding stoichiometry to Ca^{2+} with ions such as Na^{+}, K^{+}, Cu^{2+}, Zn^{2+}, Mg^{2+} not binding CatchER thus displaying Ca^{2+} specificity in a range of physiological conditions. The Kd value of CatchER was determined as 0.19 ± 0.02 mM with the minimal/maximal working fluorescence intensity observed to be between ~ 0.1 mM and ~ 6 mM Ca^{2+}. CatchER was effectively used for the first time to identify the aging related coupling of sarcolemmal excitation and sarcoplasmic reticulum (SR) Ca^{2+} release in mice thanks to its high sensitivity (Wang et al., 2012). Although extracellular cell surface Ca^{2+} is yet to be directly investigated, studies have reported a free extracellular/interstitial free Ca^{2+} as around 1 mM and total Ca^{2+} around 2 mM (Raine et al., 1993, Fogh-Andersen et al., 1995), well within the working range of CatchER.

As discussed in Section 1.4, extracellular Ca^{2+} plays a pivotal role in the proliferation/differentiation state of keratinocytes *in vitro*. Despite this, a genetically encoded GFP based Ca^{2+} sensor has not been targeted to the extracellular space to date. The properties described above make CatchER a prime candidate for an extracellular Ca^{2+} indicator. Therefore, this chapter aims to modify the targeting regions of CatchER and in turn, generate a GECI implanted into the extracellular plasmalemmal surface.

Two commonly used targeting strategies for proteins to the cell surface are Glycosylphosphatidylinositol (GPI) anchors or transmembrane regions of proteins

such as the platelet derived growth factor receptor (PDGFR). Previous investigations in my laboratory using a membrane bound luciferase targeted with a GPI anchor (Pellegatti et al., 2005), lacked sensitivity and the protein as not evenly localised across the membrane, rather appearing in clumps. Therefore here, the 50 amino acid, transmembrane region of PDGFR, used successfully in a membrane bound horseradish peroxidase sensor and also found in the pDISPLAY commercial vector (Life Technologies) will be used. The entire Catch EGFP sequence and PDGFR-TM targeting sequence will be ordered as DNA strings and using Gibson isothermal assembly, ligated together directly into a vector generating CatchPM.

3.2 Methods

3.2.1 Immunofluorescence staining of cultured cells

To investigate protein localisation in cell lines such as HaCaT keratinocytes, cells were seeded onto 13 mm coverslips at ~ 1 x 10^5 cells/ well in 12 well plates (Sigma # CLS3513) and cultured to ~ 80 % confluence. For transfections, cells were seeded at the same number and analysed 48 hours post transfection. Following this, cell growth medium was aspirated from the wells and replaced with non-sterile PBS. This wash was repeated a further two times before fixation using 4 % paraformaldehyde (PFA) for 10 minutes. The cells were again washed with PBS before addition of 50 mM ammonium chloride (NH_4CL) for 20 minutes to quench the fixation. Further washing preceded permeabilisation with 0.1 % Triton X-100 in PBS for 10 minutes. Post-washing, cells were blocked with 10 % chick serum for 30-60 minutes at room temperature. Cells were incubated with primary antibody diluted in 1 % chick serum at 4 °C overnight in a humidified chamber. The next day, cells were washed three times in PBS and incubated with secondary antibody diluted in 1 % chick serum for one hour at room temperature in a humidified, dark container. Further PBS washes were followed by immersion in deionised H20 before mounting onto SuperFrost slides using Prolong Gold AntiFade reagent. Coverslips were imaged using a Leica TCS SP2 AOBS (Leica Microsystems, Heidelberg, Germany) scanning laser confocal microscope using the 63x oil objective with 1.43 numerical aperture for high resolution imaging. Fluorochromes were excited using an argon-krypton laser source at 488 nm and a helium-neon laser at 594 nm. Images were scaled using Leica Confocal Software and exported as TIFF files.

3.2.1.1 Primary antibodies used

Antibody	Species	Product Code	Recommended Dilution
Anti-HA	Mouse	Ab18181	1:100

Table 3-1. Primary antibodies used for immunocytochemistry.

3.2.1.2 Secondary antibodies used

Antibody	Species	Product Code	Recommended Dilution
Alexafluor mouse anti-488	Goat		1:250

Table 3-2. Secondary antibodies used for immunocytochemistry.

3.2.2 CatchPM assembly

Gibson isothermal assembly was used to ligate the CatchPM Gblocks directly into pcDNA3.1+ as per the protocol described in. Briefly, reaction mix was made as per table (3:1 each insert: vector) and incubated at 50 °c for 15 minutes initially, and changed to 60 minutes. Reactions were placed on ice before transformation into XL10-GOLD unltracompetent E.Coli. Colonies were selected and screened by digestion using HindIII restriction enzyme as detailed in

	2–3 Fragment Assembly
Vector	100 ng
GBlock1	38ng
GBlock2	26ng
Gibson Assembly Master Mix (2X)	10 µl
Deionized H_2O	10-X (total of 3 fragments) µl
Total Volume	20 µl***

Table 3-3. Gibson isothermal assembly conditions for CatchPM.

3.2.3 Live cell imaging

HaCaT keratinocytes were plated onto 18 mm coverslips in 6 well plates at 200,000 cells/well. 24 hours later HaCaTs were transfected using JetPrime transfection reagent as described in Chapter 2. Coverslips were washed in supplemented 10 mM HEPES buffered saline (10mM Glucose + 1 mM Ca^{2+}) and transferred into a purpose built chamber in fresh HEPES buffered saline. For thapsigargin experiments, equal volume of HBS was added that contained 20 μM Thapsigargin. Coverslips were imaged using a Leica SP2 AOBS confocal microscope with 63x 1.43 numerical aperture oil magnification.

3.3 Results

3.3.1 Confirmation of CatchER localisation and calcium modulation

CatchER was initially transfected into HaCaT keratinocytes and very high transfection efficiency was observed (Figure 3.1A). Fluorescence was very bright and localised to a branch-like network within the cell excluding the nucleus (Figure 3.1B). To test Ca^{2+} modulation of fluorescence, transfected cells were treated with the SERCA-pump inhibitor, thapsigargin (10 μM) to inhibit uptake into the ER. Thapsigargin induced a ~ 50 % decrease in fluorescence (Figure 3.1C).

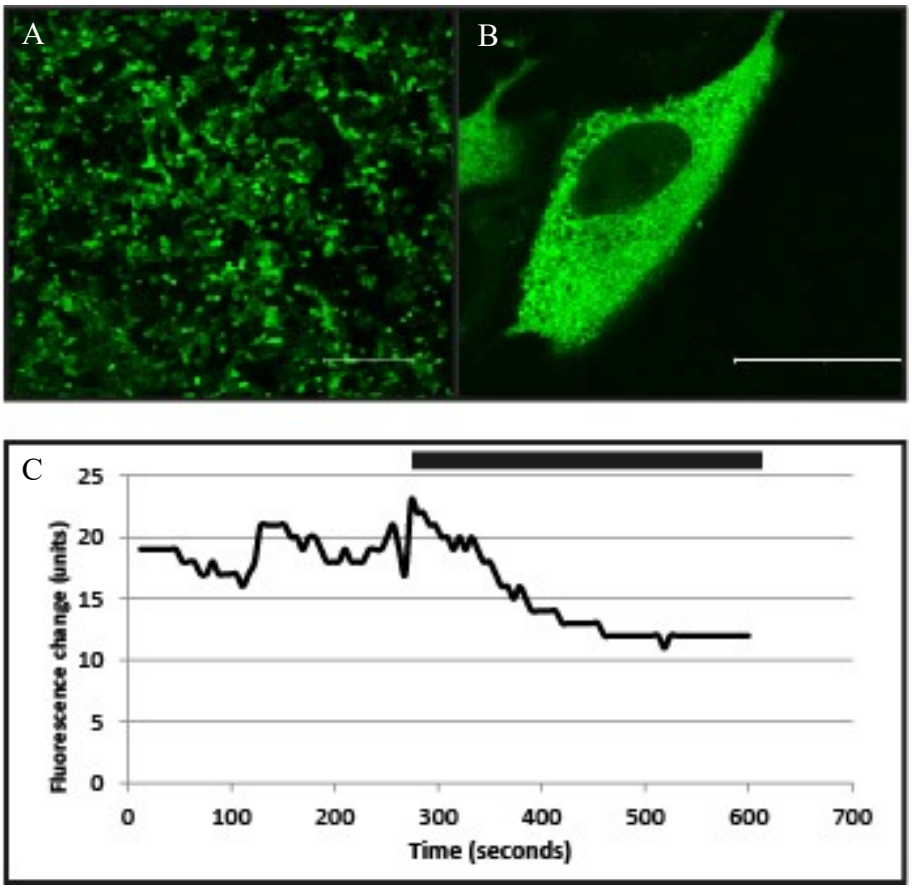

Figure 3.1. Confirmation of CatchER localisation and Ca^{2+} modulation.

A&B) CatchER was transiently transfected into HaCaT keratinocytes using JetPrime Transfection reagent (PolyPlus, Illkirch-Graggenstaden, France). 1 µg DNA was incubated at room temperature with 200 µl JetPrime buffer and 2 µl JetPrime reagent and added to growth medium. 24 hours post-transfection cells were imaged using a Leica SP2 AOBS confocal microscope using a 10x dry and 63x 1.43 numerical aperture oil magnification respectively. Scale bar is 300 µm and 20 µm respectively. C) Transfected cells were washed and placed in 10 mM HBS (+ 10 mM D-Glucose and 1 mM Ca^{2+}) before addition of 10 µM thapsigargin to inhibit Ca^{2+} uptake to the ER at around 260 seconds (bar). Live cells were visualised using a Leica SP2 AOBS confocal microscope with 63x 1.43 numerical aperture oil magnification. Representative trace shown.

3.3.2 *In silico* design of CatchPM

Using sequences of CatchER and pCAG HRP-TM, a gene of interest (GOI) was designed with N-terminal IgK leader sequence, HA-Tag, Ca^{2+} binding EGFP of CatchER and C-terminal PDGFR-TM (Figure 3.2A). Two gBlock Gene Fragments (Integrative DNA Technologies, California) were designed (Figure 3.2B), together generating the complete GOI with areas of overlap for annealing together and to pcDNA3.1+ vector. Using a codon optimisation tool (JAVA Codon Adaption Tool) to improve the codon adaption index (CAI) and GC content a new sequence was generated. This new sequence modified the original ~ 0.15 CAI value (Figure 3.3A) to ~ 0.95 (Figure 3.3B), closer to the optimum value of 1.

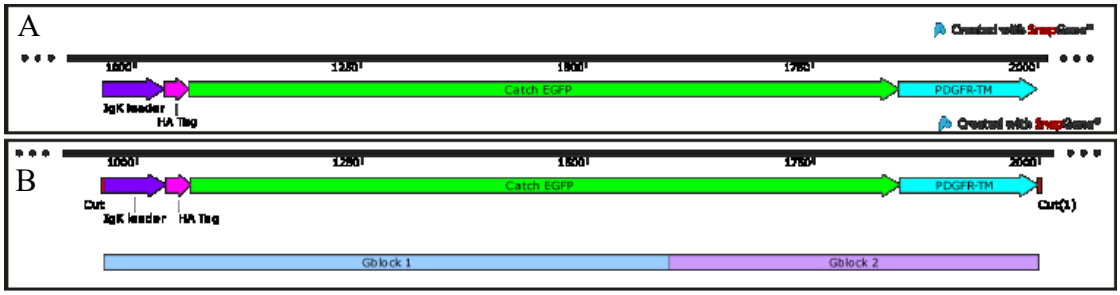

A) Using known sequences of CatchER and pCAG-HRP-TM, sequences were aligned using SnapGene. An IgK leader sequence was placed at the N-terminus followed by a HA-TAG. The CatchER EGFP sequence was inputted and an N-terminal PDGFR-TM sequence followed. B) The construct was divided into two gBlock Gene Fragments due to their size. Overlapping regions ~ 15 bps were added at each end of the fragments overlapping the pcDNA3.1+ backbone and the other gBlock (not shown here). 'Cut' represents EcoRV restriction site in pcDNA3.1+ that construct is inserted into.

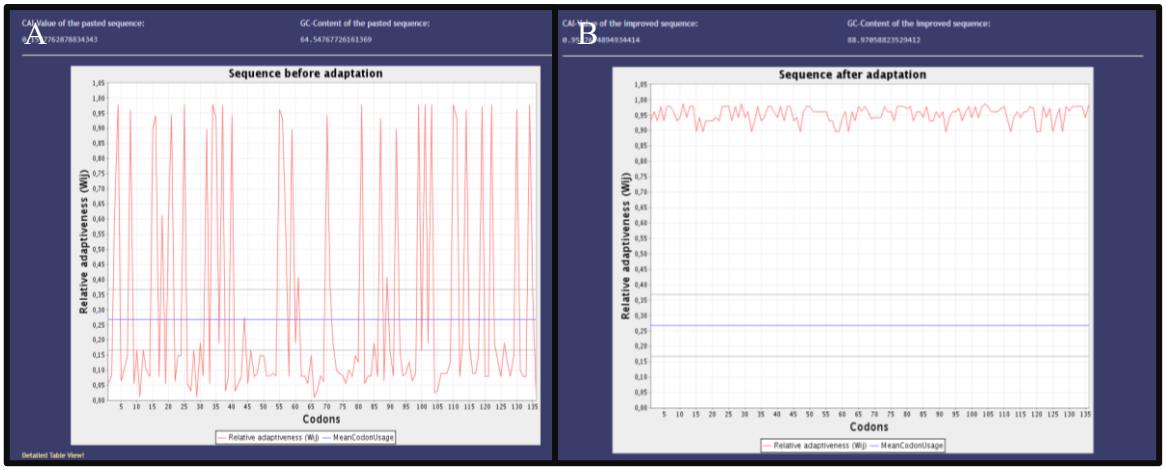

Figure 3.3. CatchPM codon optimisation

Using the online Java Codon Adaptation Tool (JCAT), CatchPM nucleotide sequence CAI value was increased in order to improve expression in human cells and cell lines. A) CAI value of original CatchPM sequence. B) CAI value post-optimisation. Images represent screenshots from online tool.

3.3.3 Cloning of CatchPM

Linearised pcDNA3.1+ vector, two DNA strings and CatchPM were ran on an agarose gel simulator using SnapGene (Figure 3.4A). Complete linearisation of the pcDNA3.1+ vector could be observed at ~ 5.5 kb in lane 1 of Figure 3.4B. Using Gibson Isothermal Assembly, GeneArt Strings were annealed together and into the EcoRV cloning site of pcDNA3.1+. The initial reaction was incubated for 15 minutes, and generated very few colonies following transformation. Ligation mix was digested using HindIII and agarose gel electrophoresis of this initial ligation identified incomplete ligation of the fragments (Figure 3.4B). With a band at ~ 6.5 kb observed, this band is likely CatchPM. However, there are also bands at ~ 5.5 kb, ~ 650 bp and ~ 450 bp, the empty vector, fragment 1 and fragment 2 respectively (Figure 3.4B). The reaction was repeated and allowed to ligate for 1 hour at 55 °c. Following this, complete ligation of the CatchPM plasmid could be observed (Figure 3.4D) as predicted by the simulator (Figure 3.4C).

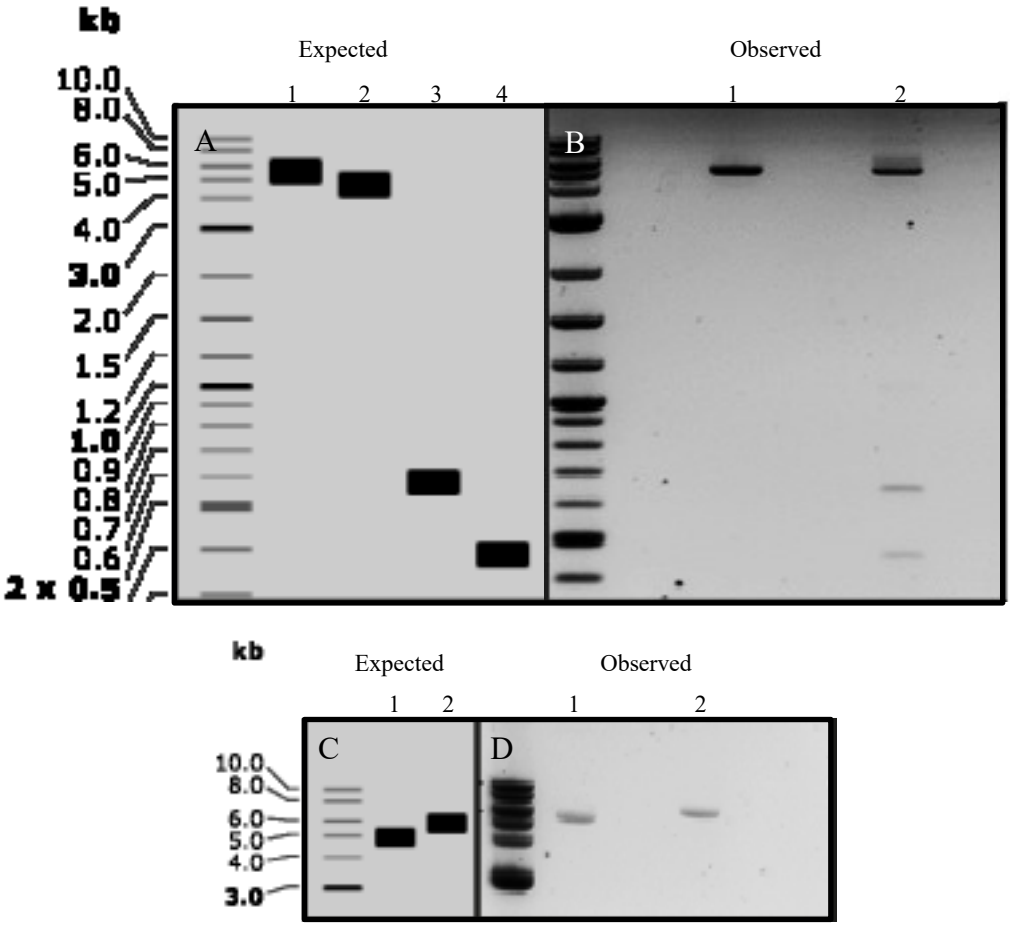

Figure 3.4. Diagnostic digests of CatchPM cloning.

Plasmids were digested using HindIII restriction enzyme to linearis. A) Lane 1 indicates complete CatchPM. Lane 2, 3, and 4 are empty vector, gBlock1 and gBlock2 respectively. Shown on separate lanes for clarity. B) Lane 1 is digested vector and lane 2 is initial ligation. 4 bands can be observed, the strongest appearing as the empty vector, a larger one (CatchPM) and 2 bands relating to each gBlock. C & D) Lane 1 and 2 show empty vector and CatchPM expected and confirmed sizes respectively. Ladder used was 2-log DNA ladder (Invitrogen). Experimental lanes were loaded with approximately 50 ng DNA in a 1 % Agarose Gel stained with Ethidium bromide. Gels were run at 120 mV for 1.5 hours before viewing on a BioDoc-It Imagining system (UVP, Upland, California).

3.3.4 Transfecting CatchPM

Initial transfections into HaCaT keratinocytes did not yield a transfection efficiency similar to that seen in CatchER (Figure 3.5A). However, 24 hours following transfection, transfected cells were observed to be brighter than the control and showing some peri-nuclear fluorescence (Figure 3.5B). After a further 24 hours, some plasmalemmal-derived fluorescence could be observed however, a large amount of fluorescence appeared clumped in the centre of a very misshapen cell, characteristic of possible cell death (Figure 3.5C).

Following 72 hours post-transfection, although some fluorescence appeared in a membrane-like shape, fluorescent cell contents appeared to have been released into the surrounding space (Figure 3.5D). *In silico* modelling of the tertiary structure showed folding of the end of the GFP and early PDGFR-TM region was disrupted (Figure 3.6).

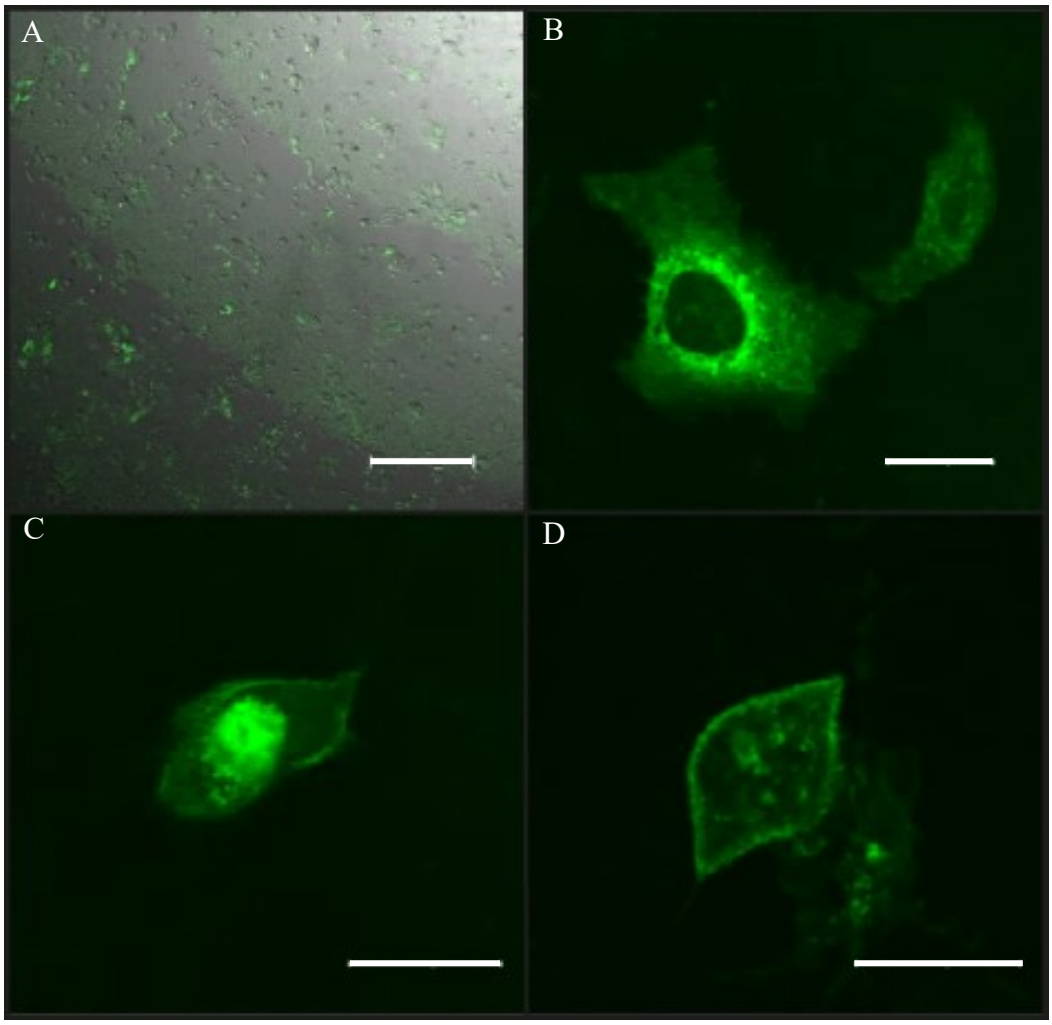

Figure 3.5. Transient transfection of CatchPM.

HaCaT keratinocytes were transfected with CatchPM using JetPrime transfection reagent as previously described. A) 24 hours post transfection, overlay with brightfield image. B, C, and D) 24, 48, and 72 hours post transfection respectively. Live cells were visualised using a Leica SP2 AOBS confocal microscope with 63x 1.43 numerical aperture oil magnification. Scale bar = 10 μm.

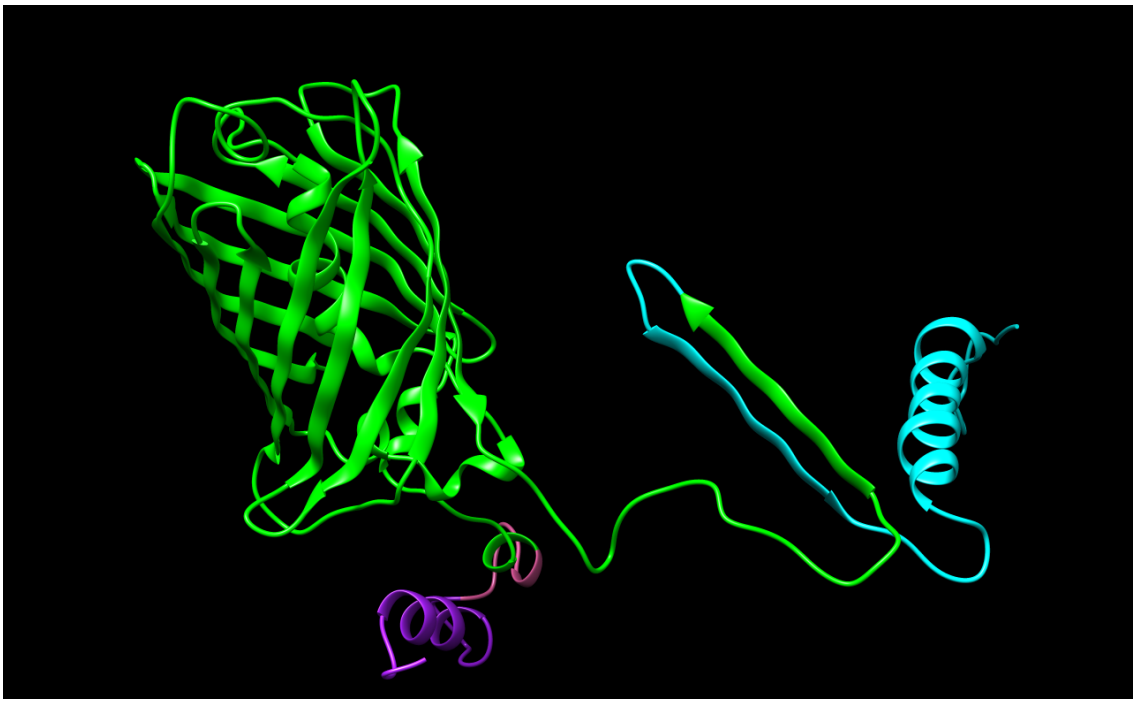

Figure 3.6. Predicted tertiary structure of CatchPM.

Using in silico tertiary modelling (Källberg et al., 2012), the predicted folding of CatchPM is modelled. Purple indicates IgK leader sequence, pink – HA Tag, green – EGFP, and blue – PDGFR-TM.

3.3.5 Redesign of CatchPM

The experiments above alluded that the protein was fluorescent and being transported to the membrane ~ 48 hours post-transfection. This information combined with tertiary structure modelling (Figure 3.6) led to the revisit of the C-terminal sequence. Like that found in CatchER, a short, flexible linker (AAGRRTKTHLRRGS) was placed in between the EGFP and PDGFR-TM targeting sequence (Figure 3.7A). Following cloning into pcDNA3.1+, the entire GOI was sequenced to ensure it was correct and in frame, the region with the flexible linker added is shown (Figure 3.7B). *In silico* tertiary structure modelling of CatchPM with the new linker added, showed correct folding of both EGFP and the PDGFR-TM region (Figure 3.8). Although the targeting region is folded up next to the EGFP, this region is flexible so would allow extension.

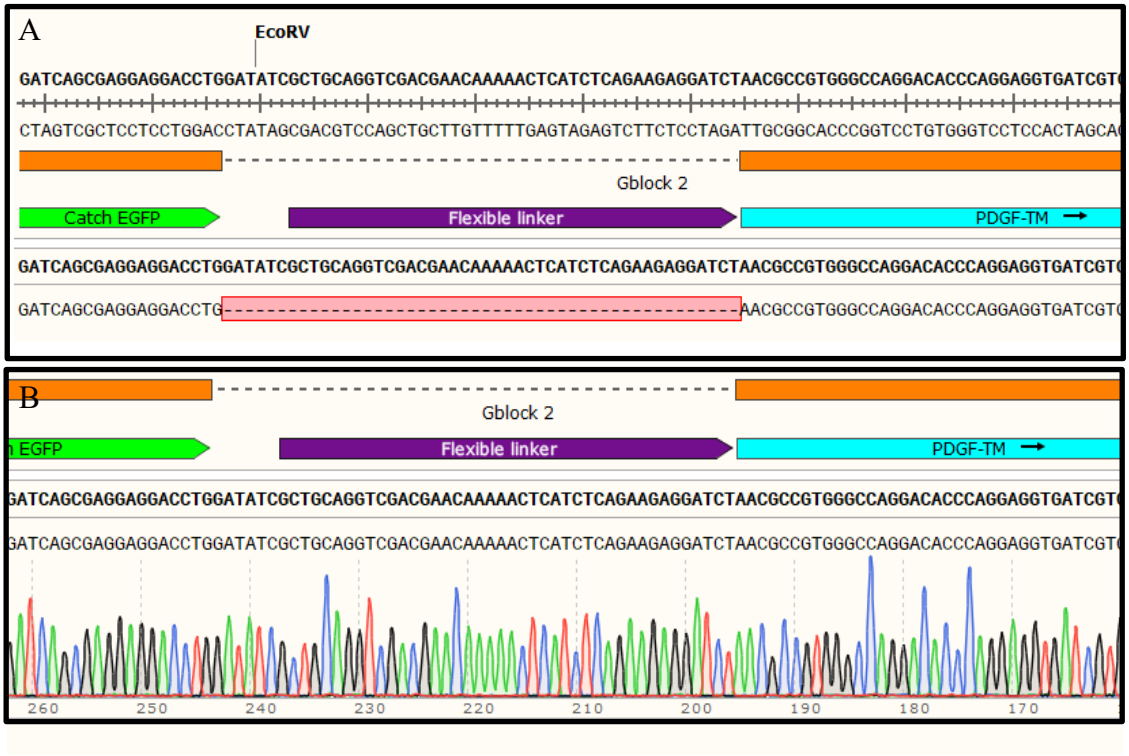

Figure 3.7. Sequencing of CatchPM with additional flexible linker.

A new gBlock2 was designed encompassing a flexible linker separating the EGFP and PDGFR-TM constructs. Following isothermal assembly, sequencing was carried out as described and chromatogram was aligned with original CatchPM sequence. A) Flexible linker and new EcoRV cloning site separate original CatchPM sequence as expected. B) Chromatogram shows correct sequence of new CatchPM, across entire sequence although no shown. Sequences and chromatograms aligned using SnapGene.

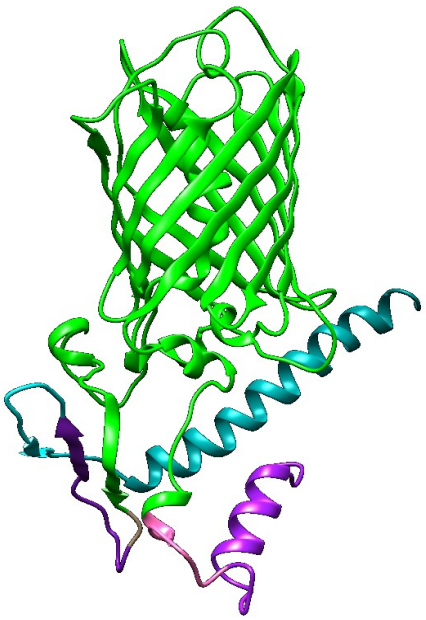

Figure 3.8. Preidcted tertiary structure of new CatchPM.

Using in silico tertiary modelling (RaptorX) , the predicted folding of CatchPM is modelled. Purple indicates IgK leader sequence, pink – HA Tag, green – EGFP, and blue – PDGFR-TM.

3.3.6 CatchPM identification

Following transfection into HaCaT keratinocytes, no green fluorescence was observed (not shown). CatchPM was transfected into HEK293 cells but again no fluorescence was observed (not shown). Using immunocytochemistry, a branched network of fluorescence was observed with some membrane-derived fluorescence (Figure 3.9A). However, to confirm translation of the complete protein, Western blotting identified a ~ 42 kDa protein with a smaller ~ 40 kDa band underneath (Figure 3.9B). This upper band is the expected size of the functional protein, with the smaller possible post-IgK cleavage.

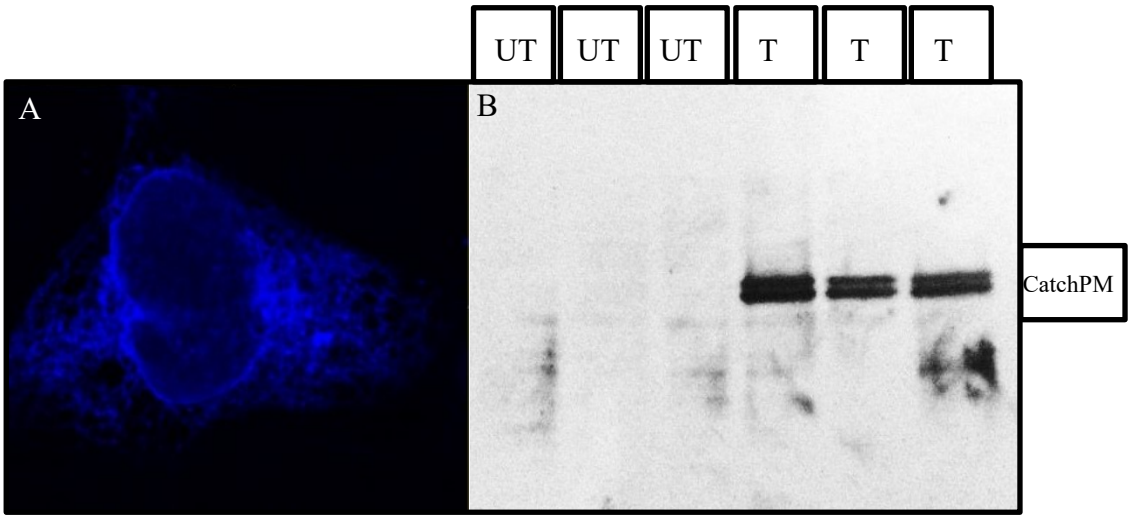

Figure 3.9. Detection of CatchPM protein.

HaCat keratinocytes were transfected with CatchPM as described. 24 hours post-transfection, anti-HA antibody was used in order to localise (A) and detect (B) CatchPM. Two bands were observed in panel B with the upper band at ~ 43 kDa, the predicted size for CatchPM. Immunocytochemistry was imaged using Leica SP5 AOBS confocal microscope with 100x 1.43 numerical aperture oil magnification. UT – Untransfected, T – Transfected

3.4 Summary

This chapter aimed to design and generate an extracellular GFP-based Ca^{2+} sensor. The initial construct, CatchER was transfected with high efficiency and appeared to localise to a branch-like network expected of the endoplasmic reticulum. Thapsigargin, a SERCA pump inhibitor has been shown to reduce uptake into the ER and therefore reduce ER stored Ca^{2+}. Here, thapsigargin treatment reduced fluorescence intensity, which is consistent with an ER based probe. Using the membrane targeting region of the platelet-derived growth factor receptor (PDGFR) and the IgK leader sequence found in pCAG HRP-TM, sequences were aligned in silico to generate a CatchPM sequence. Following codon optimisation, two GeneArt strings were designed and following ligation into a pcDNA3.1+ vector, CatchPM was formed. Initial transfections were much less efficient than was observed with the original CatchER plasmid. Following 48 hours, some plasmalemmal-derived fluorescence was discovered, however at this stage cells appeared to be undergoing cell death. The subsequent addition of a short, flexible linker separating the EGFP and TM targeting sequence, reduced cell death however no EGFP fluorescence was observed. Using immunocytochemistry to the HA tag, the probe appeared to be localised to the endoplasmic reticulum. Western blotting also confirmed the presence of a ~ 43 kDa protein, as expected from CatchPM.

3.5 Discussion

The initial construct, CatchER, was designed with a short spacer region between the C-terminal of the GFP and the KDEL ER retention sequence. When the CatchPM sequence was designed herein, this sequence was removed due to its apparent lack of need, rather a 'cloning artifact'. However, once this sequence was removed and the PDGFR-TM was added, aggregation of the protein was observed. The EGFP used to generate CatchER/CatchPM was the M153T/V163A mutation. This variant was chosen because of its high fluorescence intensity, folding efficiency, and thermostability (Nakai et al., 2001). Additionally, GFP aggregation has been widely studied, addition of a ubiquitin-driven degradation protein at either the N-terminal (Dantuma et al., 2000) or C-terminal (Bence et al., 2001) of GFP, allowed the monitoring of the GFP protein during degradation. As observed here, throughout the degradation process GFP remained fluorescent. Due to this and also as seen with protein modelling, the possible reason for the aggregation and downstream apoptosis of the cell was due to misfolding of the PDGFR-TM region.

Large quantities of unfolded or misfolded proteins are known to initiate the UPR. As mentioned, keratinocytes are in a state of constant UPR that assists in the secretory process. Although the stress intensity mechanism of the UPR is largely not described (Hetz et al., 2015) one could assume these cells are more likely to enter apoptosis following an increase in unfolded/misfolded proteins. Therefore, as the protein was shown to be misfolding, this could induce aggregation and therefore apoptosis. It has previously been shown that apoptosis is characterised by disassembly of the golgi apparatus prior to cytoskeleton rearrangement (Mukherjee et al., 2007) and cell shrinkage (Danial and Korsmeyer, 2004). As the golgi is required for protein

processing following folding, fragmentation would lead to a further clustering of fluorescence. In addition, maintenance of the cytoskeleton would ensure the structure of the membrane into late apoptosis, possibly explaining the membrane-like fluorescence after 72 hours.

With these data in mind, a short flexible linker sequence was added (AAGRRTKTHLRRGS) equal to that found in CatchER. Following assembly and transfection, no fluorescence was observed despite detection of the protein using immunocytochemistry and western blotting. As CatchPM was to be used in human epidermal models, the entire sequence was optimised using a CAI optimising tool (JCAT) in order to improve mammalian expression. Studies have identified the necessity of a translation 'speed-ramp' (Tuller et al., 2010), This ramp enables the control of tRNA speed, in conditions of low amino acids, the first ~ 50 codons contained a 'queue' of ribosomes (Ingolia et al., 2009). This model of a tight control of translational speed was confirmed by Qian *et al* (2012) where they identified that low efficiency codons are not translated at the same speed as high efficiency or cognate codons, in fact the relative tRNA concentrations and therefore codon-tRNA balance drives translation speed (Qian et al., 2012). With this in mind, over optimising the CAI could affect the subsequent cognate/non-cognate spacing and also the codon-tRNA ratio (Thanaraj and Argos, 1996). Although only a very small number of mistranslations would lead to a prevention of fluorescence, this may have occurred here.

3.6 Conclusion

This work attempted to generate a single-EGFP based Ca^{2+} sensor, targeted to the plasma membrane. The first construct was predicted to be misfolded, possibly due to the close proximity of the EGFP structure and the PDGFR targeting sequence. The addition of a small, flexible linker led to a correct, predicted tertiary structure along with a protein of the correct size located in an ER and some plasmalemmal-like pattern in repeated (> 3) transfections. Unfortunately, despite these confirmations no fluorescence was observed. The protein may therefore being mistranslated due to an over correction of the CAI producing a protein with a number of point mutations sufficient to disrupt the fluorophore.

4 Design and generation of an extracellular calcium sensor, CEPIA1pm

4.1 Introduction

As discussed previously in Sections 1.3 and 3.1, techniques available to measure changes in extracellular Ca^{2+} at close proximity to the cell membrane are limited in their real-time application and spatial accuracy. Therefore, the role of $[Ca^{2+}]_e$ *in vivo*, particularly in epidermal homeostasis, is largely understood.

The generation of genetically-encoded Ca^{2+} indicators greatly improved the ability to measure Ca^{2+} in real time. Structural data and various mutational studies have meant there is a continual improvement of GECIs. In 2014, a new range of GECIs were described (Suzuki et al., 2014). Using cfGCamp2, a calmodulin bound-GFP probe, Suzuki *et al* (2014) began to systematically mutate residues in the CaM in order to modify its binding efficiency (Kd). Initially using previously described mutations to modify the Kd, they began to make mutations of their own. In doing so, they generated a range of cfGCamp2s with Kd values from 0.9 μM to 13,400 μM. However, modifications of this kind appeared to drastically reduce the dynamic range. Cloning of the mutated calmodulins into other Ca^{2+} reporters such as G-GECO1.1 and R-GECO produced Ca^{2+} reporters with high Kd and dynamic ranges suitable for use in a variety of organelles. These probes were termed CEPIA, Ca^{2+}-measuring organelle-Entrapped Protein IndicAtor 1.

G-CEPIA1er exhibits a Kd of 672 ± 23 μM, with a dynamic range of 4.7 this probe has a minimum and maximum working range of 0.1 – 3 mM. No fluorescence

modulation was observed following Mg^{2+} titration and although a greater range in alkaline conditions, the Hill coefficient, between Ca^{2+} bound and Ca^{2+} free, is ~2 in physiological conditions (pH 7.4). This probes sensitivity to small Ca^{2+} changes allowed the identification of inverse Ca^{2+} waves with peripheral to nuclear directionality for the first time.

Despite the issues faced with folding and fluorescence of CatchPM in Chapter 3. The strategy of targeting the protein to the extracellular surface remained successful. Therefore, using a modified strategy, this chapter aims to retarget the G-CEPIA1er and R-CEPIA1er probes to the extracellular surface and subsequently make stable clones in both HEK-293 cells and HaCaT keratinocytes for characterising and use in a functional system.

The retargeting of CatchER was carried out using GBlock gene fragments containing the entire CatchPM sequence. In this chapter, the CEPIA GFP will be amplified using PCR and ligated, along with the vector, to a GeneArt string containing only the PDGFR-TM targeting sequence. Thus, maintaining the PDGFR-TM strategy but limiting modification of the original CEPIA nucleotide sequence.

4.2 Methods

4.2.1 CEPIA1pm construction

The original CEPIA1er sequence was comprised of an IgK leader sequence, CEPIA EGFP-CaM and a KDEL ER retention sequence. The IgK leader sequence is a suitable leader for secretion onto the plasma membrane and therefore this sequence was left untouched. In order to generate the PDGFR-TM sequence, without having a plasmid available, a GeneArt String (Life Technologies) was designed as seen in Figure 4.1. The NotI restriction site was the closest available site to the KDEL sequence and therefore the GeneArt string was designed with a region, spanning from the NotI site, completing the Myc tag sequence and, with a small spacer, the PDGFR-TM sequence followed by a stop codon and an XbaI cloning site. Initially, digestion of CEPIA1er with NotI and Xba1 was unsuccessful as Not1 was unable to digest the plasmid. Therefore, primers were designed to amplify a region of DNA from the next closest restriction site, EcoRV to NotI. The backbone was then digested with EcoRV and XbaI, the PCR product with EcoRV and NotI, and the GeneArt String with NotI and XbaI. The digested backbone and GeneArt String were purified using a column and as the PCR product was under 100 basepairs, this was purified using sodium acetate precipitation as described. All products were then ligated using T4 ligase as described in Section 2.3.6.

4.2.2 Addition of a flexible linker

In order to insert a linker between the EGFP-CaM and targeting sequence, primers were designed that amplified the IgK leader sequence and EGFP-CaM sequence. The forward primer here had a HindIII restriction site and the reverse a small region of

overlap with the linker. The same principle was employed for the primers amplifying the linker and targeting sequence, with small regions that overlapped the next region. Initial PCR using CEPIA1pm amplified two products, EGFP-CaM and the targeting sequence. A separate PCR using the linker added the overlapping sequences to the product. All products were purified using a column and the outside primers were used to amplify the entire gene of interest, with overlapping sequences annealing in the initial cycles. The product was digested with HINDIII and XbaI and ligated into pcDNA3.1+.

To transfer the gene of interest into pSBi and pLJM1, primers were designed that had flanking restriction sites, SfiI and Age1/EcoRI respectively. CEPIA1pm was amplified and ligated as described into the respective plasmid. Plasmid maps are represented in Figure 4.3.

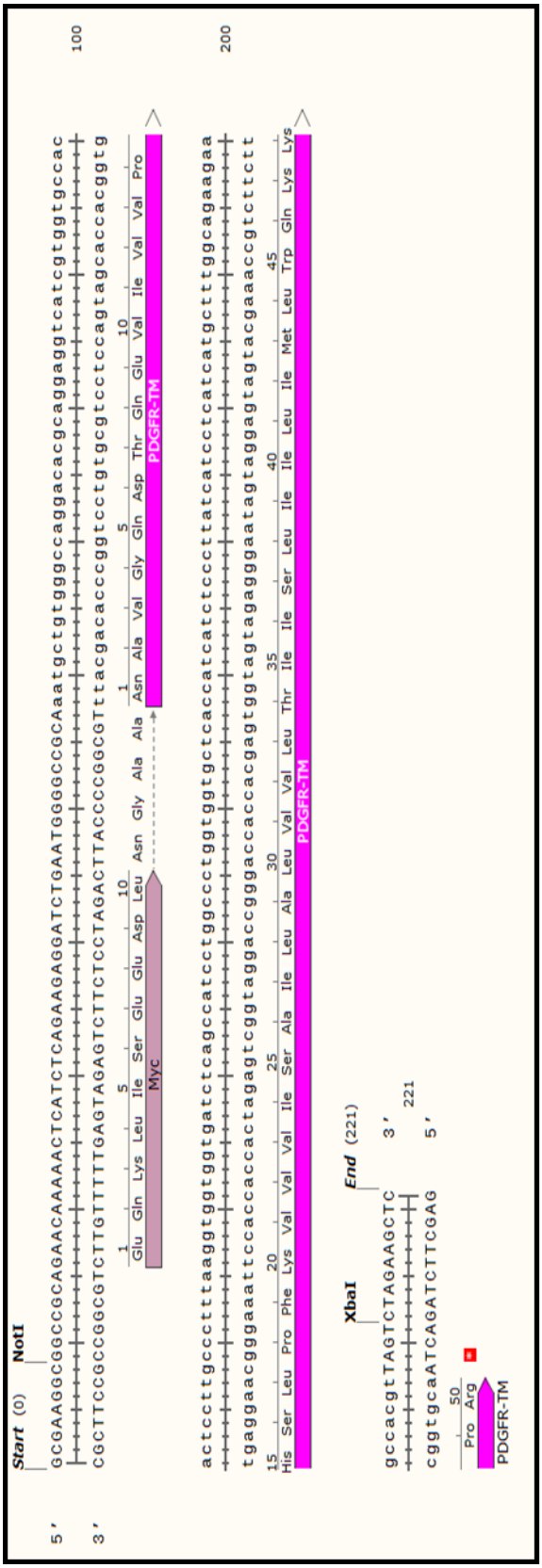

Figure 4.1. GeneArt String designed to introduce transmembrane targeting into CEPIA1er.

The NotI restriction site, the closest available site to the end of the CEPIA1er construct was at the 5' end of the GeneArt String followed by the already present Myc tag and then the PDGFR-TM sequence taken from pCAG-HRP-TM. The XbaI site was remained for ligation into pcDNA3.1+. Image taken using SnapGene.

4.2.3 Sleeping Beauty Transposon

Transposable elements (TE) or mobile genetic elements are often used as a non-viral gene-delivery system both *in vivo* and *in vitro*. Synthetic transposable elements are originally derived from the Tc1/mariner family of transposable elements originating in the fish genome (Ivics et al., 1997). Sleeping beauty, once the most widely used transposon system (Wilson et al., 2007) was derived from the salmonid subfamily (Ivics et al., 1997) and has been effectively used as a TE in animals such as zebrafish, mice, and rats (Mátés et al., 2007). As depicted in Figure 4.2, inverted terminal repeats are used to flank genes of interest, a genetically encoded transposase is then able to 'transpose' the gene of interest directly into the genome at TA dinucleotide sites (Ivics et al., 1997). The Sleeping Beauty transposon has been heavily modified in order to increase its activity, in excess of 16 modifications have been made (Mátés et al., 2009). Mates *et al* (2009), generated a novel hyperactive version of the Sleeping Beauty Transposon using high throughput screening. This new SB (SB100X) was able to support up to 50 % stable gene transfer in human cells that sustained expression for in excess of one year (Mátés et al., 2009). A study on in excess of 1000 SB insertions identified that although the insertion loci varied between cell type and culture condition, the SB transposon targeted TATA-rich regions of DNA as expected (Yant et al., 2005). SB targeted genes had no significant difference in transcriptional activity, when compared to the entire population, showing that this method is both efficient, and non-harmful to the original function of the cell (Yant et al., 2005).

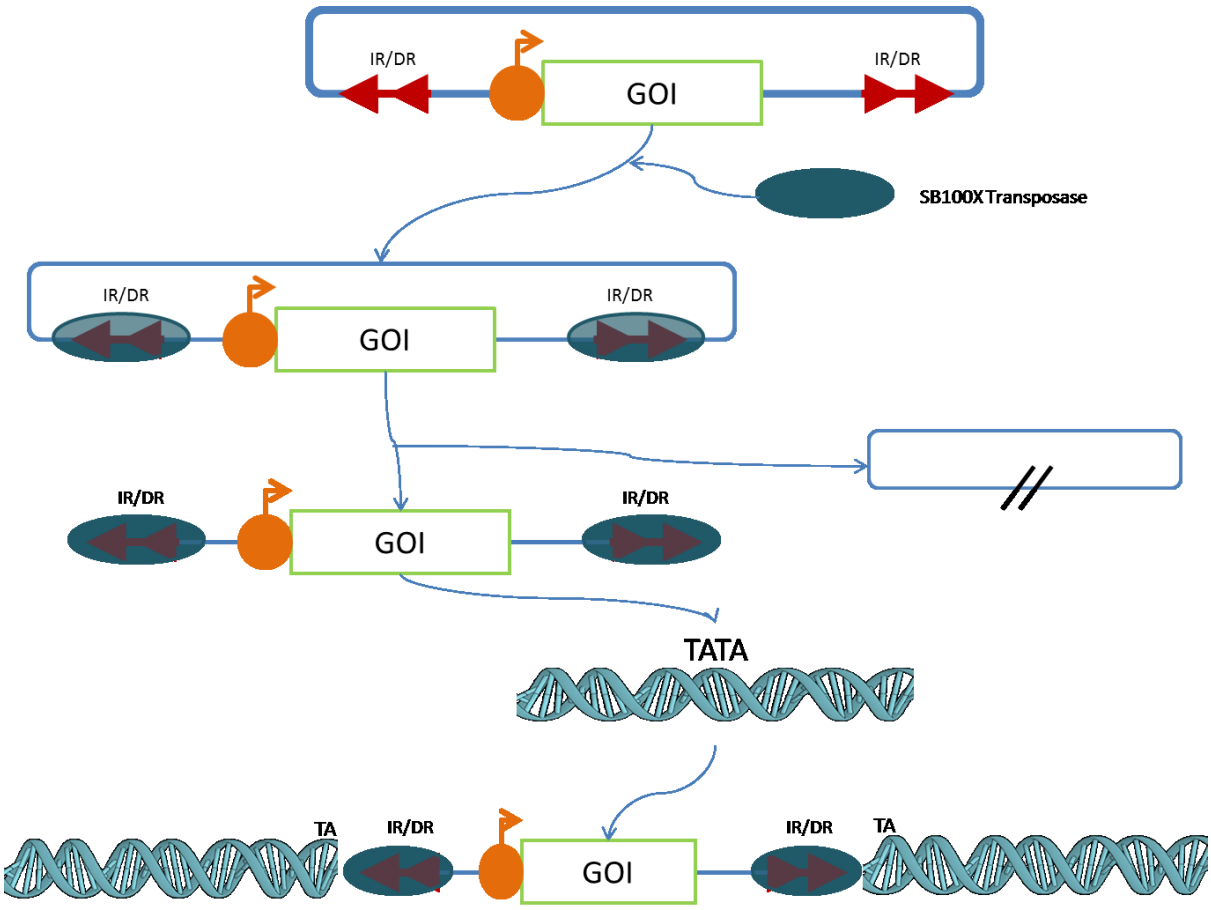

Figure 4.2. Sleeping beauty transposon mechanism of action.

The promoter and gene of interest (GOI) cassette is flanked by inverted terminal repeats (IR/DR). A genetically encoded transposase cleaves these repeats and 'transposes' them along with the GOI cassette directly into the genome at TATA sites generating stable clones without the needed for antibiotic selection.

A

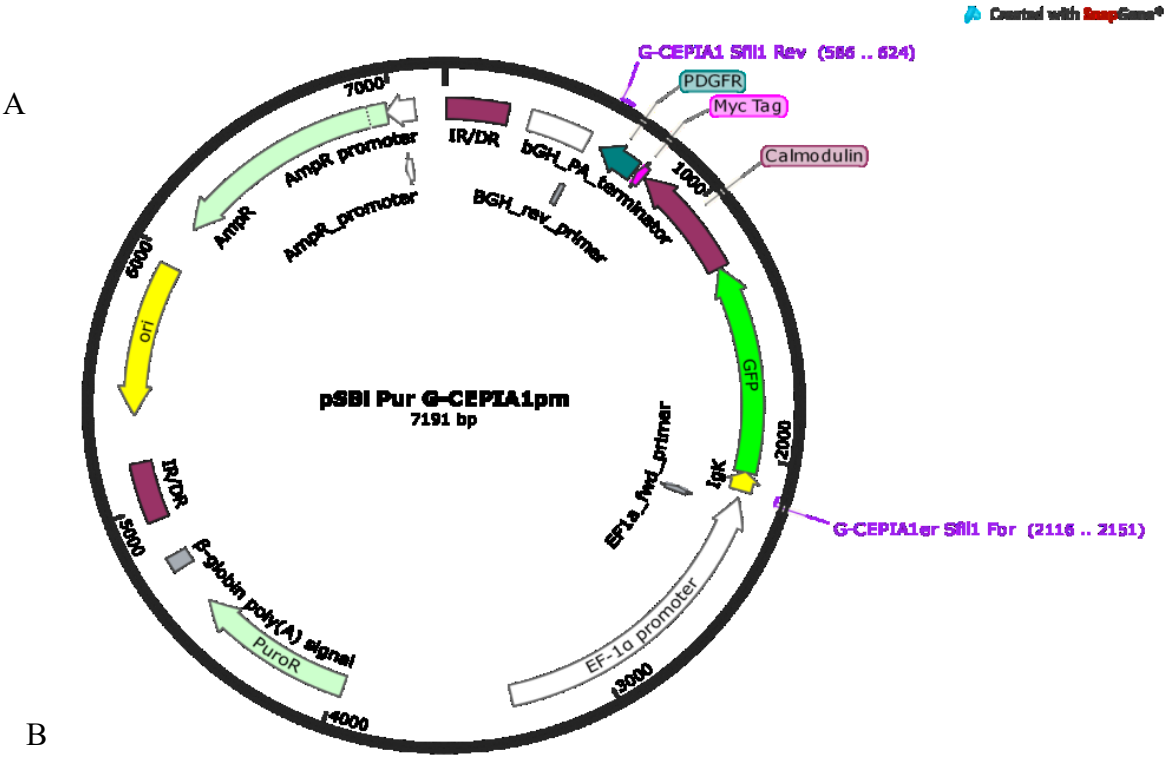

B

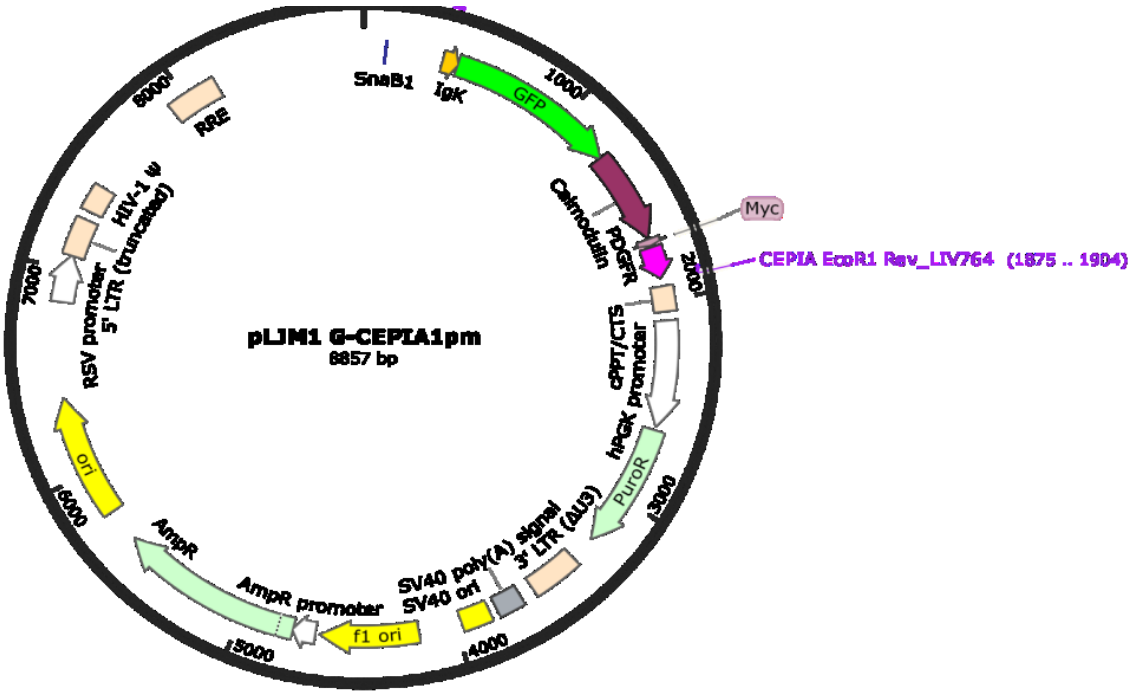

Figure 4.3. CEPIA1pm plasmid maps

CEPIA1pm constructs including IgK leader sequence, GFP or RFP (GFP shown), CaM, Myc tag, and PDGFR-TM targeting sequence were ligated into sleeping beauty vector (A) or lentiviral vector (B) for use both in transient and stable transfections. Plasmid maps were generated using SnapGene.

4.2.4 Live cell imaging

HEK293 cells or HaCaT keratinocytes were plated into 8-well chamber slide/ cover glass (Sarstedt #94.6190.802) at 125,000 cells /well. Cells were transfected as described (Chapter 2.2.1) 24 hours after plating and incubated for 72 hours. Wells were washed in HBS (+ 10mM Glucose) with 100 μM EGTA and maintained in fresh HBS (+ 10mM Glucose) with 100 μM EGTA. Wells were imaged using a Zeiss Airyscan 880 confocal microscope with 63x 1.43 numerical aperture oil magnification.

4.3 Results

4.3.1 Confirmation of targeting and Ca^{2+} modulation of fluorescence with G-CEPIA1er

G-CEPIA1er has previously been observed to exhibit endoplasmic reticulum-like fluorescence and also be modulated by changes in Ca^{2+} concentration (Suzuki et al., 2014). In order to confirm this, HEK293 cells were transfected with G-CEPIA1er. A very high transfection efficiency was observed as seen in Figure 4.4A with an endoplasmic reticulum-like fluorescence pattern as expected (Figure 4.4B). Additionally, in live cell experiments, addition of 1 mM Ca^{2+}, 10 µM ATP (+ 1 mM Ca^{2+}) and 1 µM ionomycin (+ 1 mM Ca^{2+}) to increase, decrease and again increase $[Ca^{2+}]_{er}$, modulation of fluorescence was observed (Figure 4.4C)

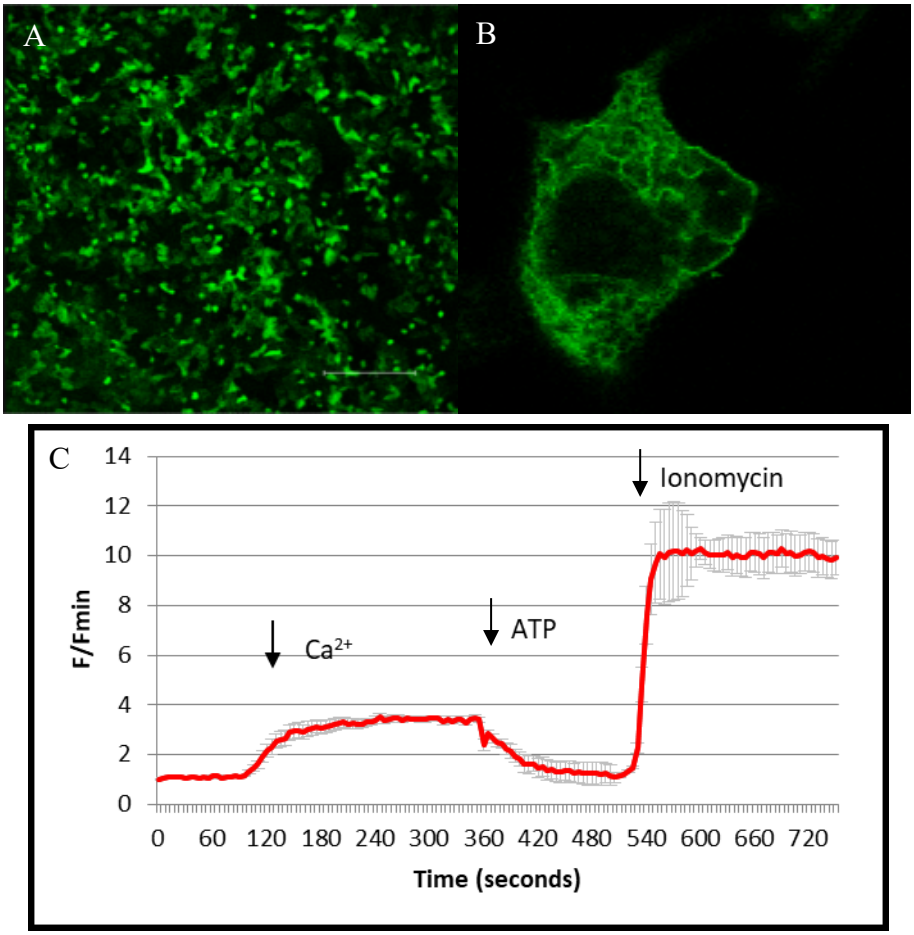

Figure 4.4. G-CEPIA1er subcellular localisation and Ca^{2+} modulation.

A&B) HEK293 cells were transfected with 1 µg G-CEPIA1er, fixed using 4% paraformaldehyde/PBS after 24 hours and imaged using a Leica SP5 confocal microscope with 10 x dry or 100 x oil objective respectively. B) Transfected HEK293 cells on coverslips were incubated in HBS with no supplemented Ca^{2+}, fluorescence modulation was observed following superfusion with 1 mM Ca^{2+}, 10 µM ATP (+ 1 mM Ca^{2+}) and 1 µM ionomycin (+ 1 mM Ca^{2+}). Imaging was carried out on a Leica SP5 confocal microscope with 10 x dry objective. Arrows indicate addition. Error bars are SEM of one field of view, n = 36 cells.

4.3.2 Cloning of CEPIA1pm

Once the activity of G-CEPIA1er had been confirmed, the KDEL ER retention sequence needed to be removed and replaced with the membrane targeting, PDGFR-TM sequence. As described in Section 4.2.1, a GeneArt String (LifeTechnologies) was designed that included a 5' NotI restriction site for ligation into the G-CEPIA1er backbone, the already present Myc tag and the PDGFR-TM sequence followed by an Xba1 site for cloning into pcDNA3.1+. The GeneArt String and the CEPIA1er plasmid were digested using NotI and XbaI, before ligation and transformation into TOP10 E.coli. Unfortunately, no colonies were formed. Using a range of diagnostic digests using control and experimental plasmids, further investigation identified that NotI was unable to digest the CEPIA1er backbone (data not shown). Therefore, using PCR, a small 60 bp region upstream of the NotI site was designed and generated (Figure 4.5A). This allowed digestion of the backbone with EcoRV and XbaI, PCR product with EcoRV and NotI, and the GeneArt String with NotI and XbaI (Figure 4.5B). Following purification, the three constructs were ligated together generating CEPIA1pm (Figure 4.5C). Both the G-CEPIA1pm and R-CEPIA1pm constructs were placed into pcDNA3.1+ for storage. G-CEPIA1pm was used from here on as the primary construct.

A layer of glycoproteins on the cell surface, termed the glycocalyx has been reported as a pH nano-environment (Krähling et al., 2009). This glycocalyx is necessary for cell adhesion and migration but importantly here, carries a large negative charge and stabilises the pH (Krähling et al., 2009). As this may have an effect on Ca^{2+} sensitivity of the G-CEPIA1pm probe, a linker was inserted between the EGFP-CaM and PDGFR-TM sequences. Using fusion PCR, primers were designed that amplified

the IgK to EGFP-CaM sequence, Sac linker and PDGFR separately (Figure 4.6A). These primers contained a region of overlap with the sequence desired to attach (Figure 4.6B). The first run of PCR amplified three products, once these had been purified, a second PCR allowed amplification of a single product using only two primers as overlapping sequences had already been generated (Figure 4.6C) This PCR product was then digested using HindIII & XbaI, SfiI, and AgeI and EcoR1 for ligation into pcDNA3.1+, pSBi puro and pLJM1 respectively.

Once cloned, colonies were selected and using PCR, were screened for correct insertion of the G-CEPIA1pm, G-CEPIA1pmSL and G-CEPIA1pmSL2 constructs. The predicted and observed sizes of the CEPIA1pm inserts are shown in panels A and B of Figure 4.7 respectively.

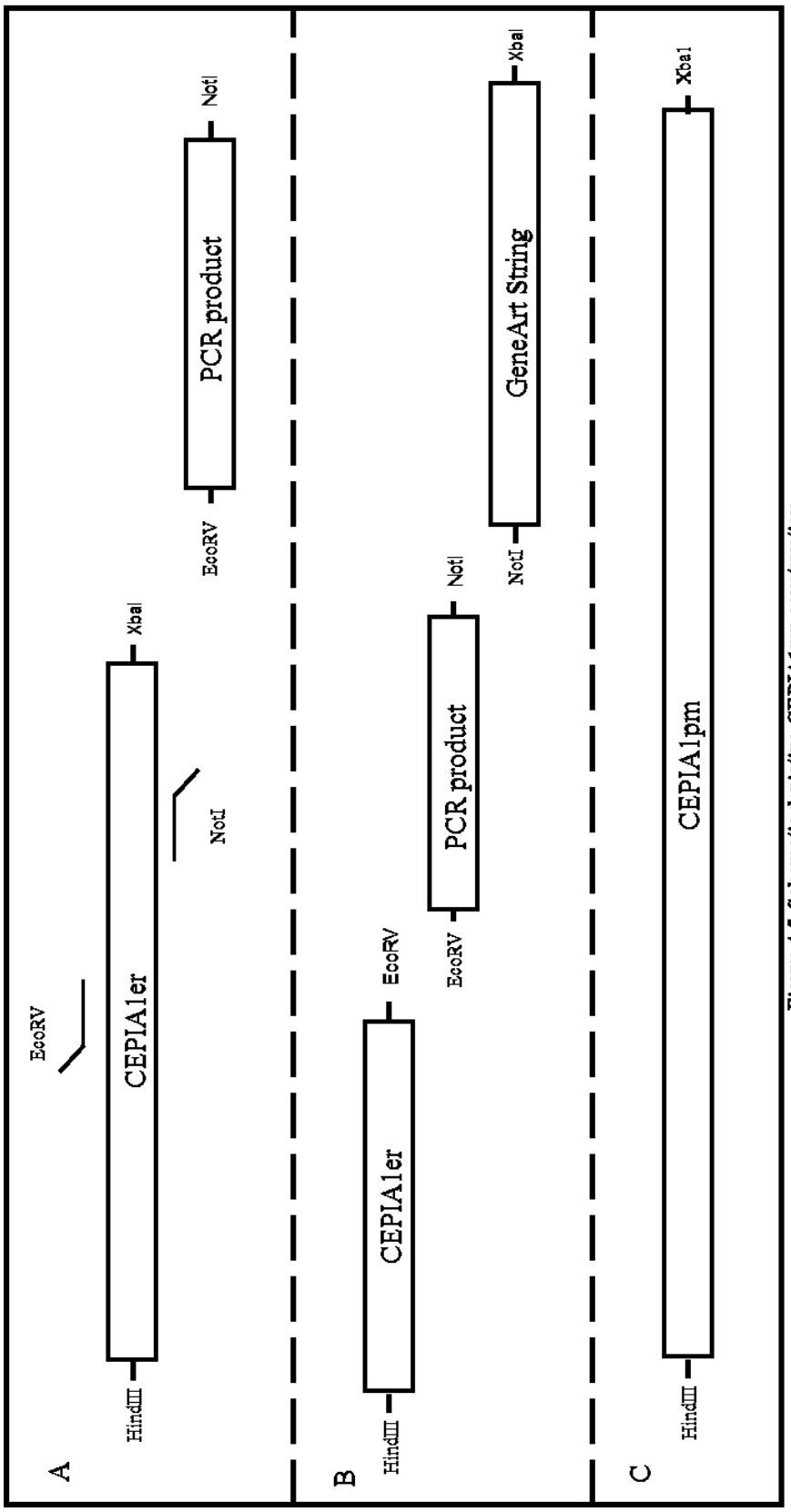

Figure 4.5. Schematic depicting CEPIA1pm construction.

A) A small, 60 basepair region was amplified using PCR, spanning from the EcoRV restriction site down to the NotI restriction site. As th NotI restriction site was non-functiona in the CEPIA1er backbone, this would allow digestion of the PCR product with NotI instead for ligation to the GeneArt String. B) Digestion of the CEPIA1er backbone with EcoRV and XbaI, the PCR product with EcoRV and NotI and the GeneArt String with NotI and XbaI allows ligation of all 3products to generate CEPIA1pm (C).

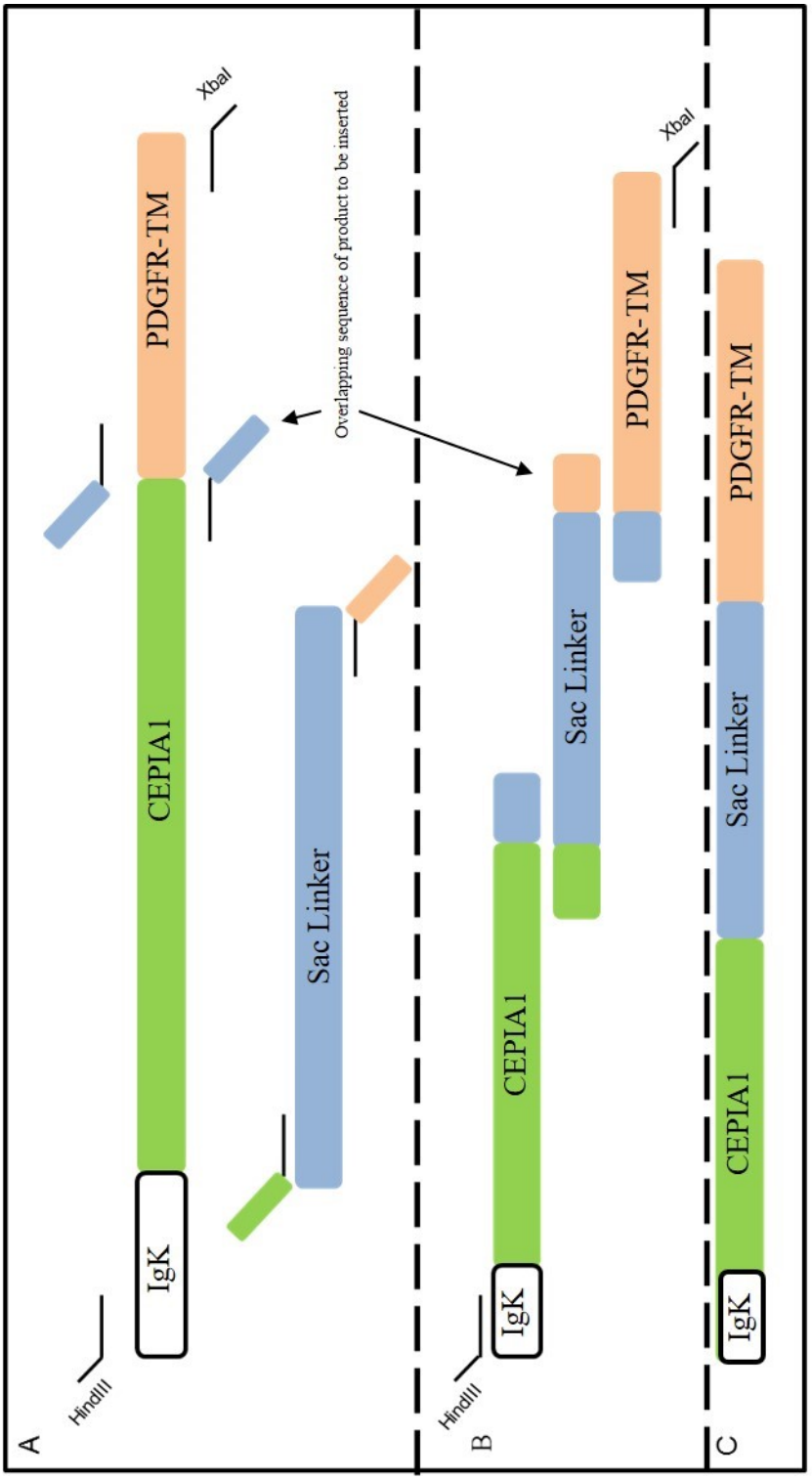

Figure 4.6. Representation of fusion PCR used to introduce Sac linker into construct, between EGFP-CaM and PDGFR-TM targeting sequence.

A) Primers were designed that amplified the G-CEPIA1pm construct and Sac PCR product with overlapping regions complementary to the product to be annealed to. B) Following the initially two PCR reactions, three products were obtained, overlapping as shown . C) The outside primers were used with all three products to generate one product, with the complementary ends of each product annealing.

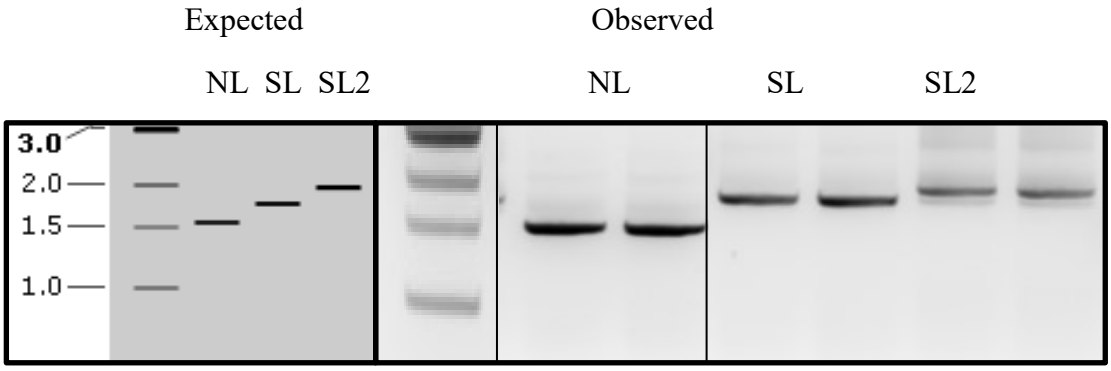

Figure 4.7. CEPIA1pm PCR screen.

A) Predicted insert sizes of CEPIA1pm constructs. B) Observed insert sizes of CEPIA1pm constructs in duplicates. Colonies were selected and screened using PCR screening primers for CEPIA1pm (CEPIA1PMFw & Xba1Rev). PCR products were run on 1 % agarose gel, ladder is NEB 1 kb ladder. NL – no linker (CEPIA1pm). SL – Sac linker (CEPIA1pmSL1), SL2 – Sac linker x 2 (G-CEPIA1pmSL2).

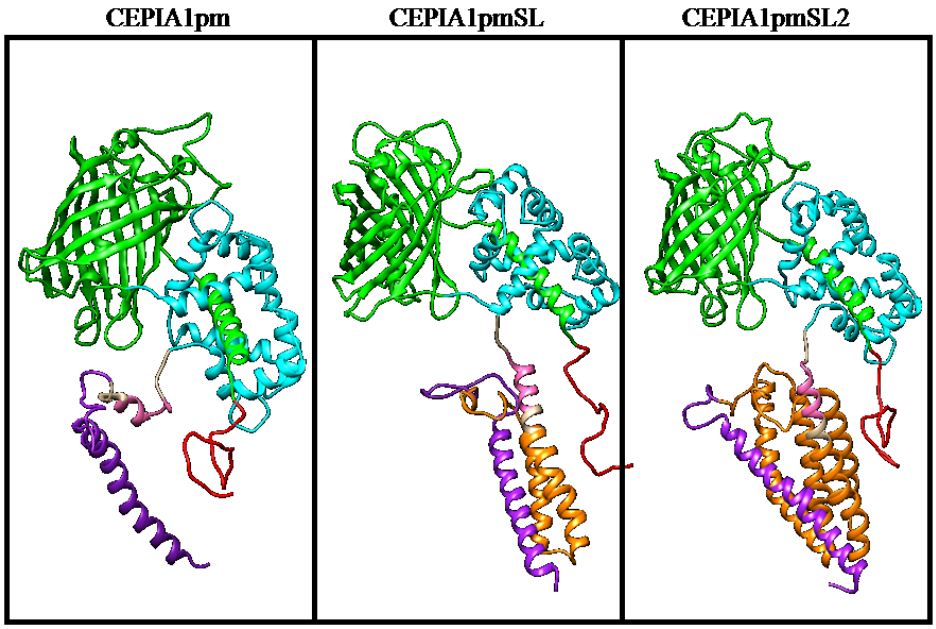

Figure 4.8. CEPIA1pm predicted tertiary structures.

Using the online tertiary structure predictor RaptorX (Källberg et al., 2012), tertiary structures were generated for all CEPIA1pm constructs. Green – EGFP, cyan – CaM, red – IgK leader sequence, pink – myc tag, orange – Sac linker, and purple – PDGFR-TM targeting sequence.

4.3.3 G-CEPIA1pm predicted tertiary structure

Using the online protein structure predictor, RaptorX (Källberg et al., 2012), tertiary predicted structures were generated in order to assess the folding of the G-CEPIA1pm constructs. The IgK leader sequence, EGFP beta-barrel (green), CaM, myc tag, sac linker and PDGFR-TM sequences can be observed (Figure 4.8).

4.3.4 Initial transfections using pSBi G-CEPIA1pm (Sleeping beauty transposase)

For pSBi, one colony was selected for each construct and 1 µg was transiently transfected (without the transposase plasmid, pCMV SB 100X) into HEK293 cells to check for fluorescence. Unfortunately, plasmalemmal localisation was difficult to ascertain due to a large amount of apparent cell death in the fluorescent transfected cells. These cells appeared rounded compared to the original morphology (Figure 4.9). The longer linker appeared to have more cells that had maintained some of their original morphology (compared to the control) but also with bright fluorescence. However, on the brightfield view, the green cells do not look as healthy as control cells (Figure 4.9H).

4.3.5 Cloning of pLJM1 G-CEPIA1pm (lentiviral plasmid)

In order to assess the effect of the promoter on protein production and cell death once transfected, the GOI was re-cloned into an available vector containing a weaker, CMV promoter or the pSBi, SFFV promoter. Following a PCR, the construct was cloned into the backbone with AgeI and EcoRI. Once cloned, colonies were selected and screened using PCR (Figure 4.10).

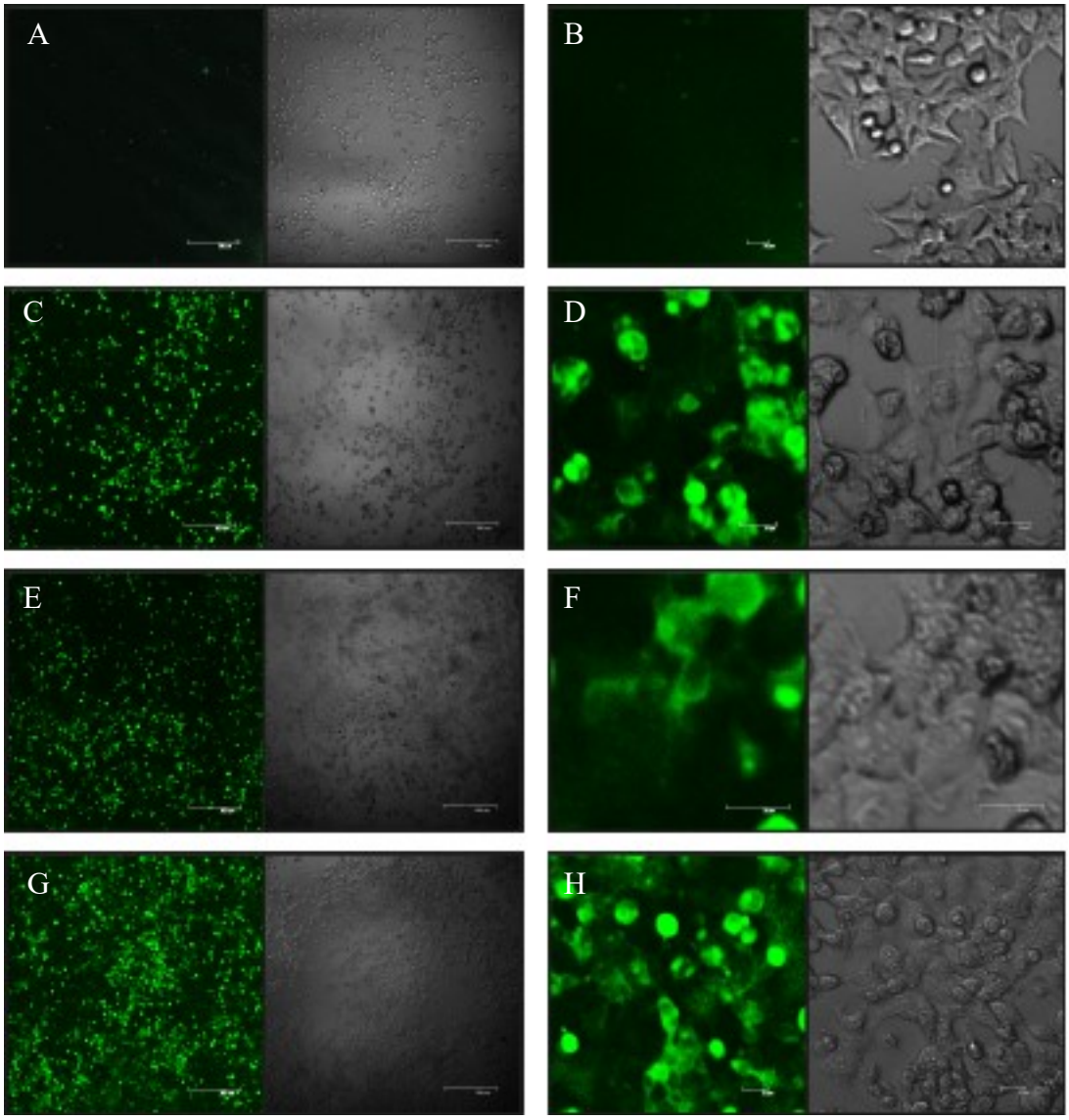

Figure 4.9. Inital pSBi - G-CEPIA1pm transfections.

A&B) Untransfected controls. C&D) G-CEPIA1pm. E&F) G-CEPIA1pmSL. G&H) G-CEPIA1pmSL2. HEK293 cells were transfected overnight with 1 µg of plasmid DNA and imaged 48 hours later in 10mM HBS (with 2 mM Ca^{2+} + 10 mM glucose). Live cells were imaged using a Leica SP2 AOBS confocal microscope with 10x dry (A, C, E, & G) or 63x 1.4 oil (B, D, F, &H) magnification.

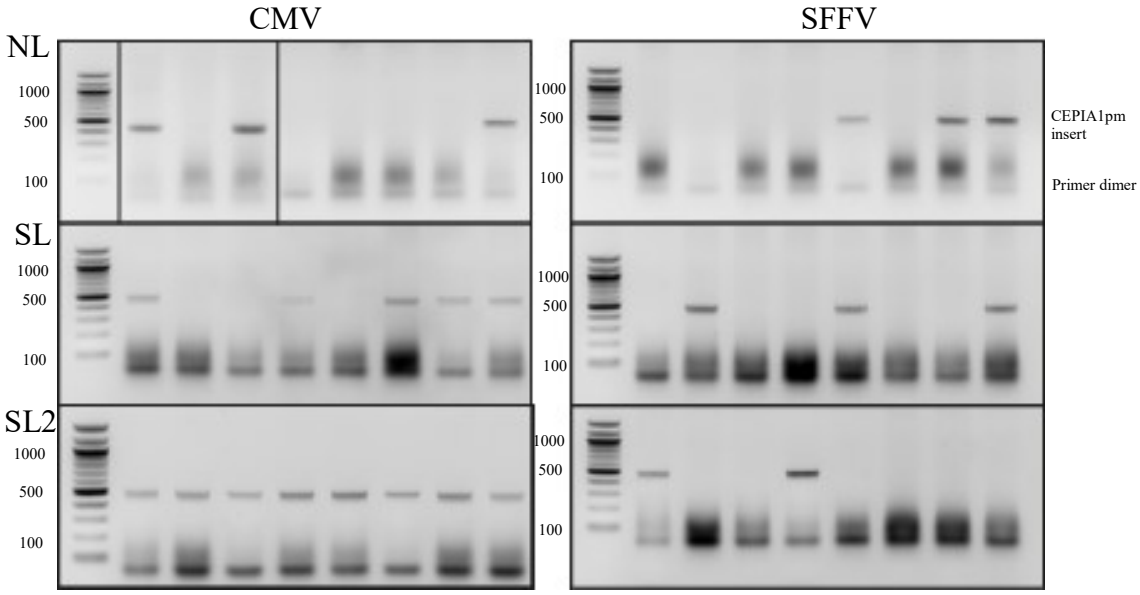

Figure 4.10. Colony screen for pLJM1 - G-CEPIA1pm constructs

Using pLJM1 PCR screening primers (G-CEPIA1er Screen For & hPGK Prom Screen Rev), colonies were selected and tested for CEPIA1pm insert with specific pLJM1 reverse promoter (expected size 579 bases). PCR products were run on a 1.5 % agarose gel with NEB 100 bp ladder. Presence of band at ~ 500 bp indicative of insertion. Lines indicate separate gels. NL – no linker, SL – single linker, SL2 – double linker.

4.3.6 Initial pLJM1 G-CEPIA1pm transfections (lentiviral plasmid)

Three colonies of each construct and promoter were selected and 1 µg was transiently transfected into HEK293 cells to check for fluorescence. Following transfection, cells were live imaged using an EVOS FLoid Cell Imaging Station (LifeTechnologies #4471136). Transfection efficiency of the CMV promoter constructs appeared high, clearly visible using a fluorescence lamp in culture medium (Figure 4.11). Additionally, cell morphology appeared to not differ from that of the control. Unexpectedly, fluorescence was less noticeable in the stronger, SFFV promoter, unlike the pSBi transfections that also contained an SSFV promoter (Figure 4.12). However, again cell morphology appeared improved. Once imaged, cells were scraped and western blotting was performed to investigate protein production of both of the CMV and SFFV overnight transfections. Concurrently with the live imaging, the CMV promoter constructs appeared to produce more protein, for all constructs (Figure 4.13). A double band was seen in clone #3 of the G-CEPIA1pm. The upper band seen in clone #3 was the correct size with the lower band appearing ~ 14 kDa lower than the predicted size. Despite this, the pattern of the bands, appearing in increasing sizes along with confirmed fluorescence suggests correct folding of the protein with both a CMV and SFFV promoter as can be seen in panels A and B of Figure 4.13 respectively.

As both protein production and fluorescence had been confirmed, plasmid DNA was retransformed, maxi-prepped and HEK293 cells were again transfected, however only with CMV constructs. Following a 72 hour incubation, cells were scraped and again a western blot was performed with both anti-Myc and anti-EGFP antibodies (Figure 4.14). Anti-myc produced many bands, this was to be expected due to the

presence of high amounts of endogenous myc in HEK293 cells (Lin et al., 2014). However, stronger bands could be seen, in a step wise manner of size similar to that seen in Figure 4.13. Interestingly, double bands were observed from every construct in Figure 4.14. The anti-EGFP western blot appeared much cleaner, with only bands attributed to the CEPIA constructs clearly visible. Again, double bands were observed for every construct with the lower band ~ 14 kDa lower than the predicted, upper band (Figure 4.14).

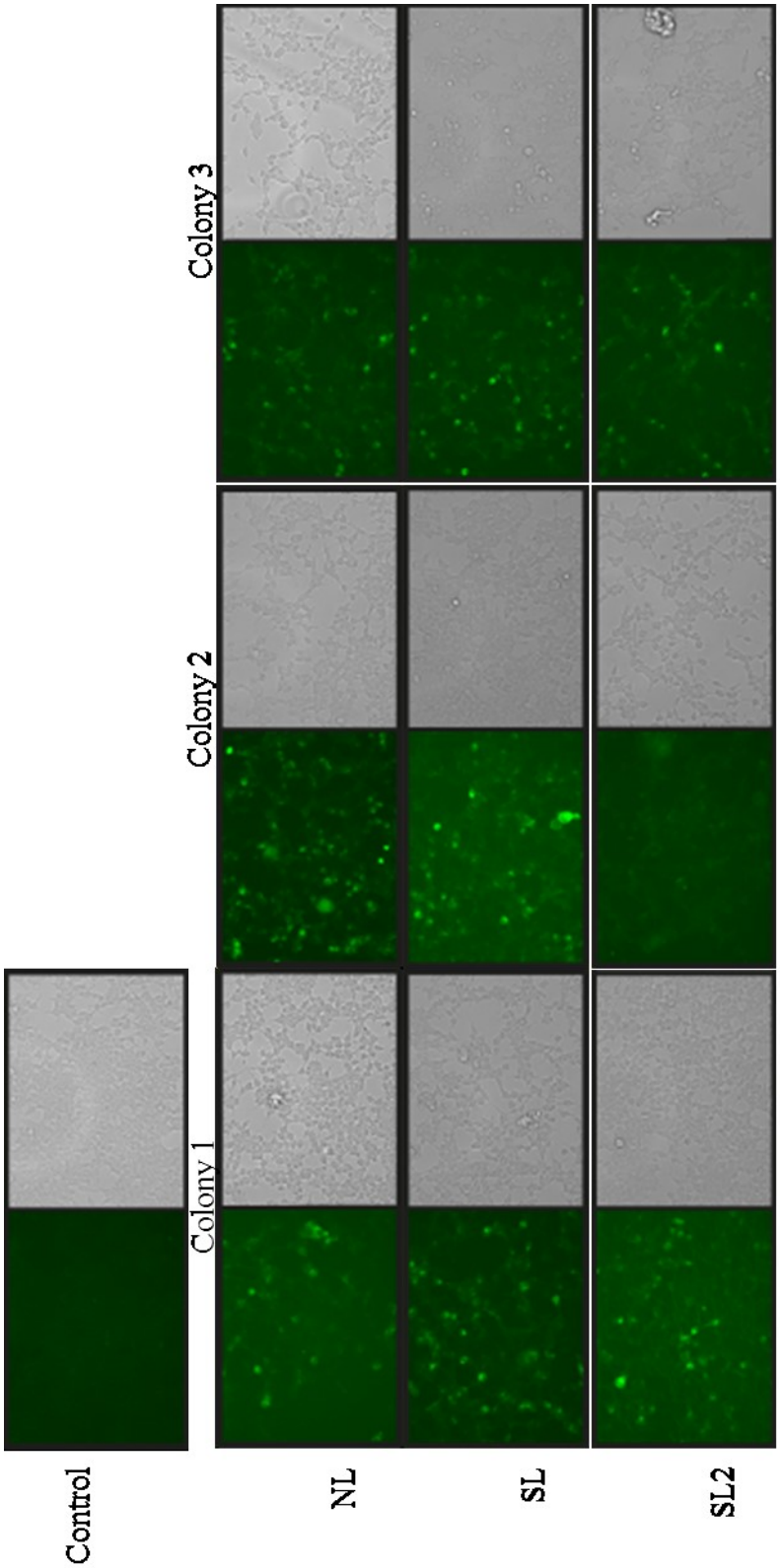

Figure 4.11. Initial pLJM1 - CMV - G-CEPIA1pm construct transfections.

HEK293 cells were transfected with 1 µg plasmid in a 6-well plate. Cells were imaged on a EVOS FLoid Cell Imaging Station (LifeTechnologies #4471136) 24 hours-post transfection in culture medium. NL – G-CEPIA1m, SL – G-CEPIA1pmSL, SL2 – G-CEPIA1pmSL2.

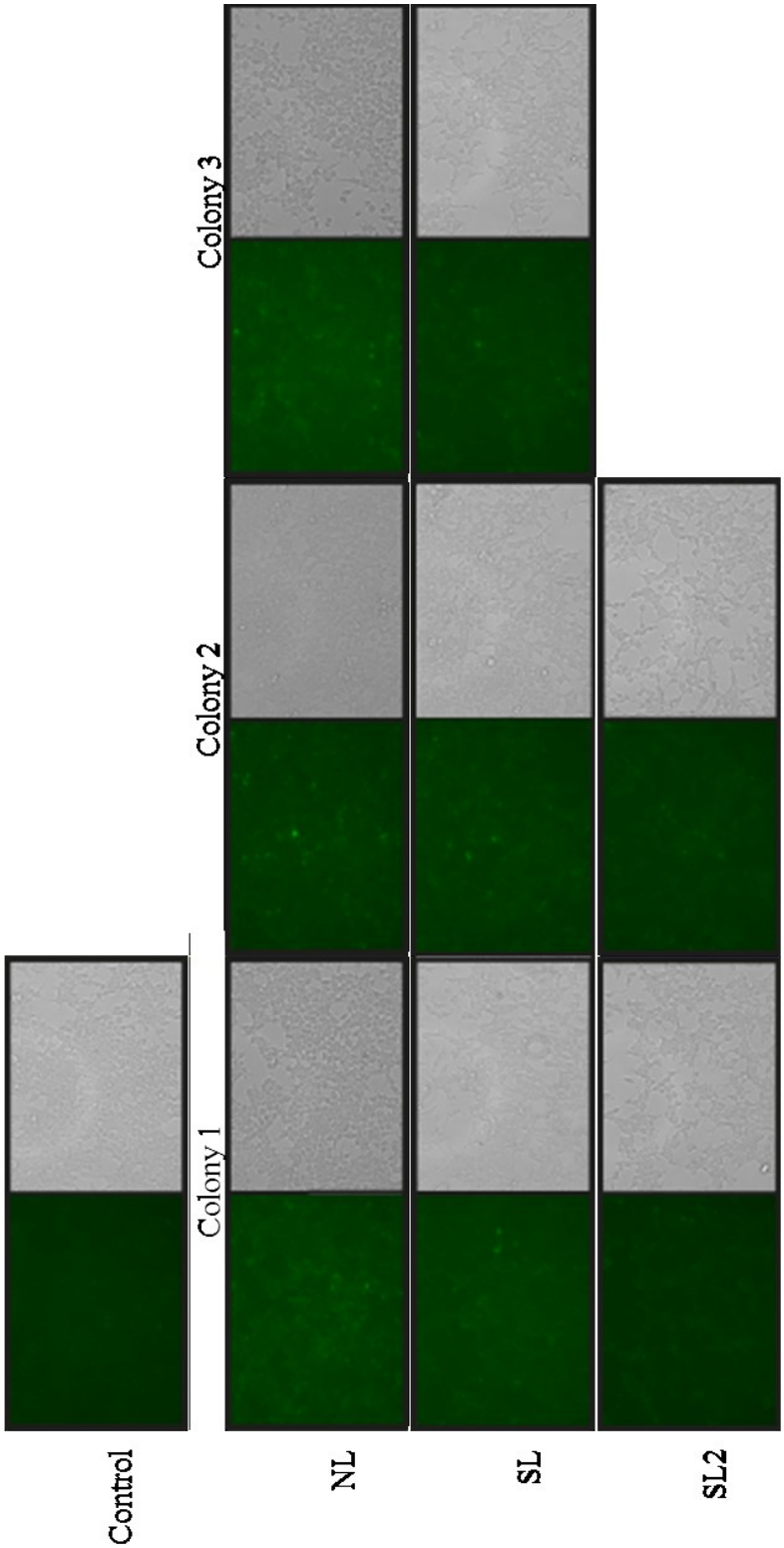

Figure 4.12. Inital pLJM1 - SFFV - G-CEPIA1pm construct transfections.

HEK293 cells were transfected with 1 µg plasmid in a 6-well plate. Cells were imaged on a EVOS FLoid Cell Imaging Station (LifeTechnologies #4471136) 24 hours-post transfection in culture medium. NL – G-CEPIA1nm, SL – G-CEPIA1pmSL, SL2 – G-CEPIA1pmSL2.

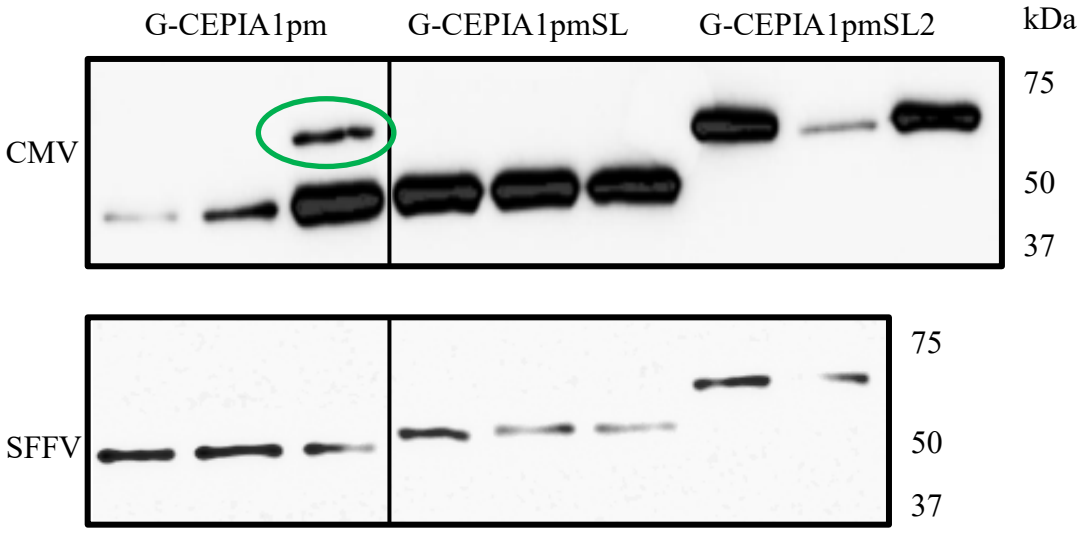

Figure 4.13. G-CEPIA1pm protein production.

Transfected HEK293 cells were collected 24 hours post-transfection and lysed for Western blotting as described in Section 2.6.3. 1/10th of each lysate was loaded per lane. Lines within blots indicate separate gels. Green circle indicates correct molecular weight for construct.

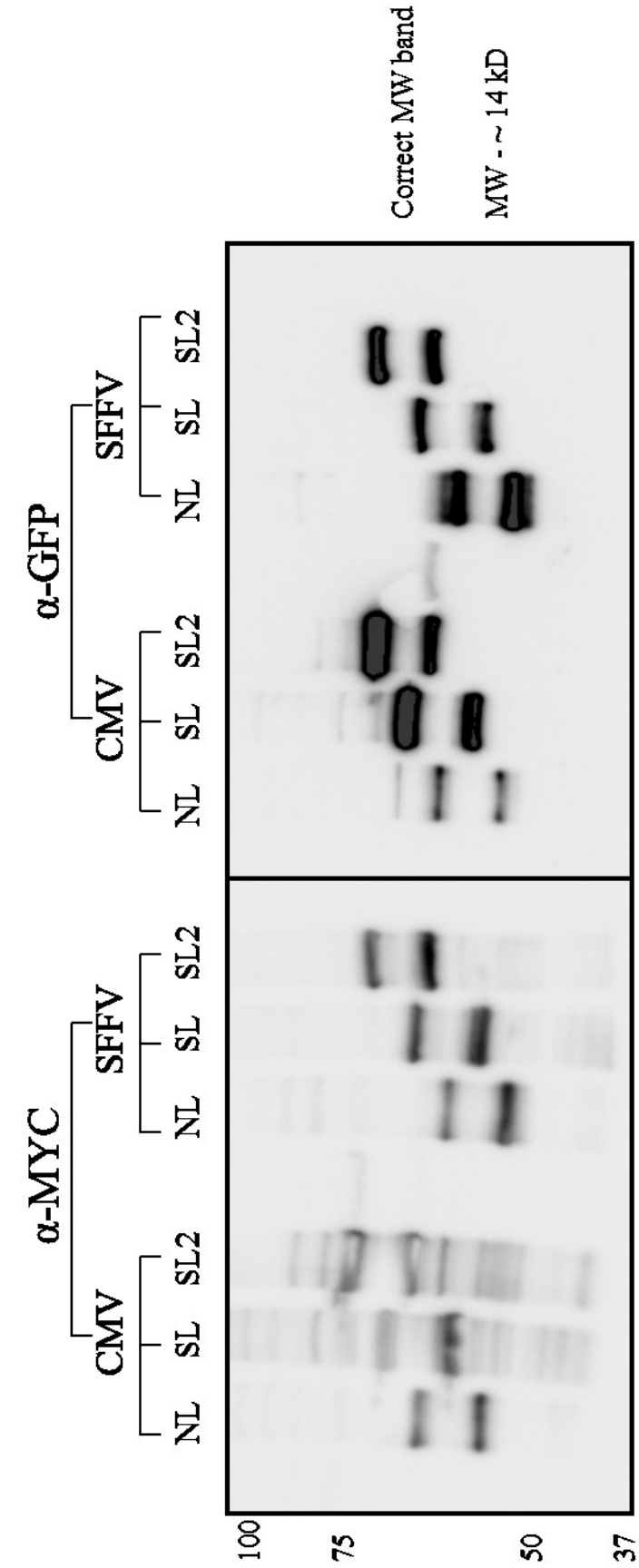

Figure 4.14. pLJM1 - G-CEPIA1pm final constructs protein production.

Transfected HEK293 cells were collected 24 hours post-transfection and lysed for Western blotting as described in Section 2.6.3. 1/10th of each lysate was loaded per lane. Lines within blots indicate separate gels.

4.3.7 Imaging of CEPIA1pm

HEK293 cells were transfected as previously described with G-CEPIA1pm, G-CEPIA1pmSL2 and also R-CEPIA1pm constructs. 72 hours post-transfection cells were placed in 2 mM Ca^{2+} in supplemented HBS for live imaging.

4.3.8 Fluorescence modulation

4.3.8.1 G-CEPIA1pm

Transfected HEK293 cells were imaged and tested for Ca^{2+} modulation of fluorescence. Although a large proportion of cells contain intracellular fluorescence, likely ER and golgi, plasmalemmal-derived fluorescence can be observed in panels A, B, and C of Figure 4.15. For live imaging, cells were washed and placed in 100 μm EGTA in supplemented HBS (10 mM glucose). Following ~ 30 seconds, equal volume HBS was added containing 2 mM Ca^{2+} (1 mM final concentration). Although an addition artefact is observed, the baseline recovers and is followed by an almost 2-fold increase in fluorescence (Figure 4.15D).

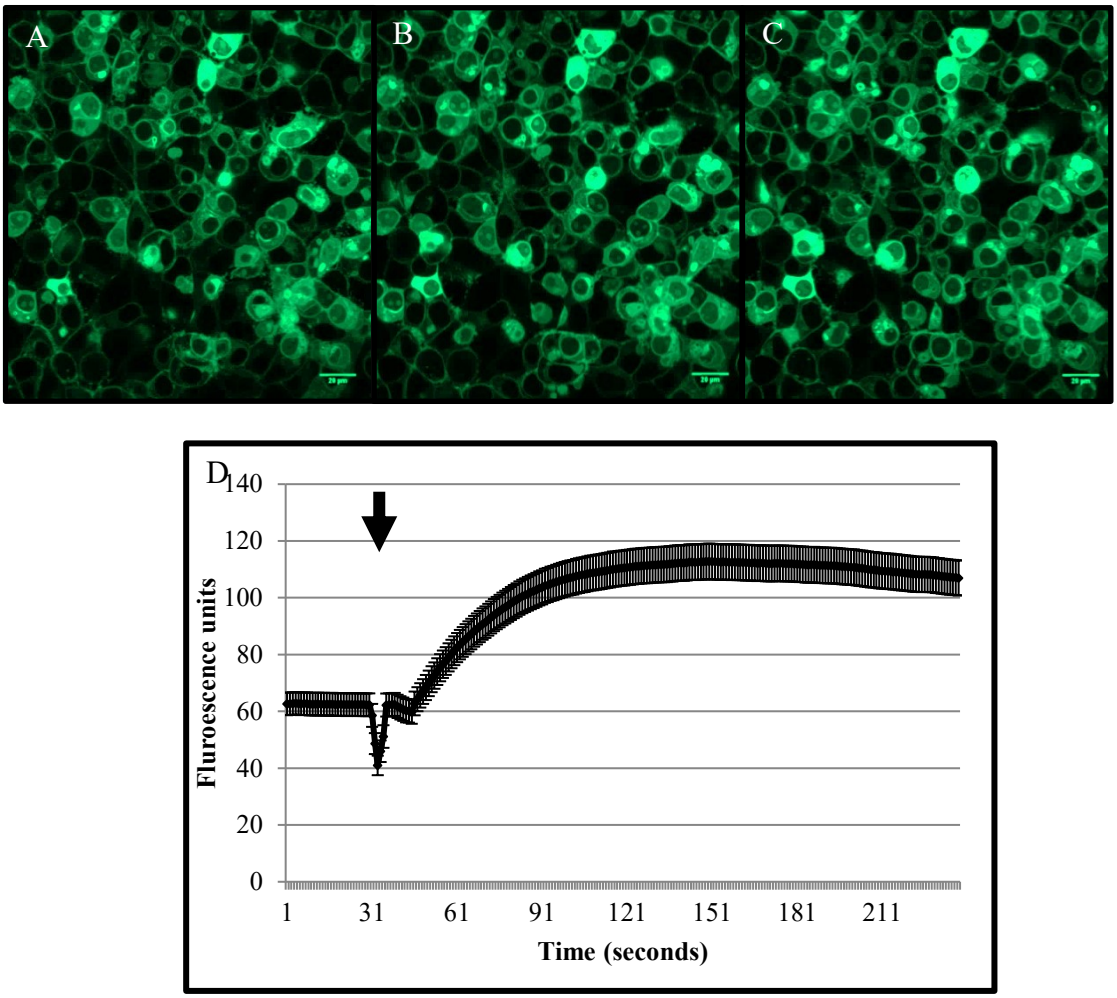

Figure 4.15. G-CEPIA1pm localisation and Ca^{2+} modulation of fluorescence.

HEK293 cells were plated onto an 8-well coverslip chamber slide at 125,000 cells/ well. 24 hours post-plating, cells were transfected with 250 ng plasmid DNA/ well at a 1:2 ratio with JetPrime reagent. 72 hours later, cells were imaged using a Zeiss Airyscan 880 confocal microscope at 1 63 x 1.4 aperture oil magnification. Cells were placed in HBS with 100 µM EGTA for imaging. A, B, &C) Z-stack of live G-CEPIA1pm subcellular localisation of fluorescence. D) After a ~ 30 second baseline, equal volume HBS containing 2 mM Ca^{2+} (1 mM Ca^{2+} final concentration) was added. Error bars – SEM. Arrow indicates addition.

4.3.8.2 R-CEPIA1pm

HEK293 cells were transfected with R-CEPIA1pm as described previously, 72-hours later cells were imaged and tested for Ca^{2+} modulation. In the same conditions as G-CEPIA1pm, R-CEPIA1pm was not as bright (Figure 4.16A), however there appeared to be less intracellular fluorescence comparatively (Figure 4.16C). It is worth noting that R-CEPIA1pm is in pcDNA3.1+ and therefore expression may vary. For live imaging, cells were washed and placed in 100 μm EGTA in supplemented HBS (10 mM glucose). After ~ 60 seconds of baseline, equal volume HBS was added containing 2 mM Ca^{2+} (1 mM final concentration). The response from R-CEPIA1pm appeared much quicker than that seen with G-CEPIA1pm. In addition, the response was more transient, falling quickly after the peak. A falling baseline can also be observed here (Figure 4.16D).

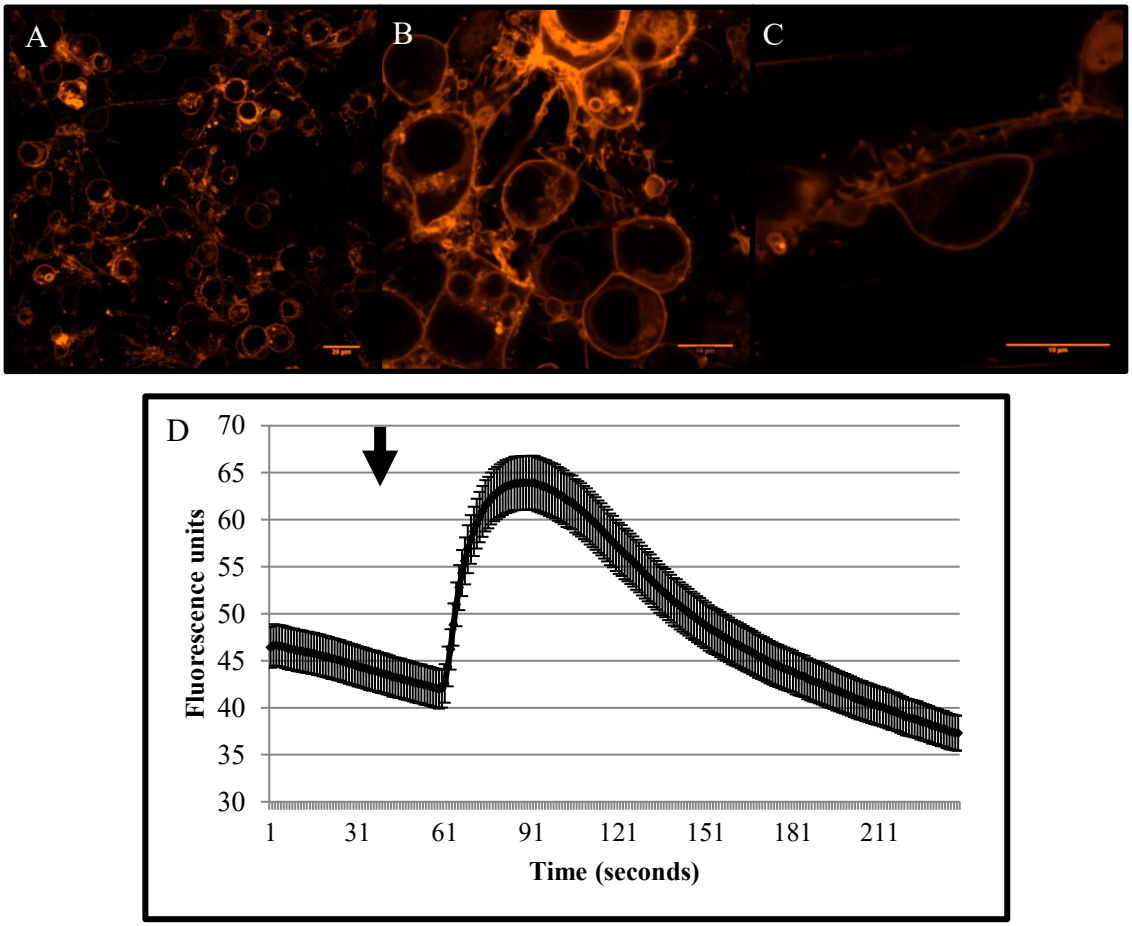

Figure 4.16. R-CEPIA1pm localisation and Ca^{2+} modulation of fluorescence

HEK293 cells were plated onto an 8-well coverslip chamber slide at 125,000 cells/ well. 24 hours post-plating, cells were transfected with 250 ng plasmid DNA/ well at a 1:2 ratio with JetPrime reagent. 72 hours later, cells were imaged using a Zeiss Airyscan 880 confocal microscope at 1 63 x 1.4 aperture oil magnification. Cells were placed in HBS with 100 µM EGTA for imaging. A, B, &C) Live R-CEPIA1pm subcellular localisation of fluorescence at various levels of zoom. D) After a ~ 30 second baseline, equal volume HBS containing 2 mM Ca^{2+} (1 mM Ca^{2+} final concentration) was added. Error bars – SEM. Arrow indicates addition.

4.3.8.3 G-CEPIA1pmSL2

HEK293 cells were transfected with G-CEPIA1pmSL2 as described previously, 72-hours later cells were imaged and tested for Ca^{2+} modulation. In the same conditions as G-CEPIA1pm, G-CEPIA1pmSL2 was less bright (Figure 4.17A), similar to R-CEPIA1pm. Although again, less intracellular fluorescence was observed whilst plasmalemmal-derived fluorescence was much clearer (Figure 4.17B). For live imaging, cells were washed and placed in 100 μm EGTA in supplemented HBS (10 mM glucose). After ~ 60 seconds of baseline, equal volume HBS was added containing 2 mM Ca^{2+} (1 mM final concentration). The response from G-CEPIA1pmSL2 was much quicker than that seen with G-CEPIA1pm, similar to R-CEPIA1pm. In addition, as seen with R-CEPIA1pm, a falling baseline is observed.

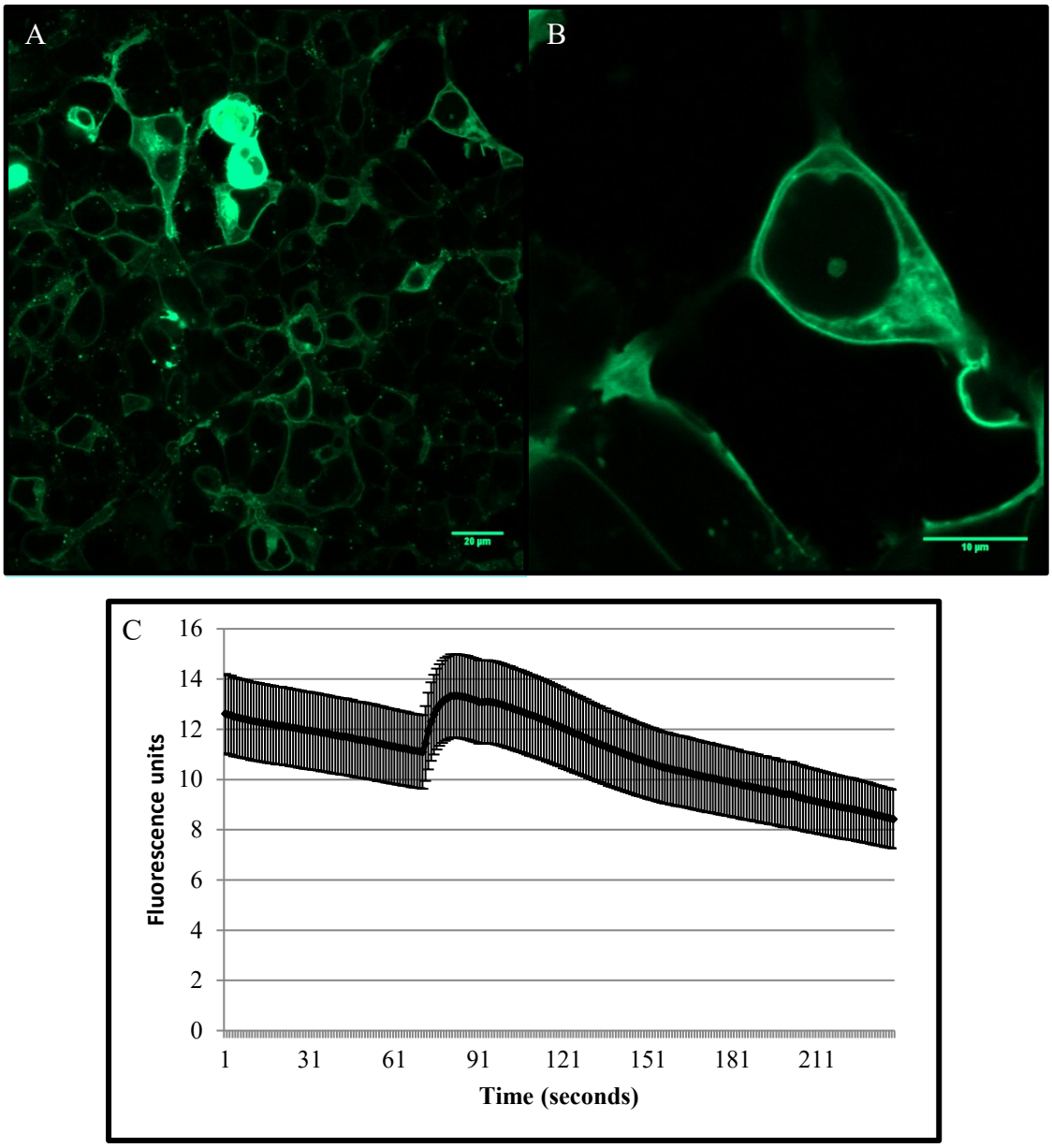

Figure 4.17. G-CEPIA1pmSL2 localisation and Ca^{2+} modulation of fluorescence.

HEK293 cells were plated onto an 8-well coverslip chamber slide at 125,000 cells/ well. 24 hours post-plating, cells were transfected with 250 ng plasmid DNA/ well at a 1:2 ratio with JetPrime reagent. 72 hours later, cells were imaged using a Zeiss Airyscan 880 confocal microscope at 1 63 x 1.4 aperture oil magnification. Cells were placed in HBS with 100 µM EGTA for imaging. A, B, &C) Live R-CEPIA1pm subcellular localisation of fluorescence. D) After a ~ 30 second baseline, equal volume HBS containing 2 mM Ca^{2+} (1 mM Ca^{2+} final concentration) was added. Error bars – SEM. Arrow indicates addition.

4.3.9 HaCaT pSBi transfections

To begin generation of stable HaCaT clones, HaCaT keratinocytes were transfected with 2:1 ratio of G-CEPIA1pm DNA and SB x100 transposase. Following 72 hours, cells were treated with 1 ug/ ml puromycin and allowed to recover. Western blotting was performed on each selected population. As seen in HEK293 cells, double bands were observed for each construct, with the upper band appearing to be the expected sizes (Figure 4.18).

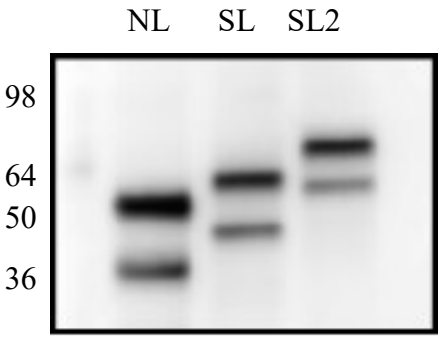

Figure 4.18. G-CEPIA1pm constructs protein expression in stable HaCaT keratinocytes.

HaCaT keratinocytes were transfected with pSBi G-CEPIA1pm constructs and pCMV SB100X at a 2:1 ratio. 24 hours after transfection, cells were treated with 1 μg/ml puromycin in culture medium for 2 weeks. Conditioned medium was then used to allow cells to recover before western blotting using α-GFP antbody. Ladder used was SeeBlue Plus 2 Protein Standard (Thermo #LC5925).

4.3.10 HaCaT clone imaging

Selected HaCaT pSBi G-CEPIA1pm cells were plated into a 96-well plate at 0.5 cells/ well and allowed to recover. Wells were checked for fluorescence at regular intervals, 8 clones were observed to be fluorescent in culture medium and these were selected for further growth. Clones 1-8 were plated into an 8-well chamber slide (Sarstedt #94.6190.802), washed and placed in 2 mM Ca^{2+} in supplemented HBS. All clones were fluorescent, however clones 1 and 2 exhibited the brightest plasma membrane-like fluorescence (Figure 4.19).

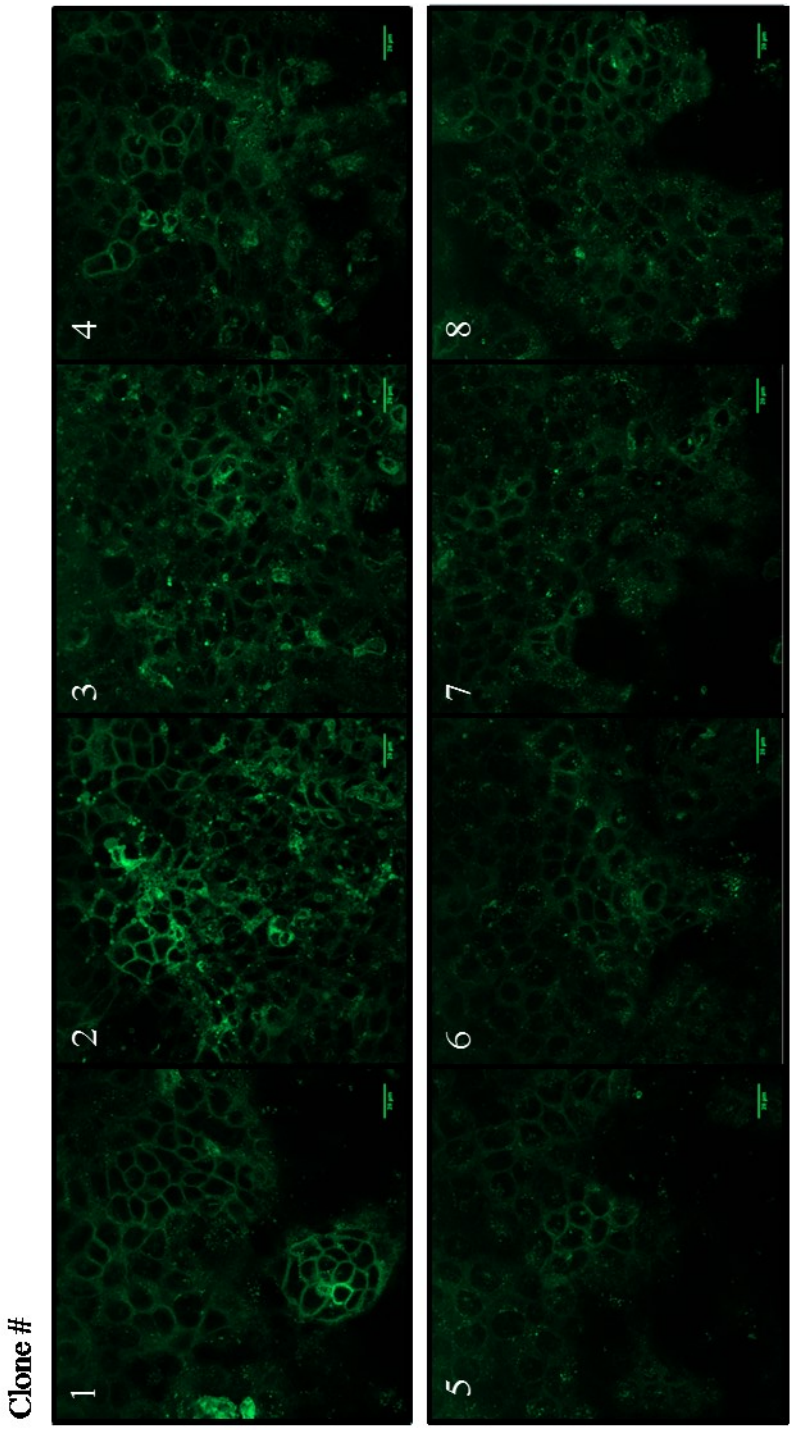

Figure 4.19. HaCaT keratinocyte pSBi G-CEPIA1pm clones.

Following transfection and puromycin selection, HaCaT keratinocyte population of pSBi G-CEPIA1pm was plated into a 96-well plate at 0.5 cells/well in growth medium. Once confluency was achieved, each well was transferred into a single well of an 8-well chamber coverslip slide for imaging. Cells were placed in 2 mM Ca^{2+} HBS and imaged using Zeiss Airyscan with 63 x 1.4 aperture oil magnification. Clones 1-4 express the clearest membrane-derived fluorescence. More tightly packed cells appear to have brighter fluorescence with little intracellular signal. Scale bars = 20 µm.

4.4 Summary

This chapter aimed to generate an extracellular Ca^{2+} sensitive probe, bound to the plasma membrane. This sensor would allow quantitative measurements of Ca^{2+} concentrations sensed by the cell in various conditions. The existing EGFP-CaM based Ca^{2+} probe targeted to the ER, G-CEPIA1er was transfected into HEK293 cells and ER-like localisation along with Ca^{2+} modulation of fluorescence was observed. A strategy was designed using PCR and a GeneArt String to retarget the CEPIA1er construct to the cell surface using a transmembrane targeting region of PDGFR. R-CEPIA1pm was also designed here and ligated into pcDNA3.1+ for storage. In addition, a single or double flexible linker was added between the CaM and targeting sequence of G-CEPIA1pm. The ~ 180 bp size increase was observed following diagnostic digests. Initially, the construct was ligated into a sleeping beauty vector for ease of making stable clones. However, following transfections of all the pSBi G-CEPIA1pm constructs, although very high efficiency was observed, a large number of cells that were fluorescent had lost normal morphology and had begun to round up. The construct was re-cloned into the viral vector pLJM1, containing a CMV promoter. The constructs were also placed into pLJM1 with an SFFV promoter, as in pSBI, for comparison.

Transfection efficiency was not as efficient with the pLJM1 plasmid as the pSBi, however, cell morphology was largely unaffected after 24 hours. Western blotting identified the presence of 3 bands, at varying sizes. The change in size was consistent with G-CEPIA1pm constructs. However, the protein appeared ~ 14 kDa smaller than predicted. In addition, the CMV promoter appeared to produce more protein than the SFFV promoter. Interestingly, in HEK293 stable clones, a double band was seen on

Western blots. The upper band was consistent with predicted sizes of each of the probes, again with a smaller band ~ 14 kDa less than predicted.

Live imaging of transient transfections G-CEPIA1pm, G-CEPIA1pmSL2 and R-CEPIA1pm probes show ER based fluorescence but also clear and distinct plasmalemmal-derived fluorescence. Ca^{2+} modulation of fluorescence of G-CEPIA1pm, R-CEPIA1pm and G-CEPIA1pmSL2 all confirm functionality of the probe.

HaCaT keratinocytes were transfected with the pSBi G-CEPIA1pm constructs along with the transposase pCMV SB x100 for stable clone generation. Once selected using puromycin and cells had recovered, the same double band western could be observed as with the HEK293 cells. G-CEPIA1pm clones exhibited plasmalemmal-derived fluorescence, clearer than seen in the transient transfections.

4.5 Discussion

Predicted tertiary structure of the G-CEPIA1pm construct was as expected, a beta-barrel GFP followed by a Ca^{2+} binding calmodulin structure, a long flexible linker with a Myc tag and a transmembrane helix. However, a flexible linker was added to move the CEPIA1pm protein away from the membrane. The linker used has a predicted length of ~ 100 nm, with a tertiary structure of two helices. The predicted structure of G-CEPIA1pm with this linker included aligns the PDGFR-TM helix and the linker helices. However, as the transmembrane region should be implanted into the membrane following translation this would not be possible. In addition, as it is a flexible linker there is no guarantee that the EGFP and CaM will be further away from the membrane as desired. However, this flexible linker was successfully used to investigate the distance of ER and mitochondria contact sites (Cieri et al., 2017).

Following generation of the CEPIA1pm constructs, transient transfections led to very high transfection efficiencies. Transfected cells expressed a range of protein amounts, as expected, due to the very nature of transient transfections. Cells with very high expression were characterised by a presence of intracellular fluorescence. As discussed in Section 1.6, proteins are folded and matured in the lumen of the ER (Ron and Walter, 2007). Therefore, cells with high copies of CEPIA1pm plasmid would show more ER fluorescence whilst the protein is being matured. In line with this, cells with less relative protein appeared to have plasma membrane-like fluorescence only.

Transient transfections of HEK293 cells led to a large amount of cell death, accompanied by very bright fluorescence. Transient transfections were used in order

to investigate localisation of fluorescence and also test Ca^{2+} modulation. Therefore, cell death following CEPIA1pm needed to be avoided. Hence the gene of interest was relocated into a new vector, containing a weaker promoter. However, as described previously, co-transfection of the Sleeping Beauty plasmid pSBi with the transposase plasmid pCMV SB 100X, allows instant generation of stable clones. This technique was therefore used to generate stable clones of HaCaT keratinocytes. Although some cell death occurred (not shown), any live cells were expressing an amount of protein not detrimental to their normal function.

Using G-CEPIA1pm, addition of 1 mM Ca^{2+} led to a ~ 2 fold change. As discussed, in optimal conditions G-CEPIA1er had a dynamic range of 4.7, saturating at around 3 mM Ca^{2+}(Suzuki et al., 2014). R-CEPIA1er has a reported dynamic range in optimal conditions of 8.8 (Suzuki et al., 2014), yet here it appeared around 1.6.

Interestingly, G-CEPIA1pmSL2 had an increase of ~ 1.15 fold on average. In the same conditions as G-CEPIA1pm, this probe appeared much dimmer. Therefore, these data indicate that in the conditions set out in this thesis, G-CEPIA1pm is more effective as a plasma membrane bound Ca^{2+} sensor. However, this may not be the case in other conditions, cell lines, or tissues.

The initial Western blot of pLJM1 transient transfections produced bands that were ~14 kDa smaller than the predicted size of the protein. Only one construct produced a second, upper band that was the predicted size. Other transient transfections, in the same conditions, produced 2 bands for each construct, using both an anti-myc tag and anti-GFP antibody. Again, the upper band was consistent with the predicted size and the smaller band ~ 14 kDa less. A study has investigating GFP as an indicator for

membrane bound protein folding, previously identified double bands on Western blots following GFP fusion with a range of proteins (Geertsma et al., 2008). As seen here, the upper band represented the predicted kDa and a smaller, (in their case 10 – 14 kDa) band was also present. Using *in gel* studies, the lower band was identified to be fluorescent following lysate preparation. Therefore they initially hypothesised that, the upper band was fully denatured protein whereas in the lower, the GFP had maintained some moiety.

By modifying promoter inducers, Geertsma *et al* (2008) identified that less protein production was accompanied by an increase in relative intensity of the lower band. In this thesis, the CMV promoter in pLJM1 appeared the brightest. Therefore, if fluorescence intensity is relative to protein production, the SFFV promoter would lead to a higher relative intensity of the lower band on a Western blot. Although not so clear using the anti-myc tag antibody, a variation in relative intensity between the upper and lower band can be observed between the CMV and SFFV constructs. The upper band for CMV - SL and CMV - SL2 is a much higher intensity than the lower. In comparison, the bands are much more equal in the SFFV constructs. Geertsma *et al* (2008) stated that the lower band is the functional protein as it is the fluorescent band on in gel studies. However, the brighter fluorescence was observed here with the CMV promoter that had more of the upper, correct kDa band. Despite these observations, a band of predicted kDa is observed in transient transfections of the final pLJM1 plasmid and also in stable populations of pSBi.

4.6 Conclusion

Following the difficulties faced with CatchPM, this chapter set out to again, attempt the generation of a GFP-based genetically encoded plasma membrane targeted Ca^{2+} sensor. As the targeting of CatchPM appeared successful, the strategy of PDGFR-TM was maintained here. As the GFP in CatchPM was the non-functional, a new EGFP-CaM based sensor was incorporated, with PCR the technique used to generate the construct, reducing the modifications made to the original construct. Initial transfections with pSBi were successful but toxic to HEK293 cells. Use of a pLJM1 vector with a weaker promoter allowed protein production with little effect on cell morphology. Ca^{2+} experiments identified Ca^{2+} modulation of fluorescence, with G-CEPIA1pm responding most similar, to the original ER based probe. Using the sleeping beauty transposase, HaCaT keratinocyte clones were made and live cell imaging showed membrane-like fluorescence.

Taken together, the fluorescence localisation, Ca^{2+} modulation, and western blot of the CEPIA1pm constructs confirm that this is a functional extracellular Ca^{2+} sensor targeted to the membrane.

4.7 Future work

Initial experiments described here show the generation of a functioning Ca^{2+} sensor located on the plasma membrane. In order for this sensor to be of use in quantifying Ca^{2+} concentrations, small increments of Ca^{2+} addition would be required to assess relative fluorescence intensities. In addition, use of the ER Ca^{2+} uptake inhibitor thapsigargin would identify the response to Ca^{2+} exhibited from plasma-membrane based protein only.

Whilst HaCaT clones of pSBi G-CEPIA1pm were generated and fluorescence was observed, Ca^{2+} modulation of fluorescence of these clones requires characterisation.

5 Investigating the role of mitochondrial calcium on keratinocyte homeostasis

5.1 Introduction

Although work has identified a role for mitochondria in differentiation (Hamanaka et al., 2013, Savignan et al., 2004) terminal differentiation of keratinocytes (Allombert-Blaise et al., 2003), extensive characterisation of $[Ca^{2+}]_m$ is lacking. *In vitro*, an increase in $[Ca^{2+}]_o$ leads to a rise in mitochondrial Ca^{2+} (Rizzuto et al., 1992), although not confirmed directly in keratinocytes. This increase in $[Ca^{2+}]_o$ has been observed to depolarise the mitochondria, more so in the hyperpolarised, basal, proliferating cells and this depolarisation is a trigger for differentiation (Savignan et al., 2004). In addition, Hamanaka *et al* (2013) identified that a Cre-mediate knock out of TFAM, a key regulator of the mitochondrial genome and in turn, ROS, inhibited differentiation both *in vitro* and *in vivo*. In addition, topical application of antioxidants had the same effect, identifying a key role for mitochondrial ROS in epidermal homeostasis (Hamanaka et al., 2013).

The subsequent identification of the mitochondrial Ca^{2+} uniporter in 2015 by independent laboratories (De Stefani et al., 2011, Baughman et al., 2011) allowed for the further investigation into the effect of mitochondrial Ca^{2+} fluxes on cell homeostasis. Although the mitochondrial Ca^{2+} uniporter is not solely responsible for mitochondrial Ca^{2+} influx, as the amplitude of the Ca^{2+} response is fine-tuned with proteins such as MICU1 and MICU2 (Patron et al., 2014), they both require the pore-forming subunit, MCU to act. As mentioned previously, studies have shown that overexpression of MCU increases Ca^{2+} influx and both knock-down and knock-out

studies show a reduction in agonist-induced mitochondrial Ca^{2+}uptake (De Stefani et al., 2011).

The studies described (Hamanaka et al., 2013, Savignan et al., 2004), highlight a role for mitochondrial Ca^{2+} as an instigator of keratinocyte differentiation *in vitro*. Therefore this study aims to generate a MCU knockout clone of HaCaT keratinocytes and in turn, use this to investigate the role of mitochondrial Ca^{2+} on epidermal homeostasis and differentiation. In addition, HaCaT keratinocytes will be grown in low Ca^{2+} medium (0.03 μM) and high Ca^{2+} medium (~ 3 μM) in order to investigate any expression changes of MCU, MICU1, and MICU2 between HaCaTs with a basal, proliferating and differentiated phenotype (Deyrieux and Wilson, 2007).

5.2 Methods

5.2.1 Low Ca^{2+} medium

For growing HaCaT keratinocyts in basal conditons, low Ca^{2+} DMEM was used. This contained Ca^{2+} free DMEM (ThermoFisher #21068028), 1 mM Sodium pyruvate (Sigma S8636), 2 mM L-Glutamine (Sigma #G7513), 30 μM Ca^{2+} chloride (Sigma #21115), 10 % FBS (ThermoFisher #10270-106) filtered with Chelex 100 Resin (BioRad #1432832) to chelate Ca^{2+}, and 1 % penicillin/streptomycin (100 units/ mL and 100 μg/ mL respectively; ThermoFisher #15140-122).

5.2.2 Genomic DNA extraction

Cells were scraped into a 1.5 mL centrifuge tube and pelleted at ~ 2000 rpm for 5 minutes followed by washing in PBS. Following centrifugation, pellet was resuspended in 300 μL Mouse Tail Lysis buffer (50mM Tris, 100mM NaCl, 1mM EDTA containing 0.2% SDS) and vortexed. Following this, 6 μL proteinase K (10 mg/ mL) and 3 μL RNAse A (200mg/ml) was added. Further vortexing preceded incubation at 55 °C overnight. The next day Proteinase K was denatured by incubation at 95 °C for 10 minutes before the addition of 1 μL Glycogen (20 mg/ mL). Tubes were vortexed and incubated on ice for ~ 30 minutes. Equal volume (~ 400 μL) isopropanol was added and samples centrifuged at 13,000 rpm for 35 minutes. Supernatant was then removed (leaving ~ 50 μL) and 500 μL of 70 % EtOH was added before further centrifugation for 10 mins. After removal of ~ 450 μL of supernatant, tubes were left at 55 °C to dry DNA before resuspension in ~ 150 μL MilliQ. Pellets were dissolved at 55 °C for 5 mins before DNA quantification.

5.2.3 The CRISPR/Cas9 system

The most recently discovered, RNA guided, gene editing tool is CRISPR (clustered regularly interspaced protospacer motifs). In the late 1980's, Ishino *et al* (1987) identified clusters of short DNA fragments separated by repeating sequences in E. coli. The origin of these sequences remained elusive until it was identified that these DNA sequences were derived from invader DNA (Bolotin et al., 2005, Mojica et al., 2005). This inclusion of foreign DNA into its own, was found to be a form of adaptable immunity (Horvath and Barrangou, 2010) By incorporating the foreign DNA into its own genome between repeated sequences, the host is able to transcribe these repeat arrays into crRNAs (CRISPR RNAs) containing fragments of each region of foreign DNA incorporated, termed protospacers. The crRNAs form complexes with tracrRNa (trans activating CRISPR RNA) and Cas (CRISPR associated) nucleases (Deltcheva et al., 2011, Jinek et al., 2012). These nucleases are directed to the pathogenic DNA upon reinfection by the crRNAs. Two nuclease domains are required for a complete double stranded break (DSB), HNH motif domain cleaving the complementary strand and RuvC-like domain cleaving the non – complementary domain (Jinek et al., 2012, Nishimasu et al., 2014). However, this cleavage is reliant on the presence of a short (2-5 nt) sequence immediately downstream (3') of the complementary sequence termed a protospacer-associated motif (PAM) (Swarts et al., 2012). Without this conserved PAM, fully complementary sequences will be ignored (Sternberg et al., 2014). The DNA, guide RNA and Cas9 complex is depicted in Figure 5.1.

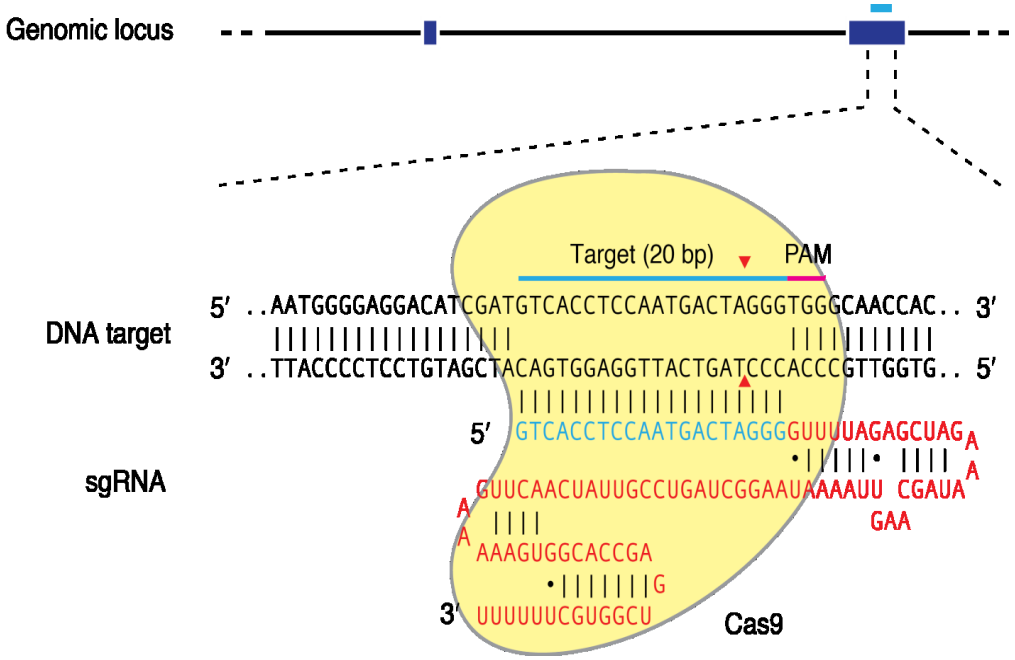

Figure 5.1. The CRISPR/ Cas9 system

A 20 bp region of DNA is identified as a target for the Cas9 complex. *In vitro* this is ligated into a plasmid vector containing a synethic single guide RNA (sgRNA), a complex of trRNA and crRNA along with CRPISPR associated gene 9 (Cas9). This short RNA strand is upstream of a protospacer-associated motif (PAM), which is required for recognition of the strand. Targeting of this complex results in a double strand break, thanks to HNH and Ruv-C like domains. This break can either be allowed to reanneal leading to a deletion or new sequences can be re-introduced by homologous directed repair using template DNA.

5.2.4 Genome editing using CRISPR

CRISPR has been adapted in order to target genomes of human and mouse and has quickly become an invaluable tool for genome editing (Jinek et al., 2012, Cong et al., 2013). In 2012, the use of CRISPR was vastly simplified with the generation of a synthetic single guide RNA, combining the sequence-specific crRNA and the fixed tracrRNA (Jinek et al., 2012). Typically, 20 nucleotides are introduced into the crRNA that are specific to the DNA target site (as per DNA-RNA complementary rules) along with a PAM site at the 3' end. This PAM site is usually NGG as it is the most efficient (Jinek et al., 2012). This targets the sgRNA-Cas complex to elicit the DSB. It has been observed that, due to CRISPR-Cas9's simplicity, multiple gRNAs can be targeted to different sequences simultaneously generating many DSBs (Cong et al., 2013).

5.2.5 CRIPSR Cloning

Guide RNAs targeting the first Exon of MCU were designed using the Broad Institute's CRISPR design tool (https://portals.broadinstitute.org/gpp/public/analysis-tools/sgrna-design). Guide sequences were synthesised as oligonucleotides and cloned into LentiCRIPSR (Addgene, Boston USA) that had been modified to include highly pathogenic retrovirus Spleen Focus-Forming Virus (SFFV) promoter (kind gift from Nicholas Harper, Liverpool UK). Plasmid was digested with BsmB1 (NEB) to remove the stuffer sequence and allow ligation of guide oligos. Following transformation colonies were screened for correct insertion then positive clones picked for mini prep and sequencing. Correctly sequenced clones were tested first in HEK293 cells by transfection for 72h as detailed below.

Guide #	Sequence	Exon
Guide #1	GTGAACTGACAGCGTTCACGC	3
Guide #2	GAGAGTTGCTATCTATTCACC	3
Guide #5	GAACAGCTCCCAAATTCTGCC	2
Guide #6	GATCGCTTCCTGGCAGAATTT	2
Guide #W1	GTGGCGGCTGACGCCCAGCCC	1
Guide #W2	GATCGCTTCCTGGCAGAATT	2
Guide #N1	GCAGGAGCGATCTACCTGCGG	1

5.2.6 T7 Endonuclease DNA mismatch assay

72h following transfection of CRISPR plasmids, cells were harvested and genomic DNA extracted as detailed above. Single CRISPR guides will produce a double-strand DNA break and this can be detected using an endonuclease and a DNA "mismatch" assay. A region surrounding Exon 1 of MCU was amplified using the following primers; MCU Exon 1 For: 5' TCAAGGGCTTTAGTTGGCCCG 3' Exon 1 Rev: 5' GAGAGGTTCAAGTCCCGTGC 3'. This PCR will contain a mix of modified and wildtype DNA homoduplexes, in order to generate heteroduplex DNA the PCR reaction was heated to 95C for 10min and then allowed to cool in a hot-block to room temperature to allow for annealing.

Following PCR of genomic DNA using relevant primers, a T7 endonuclease assay was used to identify 'smears' that would indicate heteroduplexes and therefore the efficiency of CRISPR/ Cas9 system. PCR product was heated to 95 °C for 10 mins, entire hot block was removed from heater and allowed to cool to room temperate as a complete unit. Once cooled, the following solution was made and the PCR products were digested using a T7 Endonuclease (NEB) for 45 min at 37C.

	#µl
PCR product	7.5
Buffer 2 (NEB)	2
T7 Endonuclease (NEB)	0. 5
Milli Q	10

Table 5-1. T7 endonuclease assay solution.

Following digestion 5 µl of DNA loading buffer was added and products resolved on a 12 % DNA PAGE gel

5.2.7 BrdU cell proliferation assay

The BrdU Cell Proliferation Assay Kit was purchased from Cell Signaling Technologies (#6183) and carried out as per manufacturer's instructions. Briefly, cells were plated in a 96-well plate at 10,000 cells/ well and incubated in growth medium for 24 hours. Growth medium was used to dilute BrdU solution to a 1X concentration and 100 µl of the solution was added to each well. Plate was again incubated for 24 hours. Growth medium/ BrdU solution was replaced with 100 µl Fixing/Denaturing Solution and incubated at room temperature for 30 minutes. Solution was replaced with 100 µl/ well of 1X detection antibody solution and incubated at room temperature for 1 hour. Wells were washed 3 times with Wash Buffer and 100 µl of HRP-conjugated secondary antibody solution was added per well. Wells were again washed 3 times with Wash Buffer and replaced with 100 µl 3,3',5,5'-Tetramethylbenzidine (TMB), a HRP substrate, before incubation at room temperature for 30 mins. After addition of 100 µl STOP solution, absorbance was read at 450 nm on a FlexStation3 PlateReader.

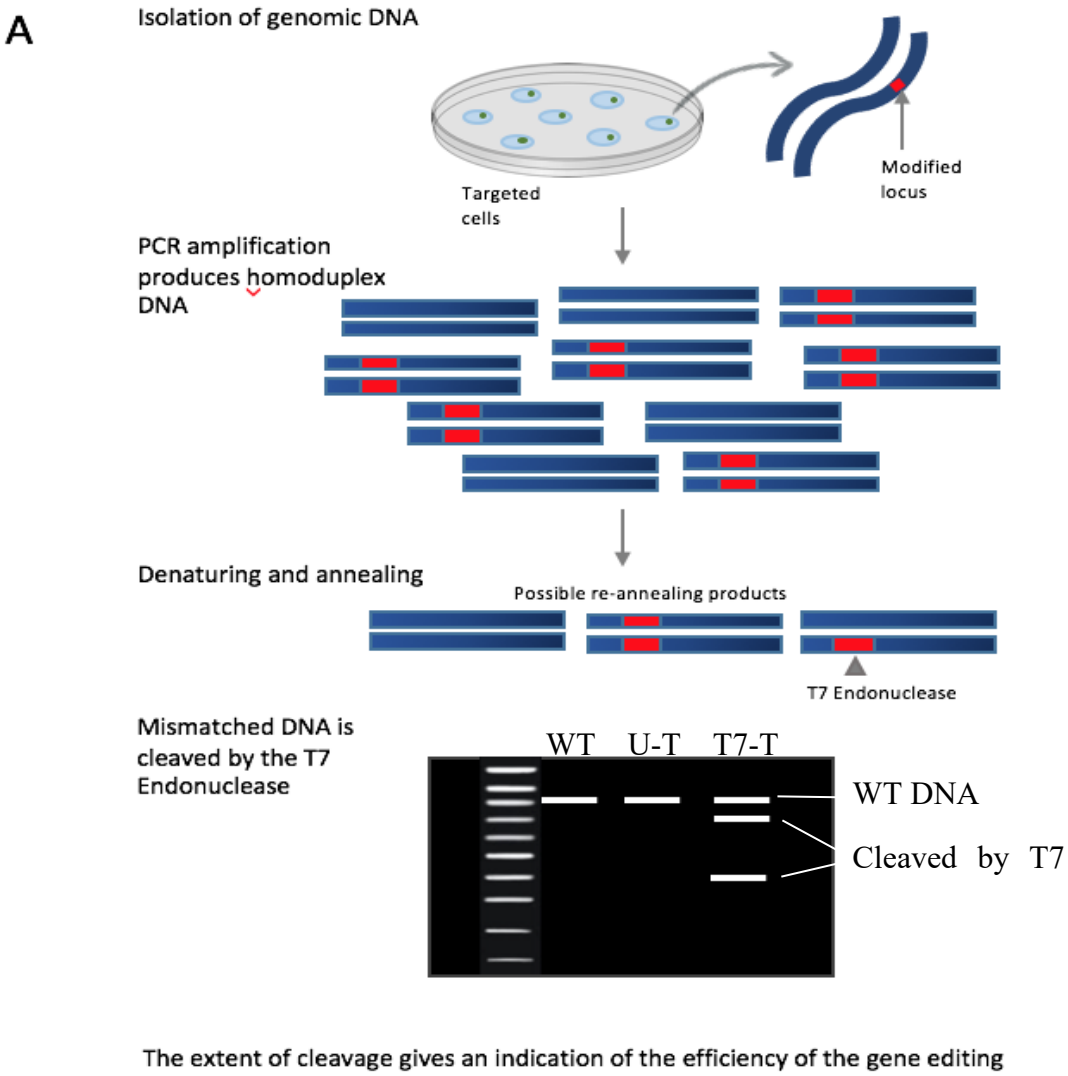

Figure 5.2. Schematic diagram of T7 endonuclease assay.

Cells are collected and genomic DNA is extracted using methods previously described, either with tail lysis buffer or using sodium hydroxide. Using a simple PCR reaction, the region spanning the modified locus is amplified. This generates amplicons of homoduplexed DNA. During the T7 endonuclease assay, amplicons are denatured and annealing in a cycling mechanism generating heterodimers which can be cleaved by the T7 endonuclease. The reaction is then run on a DNA PAGE gel. Cleavage of the heteroduplexed locus is indicated by bands below the wildtype region, indicating efficiency of CRISPR/Cas9 cleavage. WT – wildtype and untransfected, U-T – transfected but untreated with T7 endonuclease, T7-T – transfected and treated with T7 endonuclease.

5.2.8 DNA PAGE

For optimal resolution of PCR products following T7 assay, a 12 % native polyacrylamide gel was used. PCR products obtained direct from direct genomic extraction PCR or T7 assay were loaded and electrophoresed at 140 V for an appropriate time to allow separation.

	#µl
Acrylamide/Bisacrylamide	7.5
2x TAE buffer	2
Milli Q	0.5
0.1% Ammonium Persulphate	10
TEMED	30

Table 5-2. DNA PAGE gel solution.

Following electrophoresis gels were stained with Ethidium Bromide in TAE for 30 mins prior to visualisation.

5.2.9 Mitochondrial Ca^{2+} measurements

To measure agonist-evoked increases in $[Ca^{2+}]_m$, HaCaT keraitnocytes were transfected with pcDNA3.1+/mit-2mutAEQ using Lipofectamine 2000 as per Manufacturer's instructions on coverslips. 24 hours post transfection, cells were loaded with wildtype coelentrazine (2.5 µM) in the presence of EGTA/HBS. After 30 minutes, cells were superfused with fresh EGTA containing HBS before superfusion with 1 mM Ca^{2+} (HBS).

5.3 Results

5.3.1 Guide cloning

Using the online broad library, a number of guide sequences were selected in order to knock-out a region of the MCU gene that would stop the functional MCU protein being translated. Guides were positioned, where possible, spanning exons 1, 2 and 3. Exon 3 guides are shown in panel A of Figure 5.3. Each guide was cloned into the LentiCrispr V2 plasmid as described in Section 5.2.5 and depicted in panels B & C of Figure 5.3. Once the guides were cloned and screened using PCR, they were then sequenced using Sanger sequencing for confirmation (Figure 5.4)

5.3.2 Initial transfections

As all guide sequences were correct, they were therefore grown into a larger volume and maxi-prepped. Following this, 1 μg of each plasmid was transfected into HEK293 cells. Additionally, guides were co-transfected with their respective partners within the same exon. Following a 72 hour incubation, genomic DNA was extracted. DNA was re-suspended in nfH_2O and using PCR, exons were individually amplified. Exon 1 did not produce any PCR products so this was discarded (data not shown). Exon 2 produced two consistently sized bands as observed in panels A and B of Figure 5.5. Exon 3 produced 1 or 2 bands with the second band appearing slightly below the original size (Figure 5.5 C&D). Co-transfection of Guide#1 and Guide#2 resulted in a lower band, showing a deletion of ~120 base pairs. To investigate further, these guides were retransfected again both individually and co-trasnfected. The lower band is clearly observed (Figure 5.6A), with the deleted region matching up to the predicted region between the two guides Figure 5.6B)

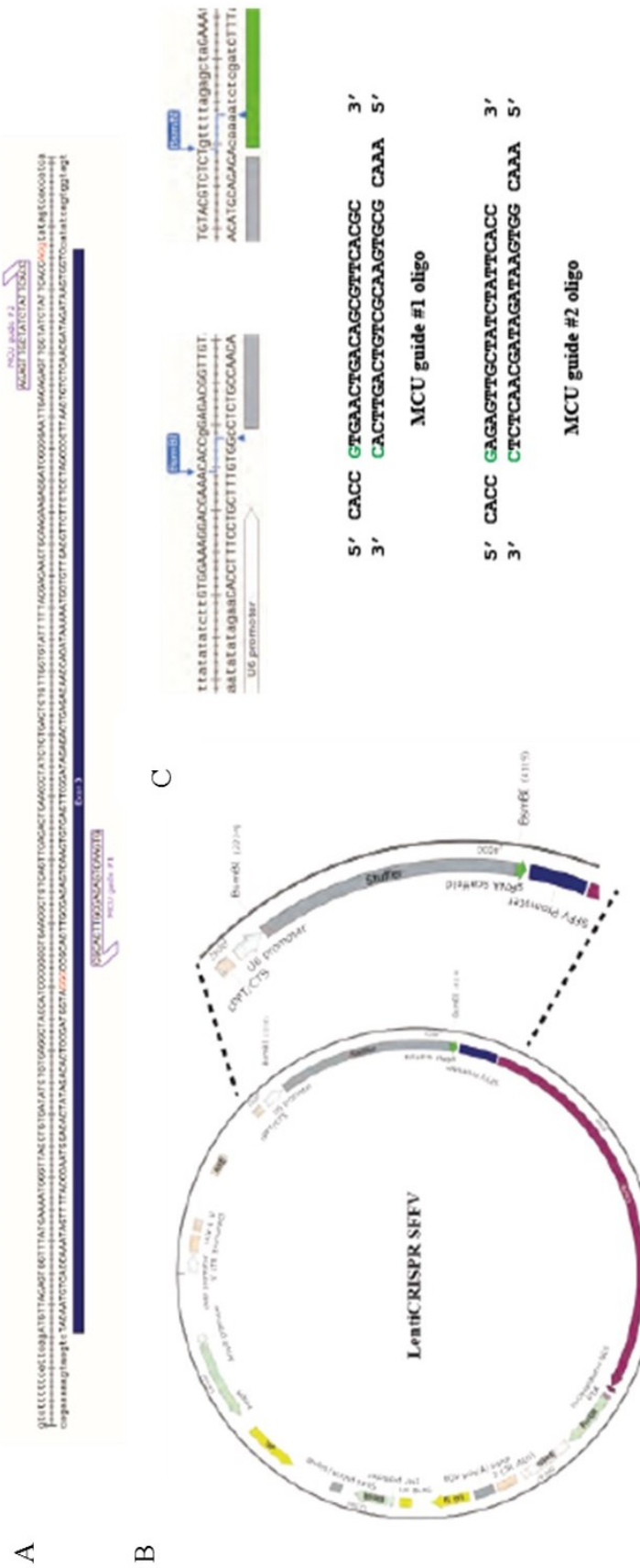

Figure 5.3. Single CRISPR guide cloning.

The CRISPR/Cas9 system is an efficient method of inducing double strand breaks that are sufficient to lead to knockout of the gene. In order to identify gene knockout quickly, two guide sequences (that target the system), were placed at each end of the MCU exons (exon 3 shown in A.). LentiCRISPR SFFV plasmid was digested with BsmB1 (NEB) to remove the stuffer sequence (B) to allow ligation of the guide oligo's (C).

Figure 5.4. Single CRISPR guide cloning continued.

The CRISPR/Cas9 system is an efficient method of inducing double strand breaks that are sufficient to lead to knockout of the gene. Once guides had been cloned into the LentiCRISPR guide plasmid as described, colonies were screened for the insertion of the guides into the plasmid using colony PCR as described. Reaction mixes were run on a 1.5 % agarose gel for identification of a band at the correct weight. Once colonies had been identified that contained the correct insert, DNA was extracted using a Qiagen Maxiprep kit as per manufacturers instructions and plasmid DNA was sequenced using a Sanger Sequencing service. As can be observed in (B), guide sequences had ligated into plasmid as expected. This process was repeated for each guide.

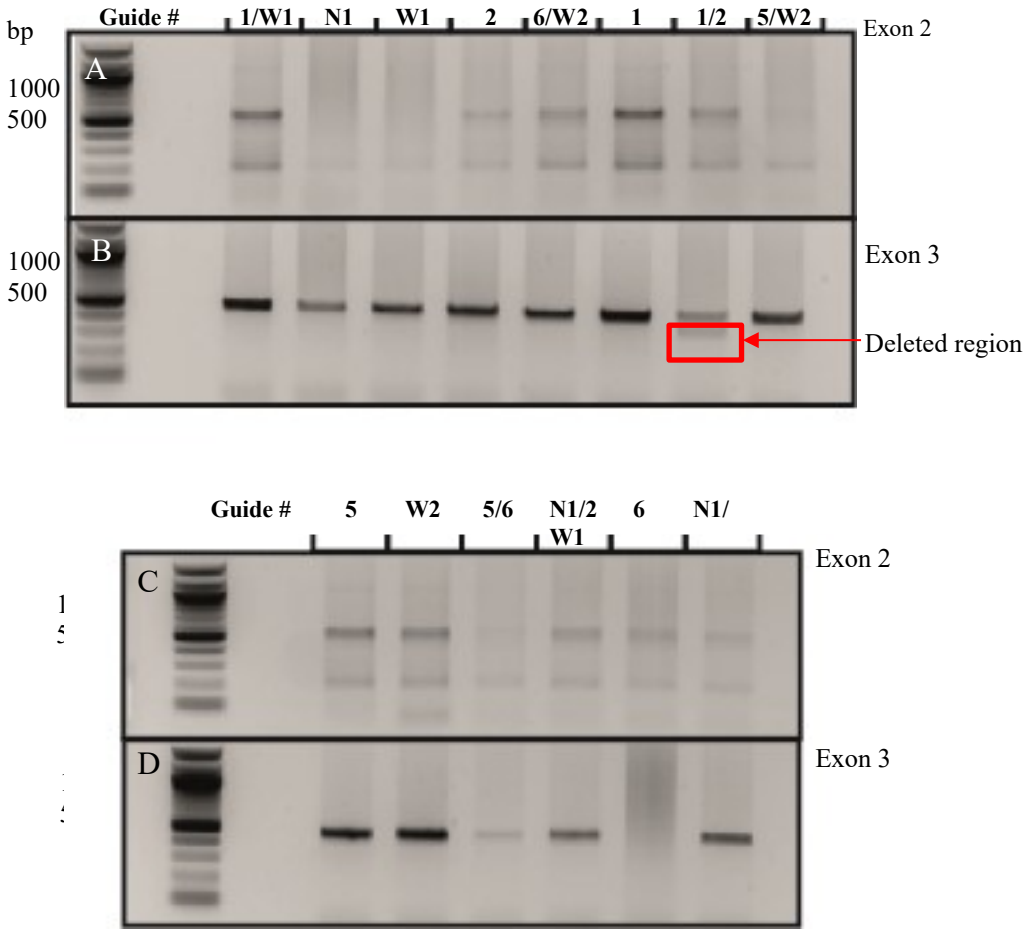

Figure 5.5. Initial guide transfections.

HEK293 cells were transfected with guides using the JetPrime method previously described. Guides were transfected individually and as pairs within the same exon to identify combinations that lead to a noticeable shift in the amplicon size. 72 hours post-transfection, genomic DNA was extracted using tail lysis buffer as described and using PCR for exon 2 (A&C) or exon 3 (B&D) samples were amplified. The PCR reaction mix was then run on 1.5 % agarose gel using NEB 100 bp DNA ladder. For exon 2, a double band can be observed for every guide or guide pair. For exon 3, a single band could be observed. However, using Guides#1 & #2, a second band, lower than the wildtype exon can be observed. This is likely due to the deleted region between the guide sequences.

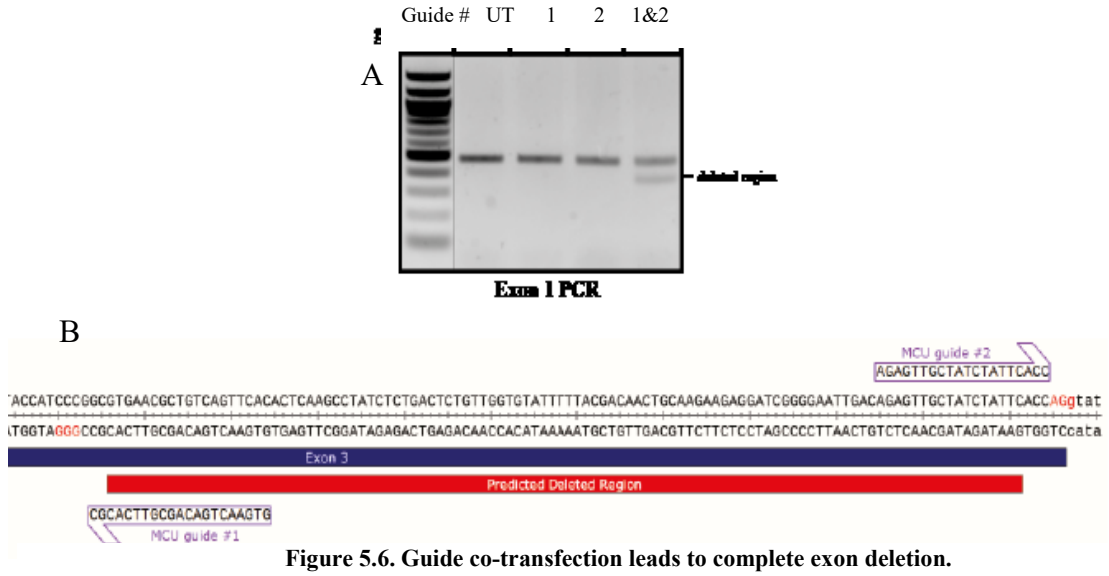

Figure 5.6. Guide co-transfection leads to complete exon deletion.

A) HEK293 cells were transfected with guide #1, guide #2, and guide #1 + guide #2. B) Predicted deleted region using two guides flanking the exon. Image created using SnapGene.

5.3.3 Deletion efficiency

A T7 assay was used to identify mismatched DNA bases that had occurred due to deletion of bases, small enough to not be resolved on an agarose gel. Using a DNA PAGE gel the deletion by the co-transfection of guide#1 and guide#2 in Exon 3 was much clearer, with smearing observed at the top of the gel (Figure 5.7A). Following the T7 endonuclease assay, the smearing had disappeared and there were now bands underneath, these bands indicate mismatched DNA (Figure 5.7B). Transfection of Guide#1 did not generate mismatched DNA and is therefore very inefficient. However, Guide#2 generated two lower bands, although very light some deletion has occurred. With co-transfection, the endogenous exon 3 band is much lighter, the lower band identifying the ~ 120 bp deletion is clear, with two lower bands highlighting deletion of just a few base pairs. Interestingly, both guides appeared to act more efficiently when co-transfected as opposed to individually (Figure 5.7).

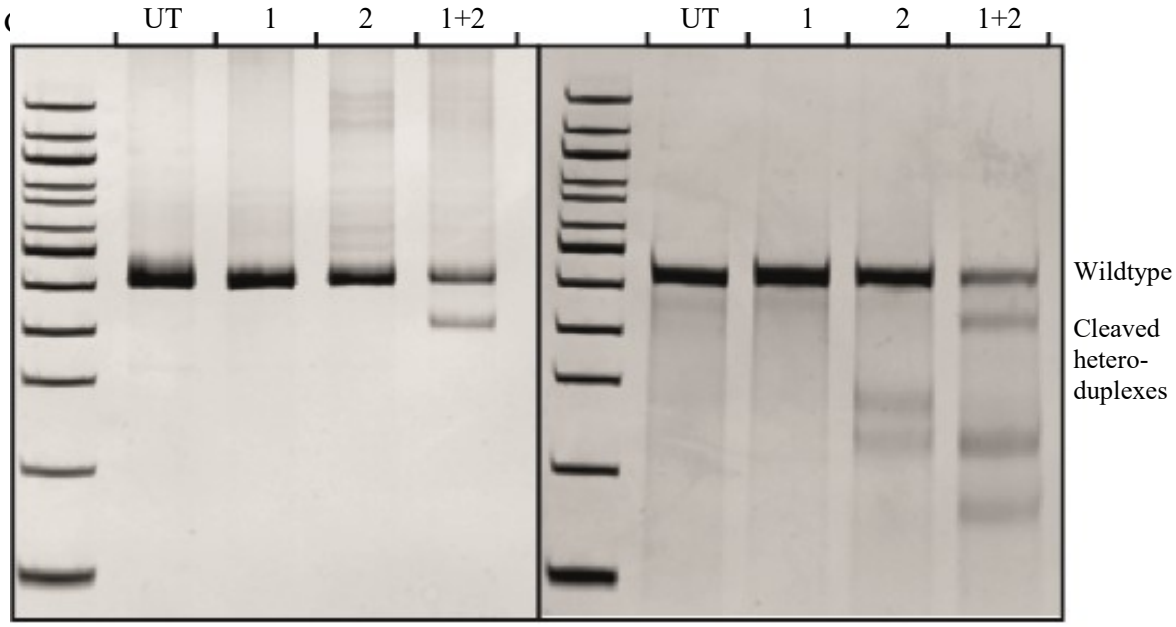

Figure 5.7. T7 endonuclease assay.

HEK293 cells were transfected with guide plasmids 1, 2, and co-transfected with both as previously described using JetPrime. Cells were maintained in transfection mix for 72 hours, following this genomic DNA was extracted and exon 3 was amplified using PCR. A T7 endonuclease assay was carried out as per manufacturer's instructions on half of the PCR reaction. The reaction mixes were run on a 12 % native polyacrylamide gel. Panel A shows before incubation with T7 endonuclease, where the expected size for exon 3 can be seen in the untransfected, single guides, and also as an upper band in the cotransfected. Here, a lower band can also be seen with the cotransfected as seen previously. Here, there are also smears at the top of the gel, these can be attributed to heteroduplexes of cleaved and uncleaved DNA, as this generates 'bubbles' in the double strand and therefore affected migration. Panel B shows post incubation with T7 endonuclease. The smears above the bands are now cleared as these were digested by the T7 endonuclease and can now be seen as bands below the wildtype region. Interestingly, both guides appeared more efficient when co-transfected, with more bands below the wildtype. UT - untransfected.

5.3.4 Double guide cloning

To negate the need to co-transfect, the two guides were cloned into the same LentiCrispr V2 plasmid, each with individual promoters. Firstly, plasmids containing single guides were digested using EcoRI to allow insertion of the other guide cassette (Figure 5.8A). Entire cassettes were amplified using PCR (Figure 5.8B) and ligated into the other guides' plasmid (Figure 5.8C). Generating two heteroduplexed guides in opposite conformations.

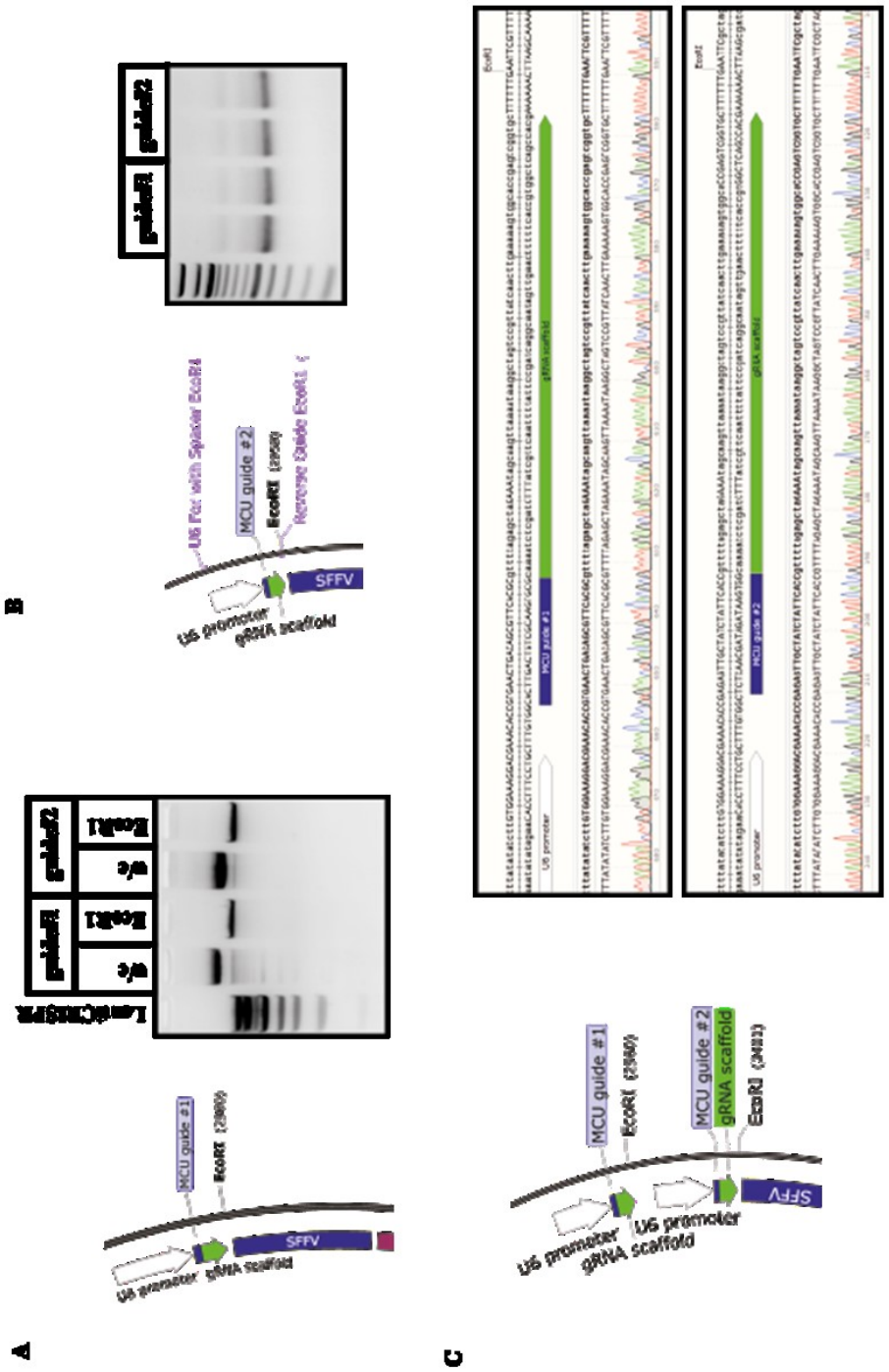

Figure 5.8. Multiplexing MCU guides into LentiCRISPR V2.

Linearisation of LentiCRISPR using EcoR1 downstream of the MCU guide cassette. B). PCR amplification of MCU guide cassettes. C) Schematicand sequencing of multiplexted guide sequences in LentiCRISPR V2.

5.3.5 Transfection of multiplexed double guide

HEK293 cells were then transfected with single guides, co-transfected with both guides and transfected with the two double guides, one with Guide#1 followed by Guide#2 and the other with Guide#2 followed by Guide#1. With the double guides, the efficiency of deletion seemed even more pronounced (Figure 5.9). Guide#1+2 was then run on a DNA PAGE gel for increased resolution of the separation of the two bands. The two bands were extracted, purified and sequenced using Sanger sequencing (Figure 5.10). As shown, the deleted region sits 3 base pairs from the PAM sequence as expected (Figure 5.10).

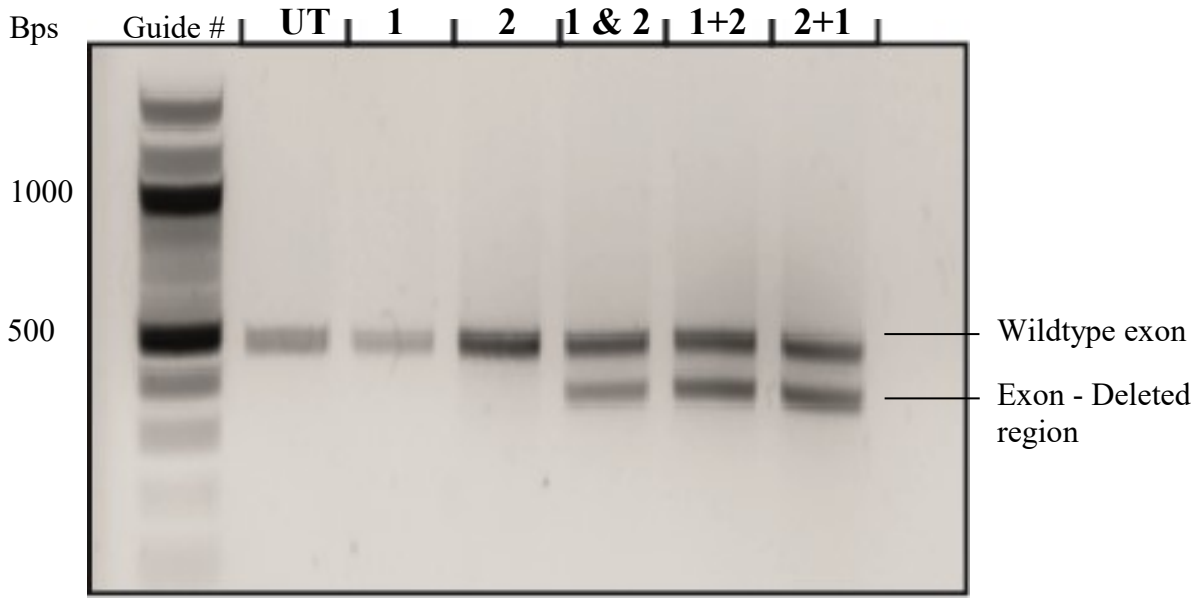

Figure 5.9. Transfection of multiplexed guides.

HEK293 cells were plated and transfected with guides as described previously using JetPrime transfection reagent in a 6-well plate. The first well was untransfected (UT), guides #1 and #2 were transfected individually and together (1 µg total DNA). Cells were also transfected with multiplexed guides of #1+2 and 2#1/ 72 hours post transfection, each well of cells was collected, and genomc DNA extracted using tail lysis buffer as described. Using PCR and primers directed to exon 3, the exon was amplified. In UT, guide #1, and guide #2, only the expected size of the amplicon can be observed as expected. Following cotransfection and transfection of multiplexed guides, a lower band can be observed. This is the expected size of exon 3 with a region deleted between the guides, resulting in a smaller amplicon. UT – untransfected. Ladder used is NEB 100 bp ladder.

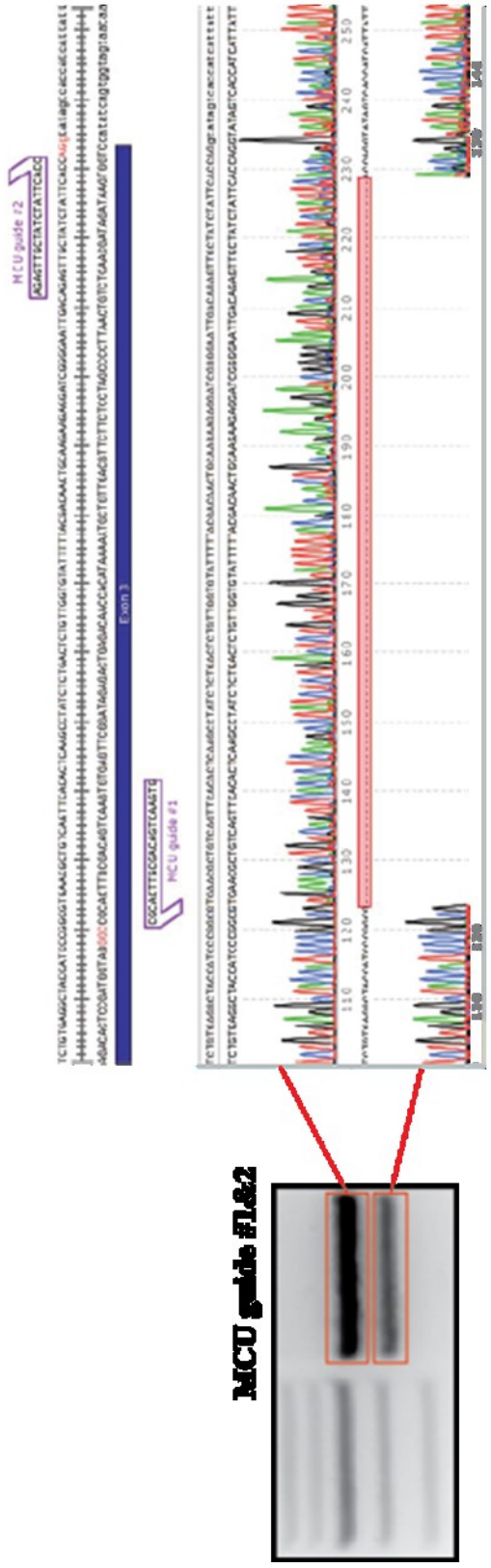

Figure 5.10. Sequencing deleted region.

PCR products were extracted from agarose gel, purified and sequenced. Chromatographs were aligned using SnapGene.

5.3.6 Antibiotic selection

In order to both assess the transfection efficiency and also effectively remove non-transfected, and therefore by assumption non-cleaved DNA, a puromycin selection gene was included into the plasmid. Previously in my laboratory, a selection curve identified 1-3 µg/mL puromycin the most effective for selection of most cells including HEK293 and HaCaT keratinocytes.

HEK293 cells were transfected with guide #1+2 and were treated with either 1 µg /ml or 2 µg /ml of puromycin (72 hours post-transfection). Transfected cells appeared healthy and largely undisturbed 48 hours after 1 µg /ml puromycin treatment, with slightly more cells appearing rounded up using 2 µg/ ml puromycin. However, in untransfected cells, a large number had begun to round up and die in 1 µg/ ml. With 2 µg/ ml, almost all the cells had died.

To assess the transfection efficiency after 24 hours, both concentrations of puromycin were added to cells 24 hours post-transfection. More cells appeared morphologically unhealthy to the control in both concentrations. Alluding to a lower transfection efficiency. These cells, along with untransfected, transfected yet unselected, and selection post-72 hour transfection were all harvested for genomic DNA extraction. Previously harvested cells were used as a PCR control here. Addition of puromycin appeared to ‘enhance’ the lower band compared to that of the control, especially when added 24 hours after transfection. Additionally, 2 ug/ ml puromycin had a stronger lower band than 1 ug/ ml compared to the control and also the untreated. Cells were taken from the 2 µg/ ml pool, 72 hours post-transfection and counted before seeding into a 96 well plate, 0.5 cells/ well.

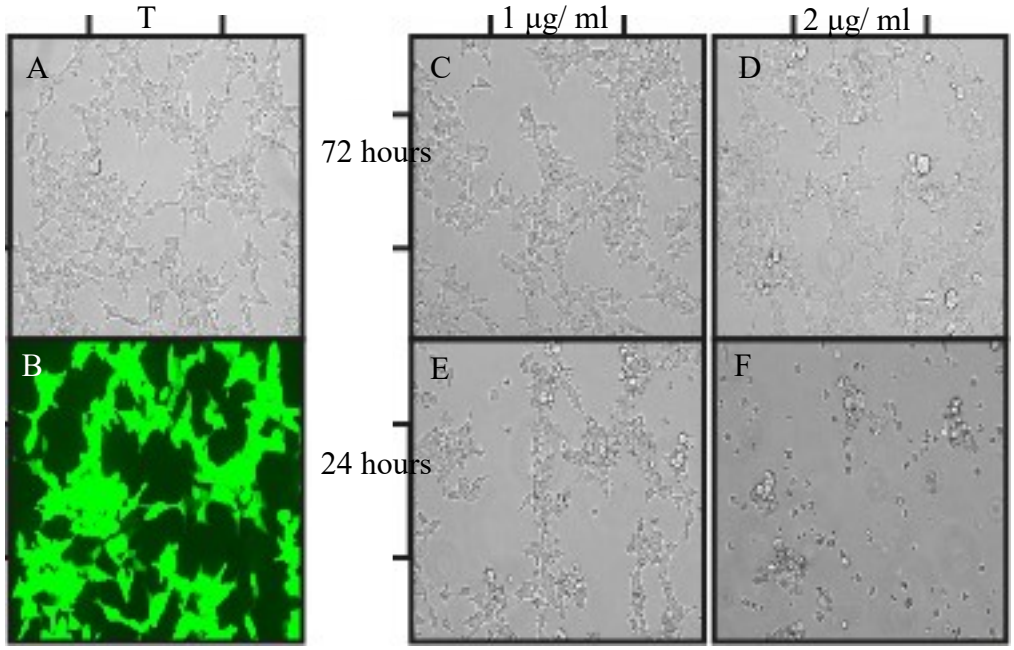

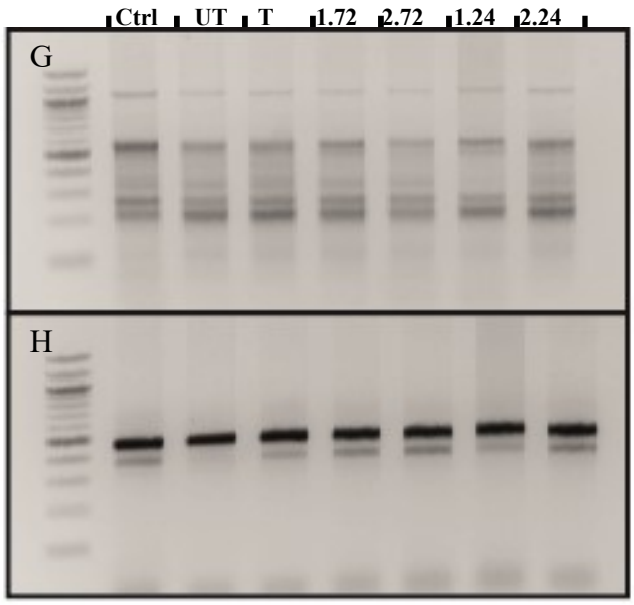

Figure 5.11. Antibiotic selection of CRISPR-Cas9 positive cells.

HEK293 cells were transfected with guide #1+2 and treated with puromycin 72 hours or 24 hours later. 48 hours after puromycin treatment cells were imaged using an EVOS FLoid Cell Imaging Station (LifeTechnologies #4471136). A&B) HEK293 cells transfected with a GFP control, highlighting no apparent transfection induced cell death. C&D) 72 hour post-transfection HEK293 cells treated with puromycin for 48 hours, E&F) 24 hour post-transfection HEK293 cells treated with puromycin for 48 hours. Ctrl – PCR control of previous sample. UT – untransfeced cells. T – transfected but not selected.

5.3.7 Genomic extraction optimisation for 96-well plates

In order to screen clones in 96 well plates, an efficient and sensitive method needed to be identified. Initially, wild type HEK293 cells were plated into a 96 well plate and allowed to reach confluence. Firstly, to test the use of Tail Lysis Buffer (TLB) for extraction, TLB was added to wells in triplicates, at 50 µL, 75 µL, and 100 µL. The first set was incubated at 55 °c for 30 mins before 10 mins at 95 °c, once the reaction had cooled to ~ 16 °c, 1 µL, 2 µL, or 4 µL of this reaction mix was used in a 10 µL PCR reaction. This method did not produce any bands as shown in Figure 5.12. The same amounts of TLB were added to other wells, this time incubated at 55 °c for ~ 16 hours before 95 °c for 10 mins and immediate PCR. Although bands were observed here, they were very faint alluding to an inefficient method. A documented method in our laboratory is the use of sodium hydroxide (NaOH) to lyse cells for genomic PCR. Therefore 25 mM NaOH with 0.1 mM EDTA was added to wells, again in triplicates with 50 µL, 75 µL, and 100 µL. The samples were incubated at 95 °c for 10 mins and 1 µL, 2 µL or 4 µL of this reaction was used in a 10 µL PCR reaction. Bands were not always seen when 1 or 2 µL was used in the PCR reaction however 4 µL appeared to produce bands for every amount of NaOH added (Figure 5.14). Before the samples were frozen for storage, 10 % 1M Tris-base was added to quench to NaOH. However, following this, a repeat PCR reaction was no longer successful.

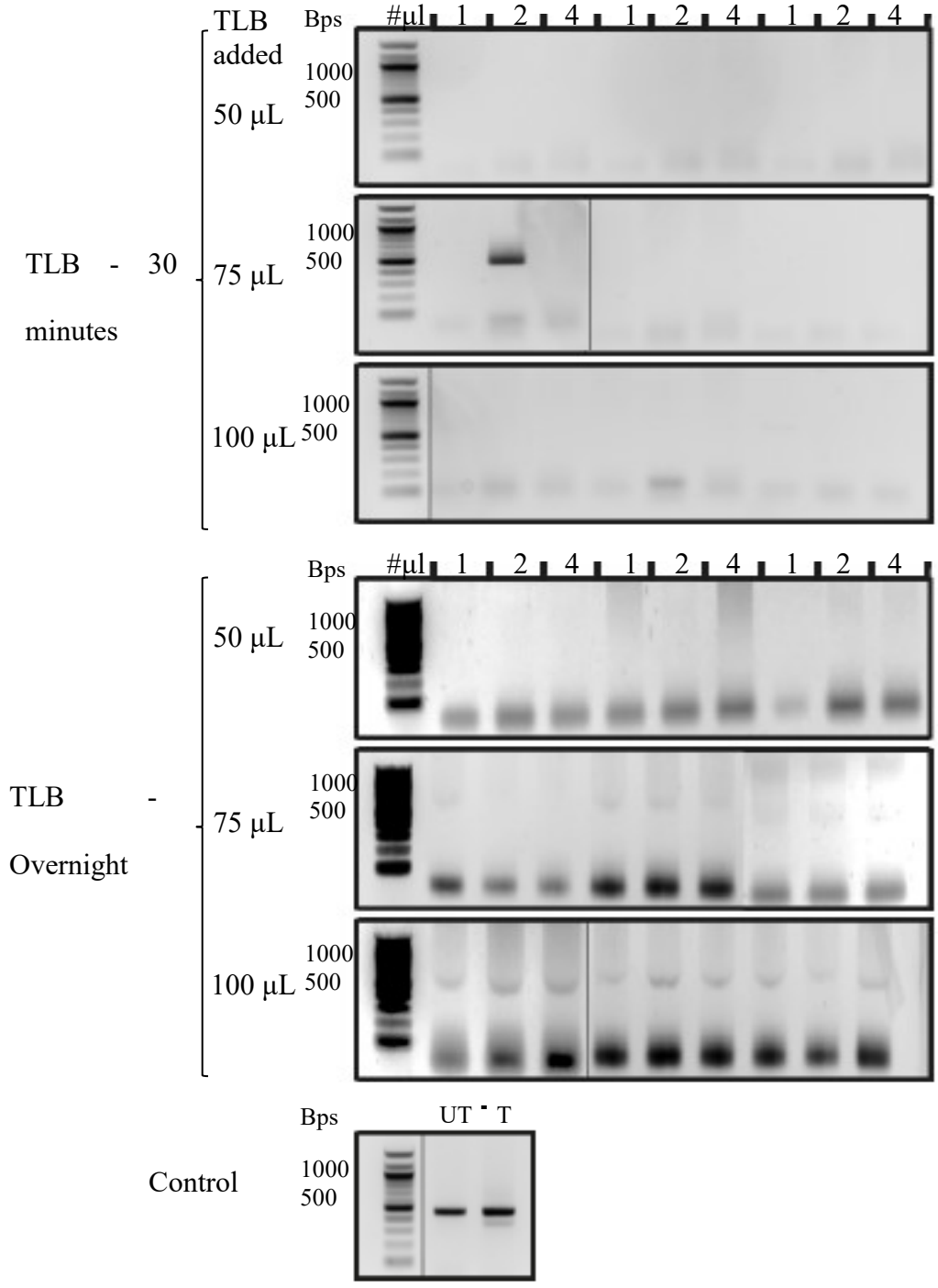

Figure 5.12. Tail Lysis Buffer for genomic extraction from 96-well plates.

Wildtype HEK293 cells were used to investigate the efficacy of TLB to extract genomic DNA from a small number of cells (confluent 96-well plate well). TLB was added in triplicates at 50 µL, 75 µL, and 100 µL. The first set was incubated at 55 °c for 30 mins before 10 mins at 95 °c, once the reaction had cooled to ~ 16 °c, 1 µL, 2 µL or 4 µL of this reaction mix was used in a 10 µL PCR reaction. Overnight reactions were incubated at 55 °c for ~ 16 hours before 95 °c for 10 mins and immediate PCR Only one replicate, 75 µL TLB for 30 mins and 2 µL for PCR reaction generated a clear band at ~ 500 bp, and only once in triplicate. UT – untransfected, T – transfected . Ladder – NEB 100 bp.

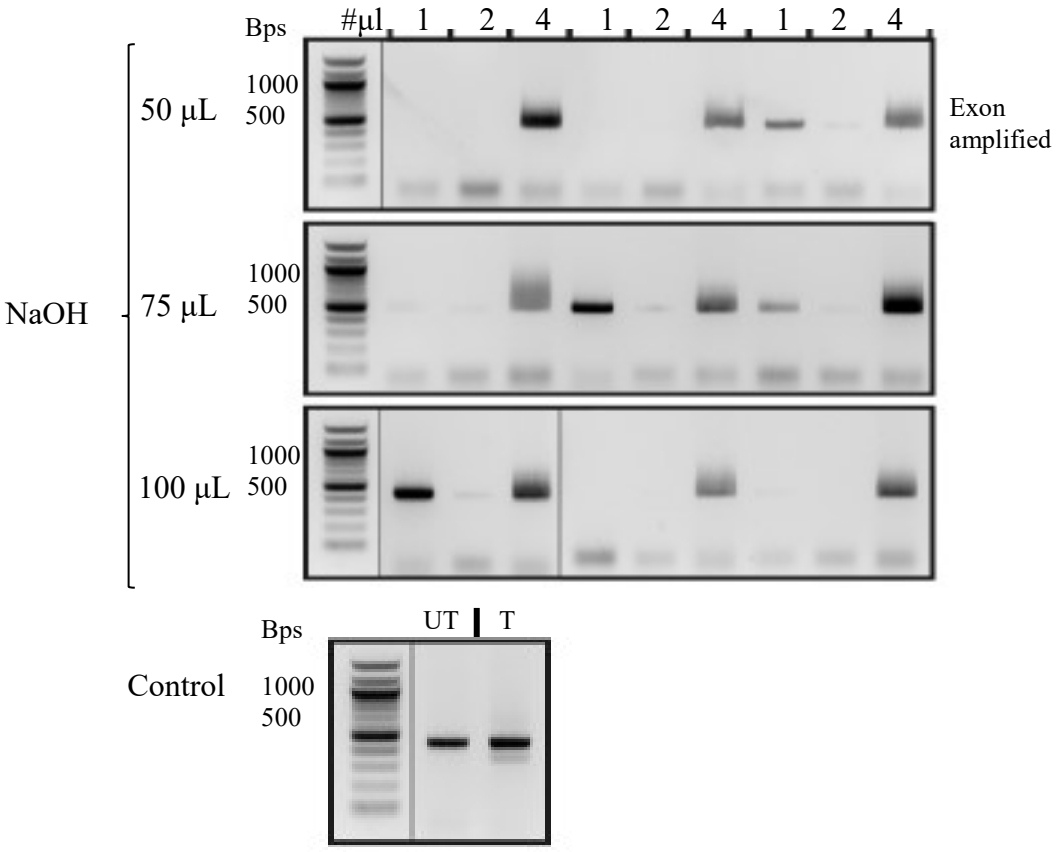

Figure 5.14. Sodium hydroxide for genomic extraction from 96-well plates.

Wildtype HEK293 cells were used to investigate the efficacy of 25 mM NaOH with 0.1 mM EDTA to extract genomic DNA from a small number of cells (confluent 96-well plate well). NaOH was added in triplicates at 50 µL, 75 µL, and 100 µL. The samples were incubated at 95 °c for 10 mins and 1 µL, 2 µL or 4 µL of this reaction was used in a 10 µL PCR reaction to amplify exon 3. Although a small number of samples that used 1 µL or 2 µL in the PCR reaction generated clear bands where expected, addition of 4 µL to the PCR reaction, at any amount of NaOH added generated a single band where expected similar to that of the transfected control. UT – untransfected, T – transfected.

5.3.8 Clone screening

Once single clones had reached confluence, they were split into duplicate 96-well plates and the above NaOH genomic screening method was employed. To each well, 50 µL 25 mM NaOH 0.1 mM EDTA was added, following a 10-minute incubation at 95 °c, 4 µL was used for PCR screening. Of the 4 columns screened (24 clones), 8 produced only the lower band, indicating complete deletion of the exon 3 region targeted (Figure 5.15). Surprisingly, there was a high number of heterogeneous clones as shown by a two bands. The 8 clones with a single lower band were selected, and cultured further before further genotyping using TLB to confirm the presence of only the lower band (Figure 5.16). Unfortunately, all of the clones contained both, although at varying percentages, of the bands. Looking back, all of the clones selected had a smear above the band in the original NaOH mediated extraction (Figure 5.15). This smear may be the small amount of upper band observed when using the more sensitive extraction method. As clone 11G contained the least amount of the upper band (Figure 5.16), these cells were used for a Western blot to identify if a reduction in protein could be observed. There was no visible band at ~ 37 kDa in the clone compared to the wildtype HEK293 cells (Figure 5.17).

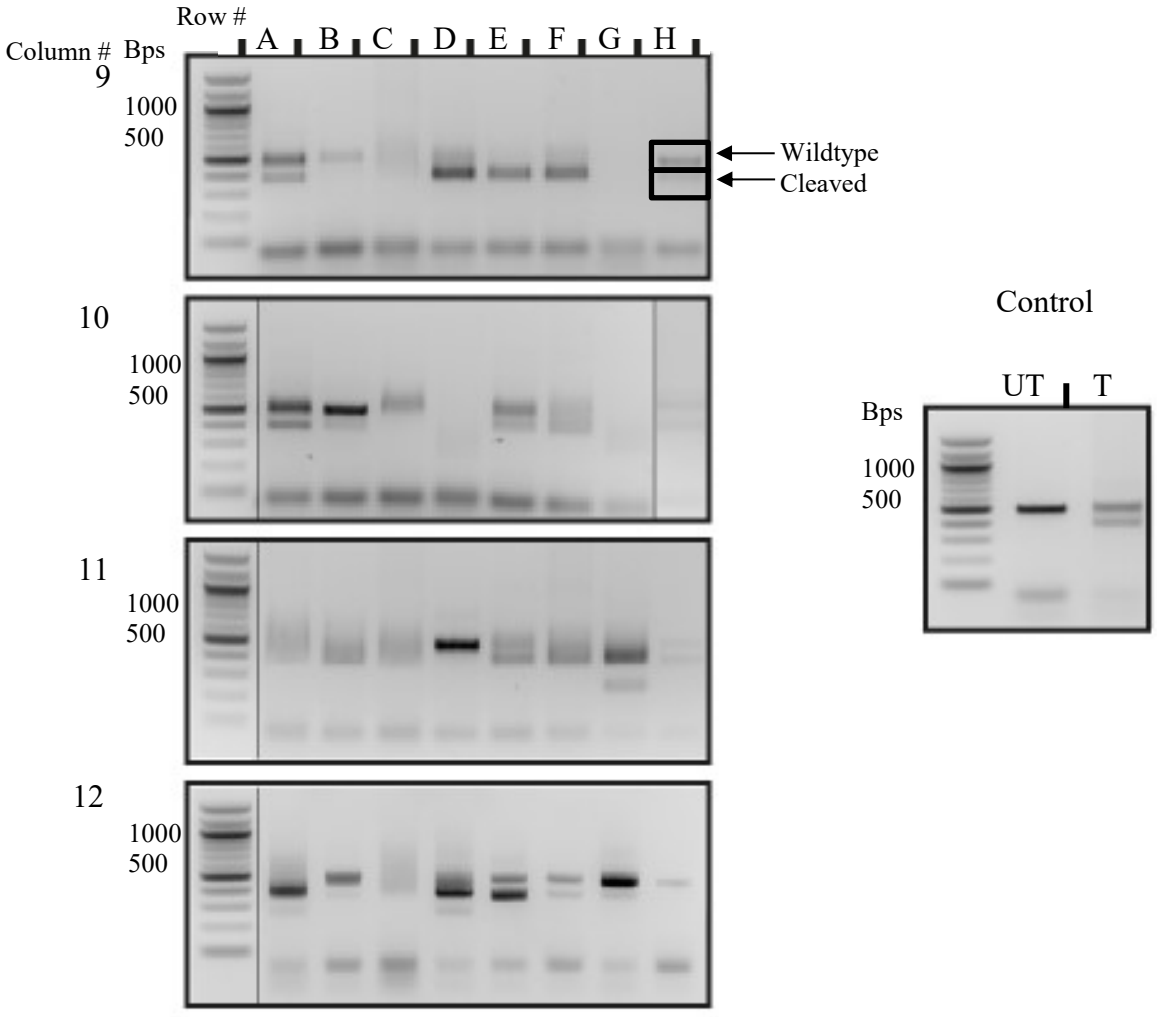

Figure 5.15. HEK293 MCU -/- clone screening.

HEK293 cells were transfected with guide #1+2, selected using puromycin as described previously and allowed to recover. Once confluence had reached, cells were plated at 0.5 cells/well in a 96-well plate. Again, once confluence had occurred, cells were split into 2 x 96 well plates therefore generating a duplicate. Both plates were allowed to reach confluence. Cells were collected and genomic DNA was extracted using NaOH as described. Using primers for exon 3 and PCR, each well was then screened for presence of only the lower band. Upper band represents wildtype exon 3 and therefore no deletion of expected region. Reaction mix was run on 1.5 % agarose gel. Smearing could be observed in many of the lanes, this could be due to presence of PCR reaction mix and acidic NaOH. However, 8 clones generated a clear single lower band. Clones were identified column/row number/letter respectively, e.g. 12E

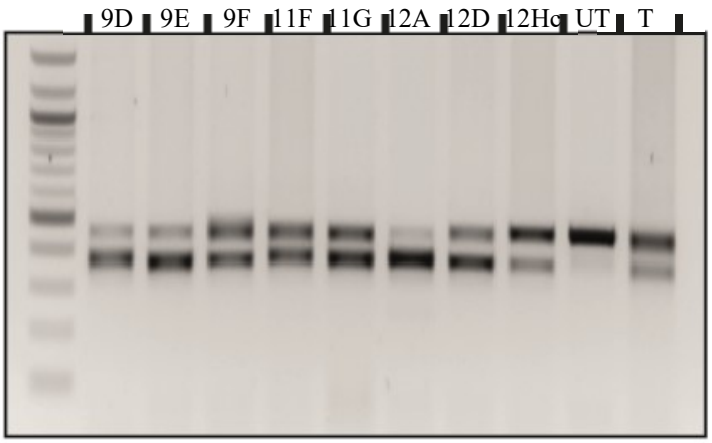

Figure 5.16. HEK293 MCU -/- clone selection.

In Figure 5.15 24 clones were screened, of which 8 appeared to have only the lower band. These clones were grown to confluence in larger wells before TLB was used to extract genomic DNA and loci were screened for the presence of the lower band. UT – untransfected, T - transfected

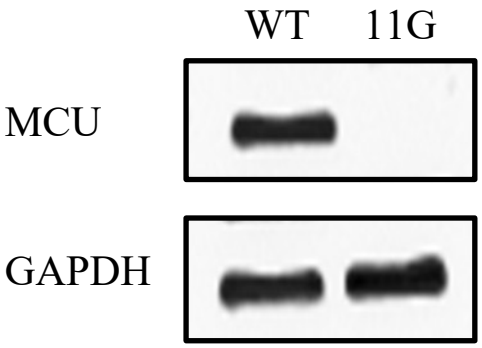

Figure 5.17. MCU protein is deleted in MCU -/- HEK293 clone 11G.

Western blotting was performed on clone 11G as described in Section 2.6.3. WT – wildtype HEK293 cells. GAPDH was used as loading control.

5.3.9 HaCaT keratinocyte clone generation

Once ablation of protein using the method employed so far had been confirmed, HaCaT keratinocytes were transfected with 1 µg Guide #1+2 after 72 hours puromycin was added in concentrations of 1 or 2 µg/ ml and allowed to recover. The cells were then genotyped using TLB. In contrast to HEK293 cells, 1 µg/ ml puromycin appeared to concentrate the lower band more than 2 µg/ ml, compared to 72 hours after transfection without selection. Therefore these cells were diluted and plated at 0.5 cells/ well of a 96 well plate. Again following recovery and passage into duplicate plates, HaCaT keratinocyte colonies were screened following NaOH mediated extraction. From 39 clones screened, 3 clones appeared to contain only the lower band, this time without smearing (Figure 5.18). These clones were termed 8G, 11E and 12D. Unfortunately, clone 11E did not survive passaging. Clones 8G and 12D were given time to reach confluency in a larger flask and genomic DNA was extracted using TLB. Compared to the transfected population, clone 8G contained no clear presence of the upper band (Figure 5.19). A western blot was performed and as with HEK293 cells, no band was observed at ~ 37 kDa (Figure 5.20), confirming ablation of the MCU protein.

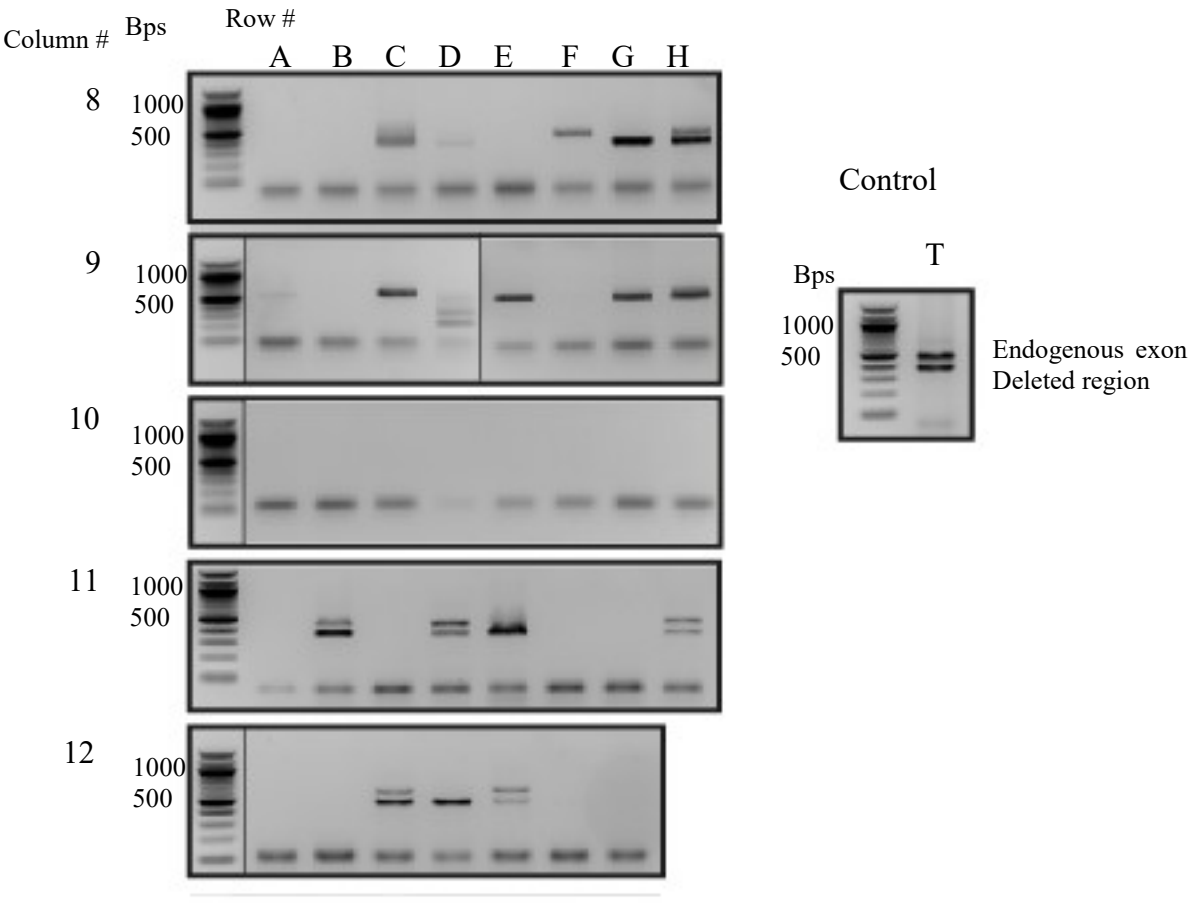

Figure 5.18. HaCaT keratinocyte MCU -/- clone screening.

HaCaT keratinocytes were transfected with guide #1+2 as described using JetPrime transfection reagent. 72 hours post transfection, cells were treated with puromycin and allowed to recover. Once confluency was achieved, cells were plated into a 96 well plate at 0.5 cells /well. Cells were then again allowed to reach confluence before colonies were split into two plates, generating a duplicate. Genomic DNA was extracted using NaOH as described before PCR using primers for exon 3. Reaction mix was run on 1.5 % agarose gel to identify amplification of exon 3. A large number of wells contained no cells or not enough to generate a signal. As with HEK293 cells, many wells contained heterogeneous clones (identified with 2 bands) and some appeared untransfected (presence of only endogenous upper band). A small number of wells contained colonies that led to a single lower band, the exon with deleted region removed. Clones were identified column/row number/letter respectively, e.g. 12E. T – transfected control

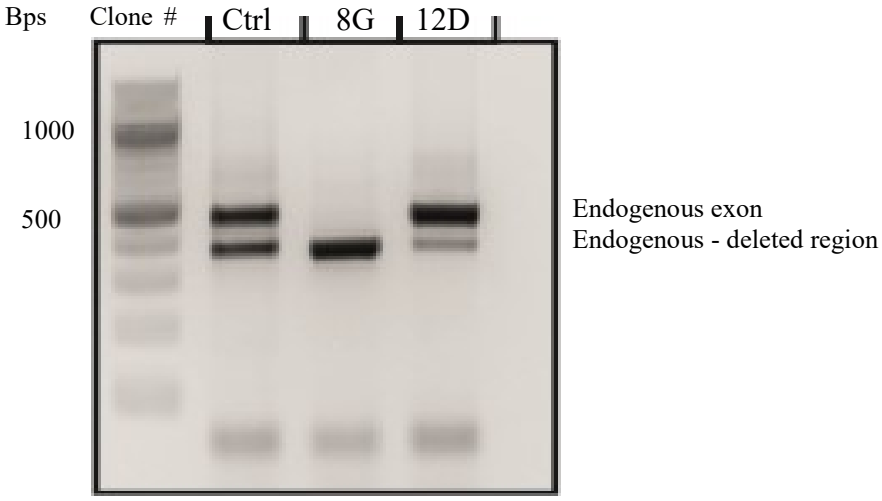

Figure 5.19. HaCaT MCU -/- clone selection.

In Figure 5.19 3 of the clones screened appeared to only have the lower band. These clones were grown to confluence and genomic DNA was extracted using tail lysis buffer as previously described. Using PCR with primers directed to exon 3, the region was amplified and reaction mix was run on a 1.5 % agarose gel.. In the transfected and non-puromycin selected control (ctrl(, two bands can be observed with the upper band the exogenous exon. The lower band is the exon with the expected deleted region removed. Clone 8G contains only the lower band, therefore homogenous for the deletion. Clone 12D contains mostly the upper band and therefore this was discarded.

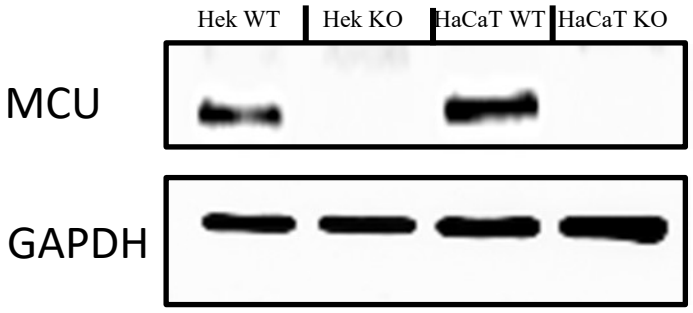

Figure 5.20. HaCaT MCU -/- clone is devoid of MCU protein.

Western blotting was performed to confirm ablation of MCU protein in wildtype HEK293 cells, clone 11G (HEK293 KO), wildtype HaCaT keraitnoyctes (HaCaT WT) and clone 8G (HaCaT KO) as described in Section 2.6.3. WT – wildtype cells. GAPDH was used as loading control.

5.3.10 Topical addition of Ca^{2+} initiates a transient increase in $[Ca^{2+}]_m$

HaCaT keratinocytes were grown in basal (0.03 mM) and differentiating (3 mM) medium and transfected with mutated aequorin. In both conditions, cells were transfected for 24 hours using lipofectamine 2000 and wild type coelentrazine (2.5 μM) was added 30 minutes prior to experiments in Ca^{2+} free HEPES buffered saline (+ 10 mM Glu). Upon superfusion with 1 mM Ca^{2+}, a transient increase in $[Ca^{2+}]_m$ was observed (Figure 5.21). In addition, low Ca^{2+} HaCaTs displayed an increased $[Ca^{2+}]_m$ peak compared to those grown in high Ca^{2+}. Alluding to a change in expression of MCU or its cofactors.

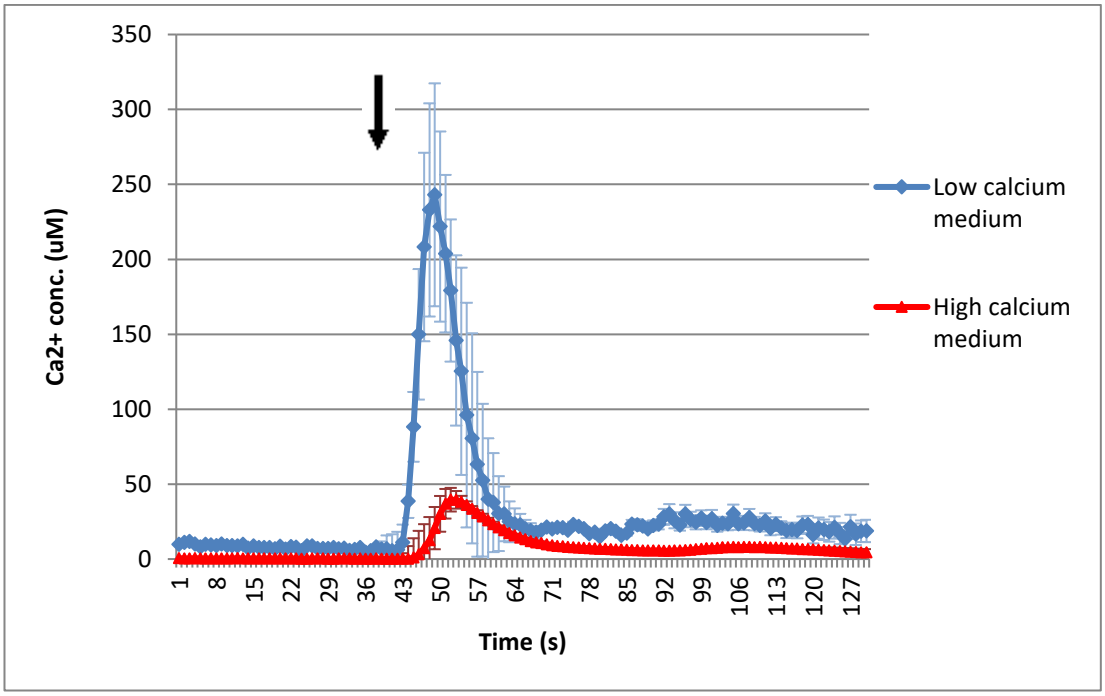

Figure 5.21. Mitochondrial Ca^{2+} transients in basal and differentiating HaCaT keratinocytes.

HaCaT keratinocytes that were grown in 0.03 mM or ~ 3 mM Ca^{2+}, were transfected with pcDNA3.1+/mit-2mutAEQ using Lipofectamine 2000 as per manufacturer's instructions on coverslips. 24 hours post transfection, cells were loaded with wildtype coelentrazine (2.5 µM) in the presence of EGTA. After 30 minutes, cells were superfused with fresh EGTA containing HBS before superfusion with 1 mM Ca^{2+} (HBS). Arrow indicates initiation of 1 mM Ca^{2+} superfusion. Error bars indicate SEM of 10 coverslips.

5.3.11 MICU2 is decreased in basal HaCaT keratinocytes

Western blotting of MCU in HaCaTs grown in low and high Ca^{2+} showed no change in MCU protein level (Figure 5.22A). This was confirmed using qPCR analyses (Figure 5.22B). Interestingly, a ~ 10 % decrease in MICU2, the MCU inhibitor, was observed (Figure 5.22B).

5.3.12 MCU -/- HaCaTs proliferate slower than wildtype HaCaT keratinocytes

Using a BrdU assay, the proliferation rate of wild type HaCaTs grown in high and low Ca^{2+} conditions was compared to MCU -/- HaCaTs grown in the same conditions (Figure 5.23). As expected, HaCaTs grown in low Ca^{2+} medium proliferate faster than those grown in high Ca^{2+} conditions (Figure 5.23). Interestingly, MCU -/- HaCaTs grow much slower in high Ca^{2+} than the control. The proliferation rate of MCU -/- HaCaTs is recovered when grown in low Ca^{2+} medium, although still lower than the wildtype in the same conditions (Figure 5.23).

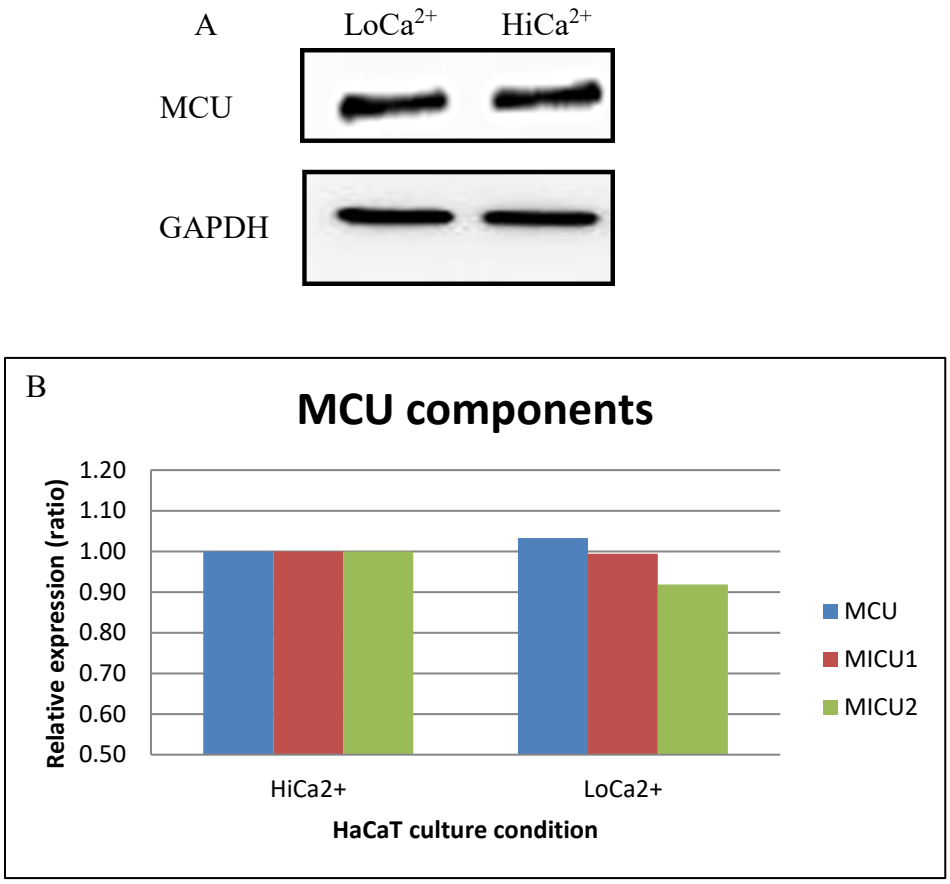

Figure 5.22. Western blot and qPCR analyses of MCU family expression.

HaCaT keratinocytes were grown in 0.03 mM or ~ 3.6 mM Ca^{2+} containing growth medium. These concentrations induce proliferation or differentiation respectively and the cells therefore mimic wildtype keratinocytes. A) Proliferationg ($LoCa^{2+}$) or differentiating ($HiCa^{2+}$) cells were used for Western blotting as described to identify any expression changes of MCU protein. As observed here, no change in protein expression was observed with this method. B) HaCaT keratinocytes grown in proliferating or differentiating conditions were collected for qPCR at the same time point to identify mRNA expression of MCU and also two of its regulators. qPCR was performed as described in Section 2.4. As in A), little change was observed in MCU mRNA expression. However, a ~ 10 % decrease in MICU2 was observed, the MCU inhibitor.

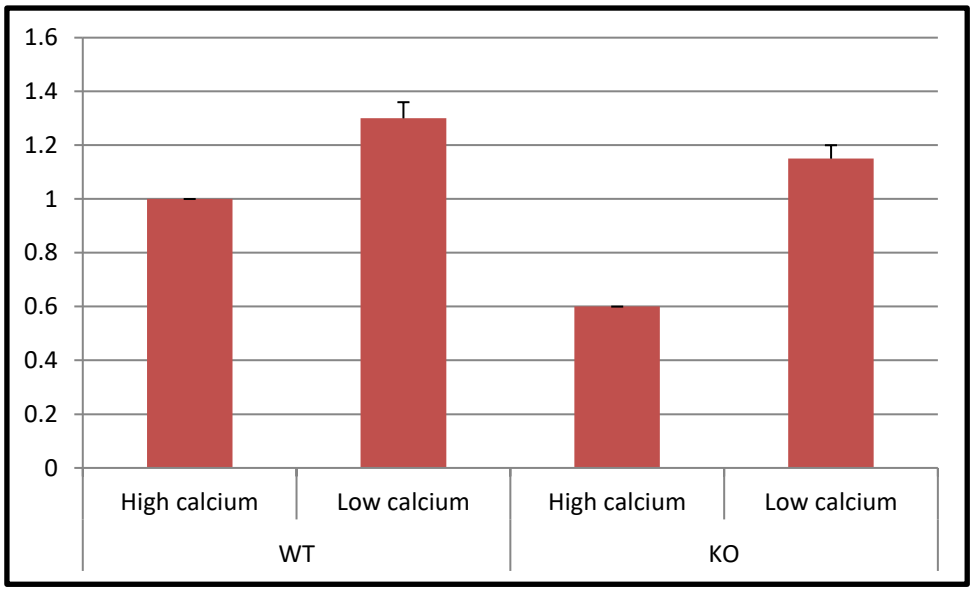

Figure 5.23. MCU knockout on HaCaT keratinocyte proliferation rate.

BrdU proliferation assay was performed as described. Briefly, 10,000 HaCaT keratinocytes were plated into 3 wells of a 96-well plate / condition. The 3 readings were averaged, and normalised to the average of the high calcium wildtype as this is the most common growth condition. This assay was run twice, in successive weeks, and data was averaged in total to generate graph. Therefore n = 6 for each bar.

5.3.13 Differentiating MCU -/- HaCaTs appear morphologically different from wildtype

As it was observed that HaCaT keratinocyte proliferation rate is affected by the deletion of MCU, the morphology was investigated. To ensure the process of deleting MCU had no effect on cell morphology, the HEK293 MCU -/- clone was imaged. There does not appear to be morphological difference compared to the wild type (Figure 5.24).

HaCaT keratinocytes grown in supplemented DMEM appear cuboidal whereas those grown in low Ca^{2+} appear more elongated, spindle-like as expected and discussed in Section 1.4 (Figure 5.24). MCU -/- HaCaT keratinocytes grown in high Ca^{2+} are characterised by an enlarged cytoplasm compared to the wild type (Figure 5.24). In addition, cell death appears to be increased, with more cells rounded up. In contrast, MCU -/- HaCaTs grown in low Ca^{2+} show a similar spindle-like morphology to the wild type (Figure 5.24).

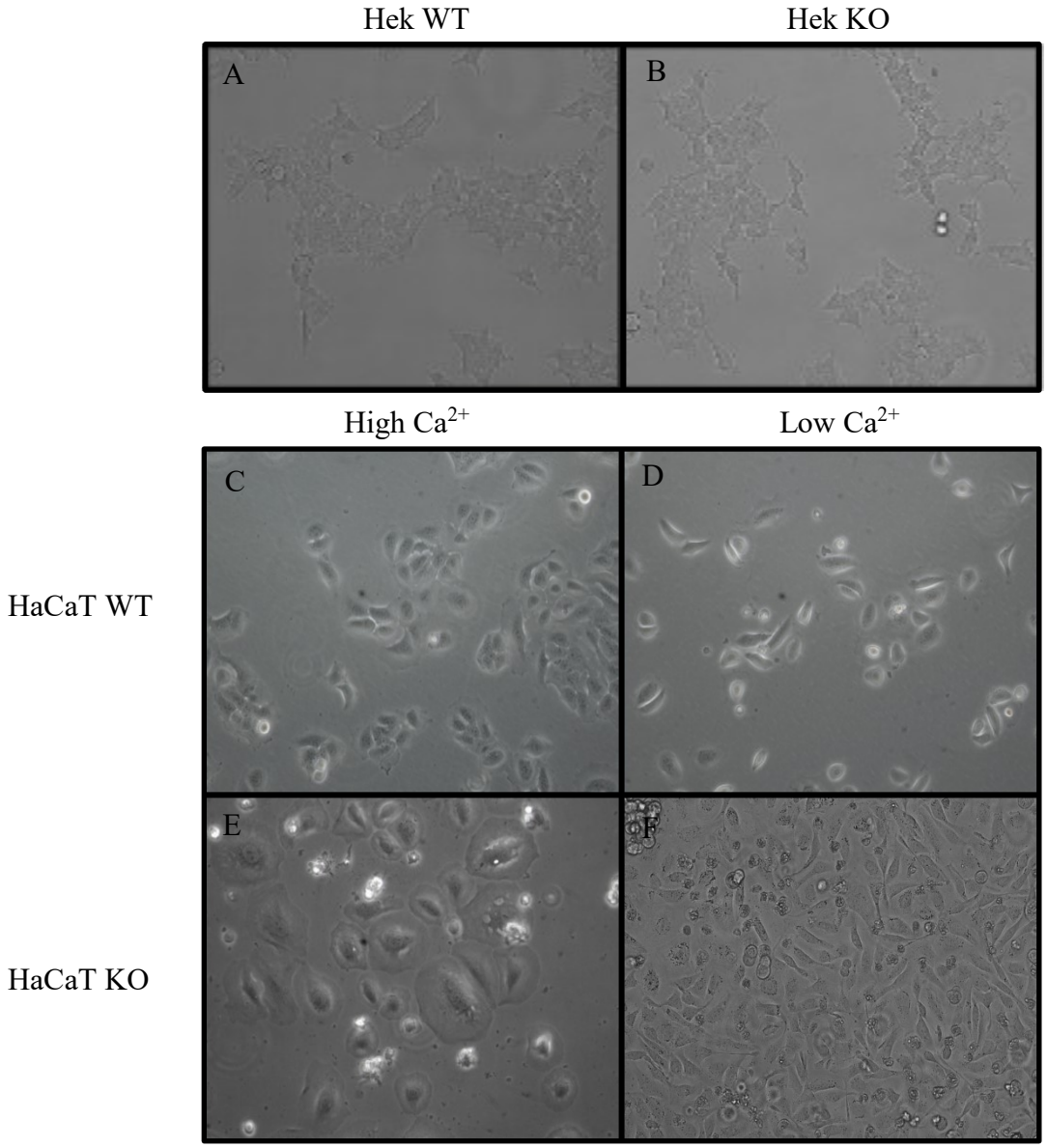

Figure 5.24. HEK293 and HaCaT keratinocyte MCU -/- cell morphology.

Cells were imaged using an EVOS Floid Cell Imaging Station with 20 X objective, 460X overall magnification with 0.45 numerical aperture. Camera used Sony 1.3MP 1/3" ICX445 EXview HAD CCD.

5.4 Summary

The aim of this chapter was to generate an MCU -/- HaCaT keratinocyte cell line and subsequently use this cell line to begin investigating the role of mitochondrial Ca^{2+} on epidermal differentiation. Initially, single guides were designed, with two guides directed to each exon. Following co-transfection into HEK293 cells of guides within the same exon, a clear deletion of ~120 bases could be seen in exon 3. This deletion was enough to inhibit translation of the MCU protein, as confirmed by western blotting. This process was repeated in HaCaT keratinocytes, with a single clone being generated that was devoid of MCU protein, again confirmed by western blot.

Western blot analyses identified no change in MCU protein level between HaCaT keratinocytes grown in high and low Ca^{2+} medium. This was confirmed with qPCR analyses. However, one of MCUs cofactors, MICU2, was increased by almost 20%. Mitochondrial aequorin experiments identified a larger accumulation of Ca^{2+} in HaCaTs cultured in low Ca^{2+} compared to those in high Ca^{2+} culture, in response to the topical addition of Ca^{2+}. Additionally, using BrdU proliferation assay, it was observed that HaCaT keratinocytes grown in the low Ca^{2+} medium were more proliferative than those in the high Ca^{2+} medium as expected. However, MCU -/- HaCaT keratinocytes grown in high Ca^{2+} had a dramatically reduced proliferation rate that was partly rescued when grown in low Ca^{2+}. Morphologically, MCU-/- HEK293 cells did not appear to be different from the wildtype. However, MCU -/- HaCaT keratinocytes appeared to have a larger cytoplasm than the wild type when grown in differentiating conditions. However the morphology recovered, to that of the wild type, when grown in proliferating conditions.

5.5 Discussion

In this study, the CRISPR/Cas9 system was used in order to delete the MCU protein and use the subsequent cell line, to investigate the role of MCU keratinocyte proliferation state, morphology and allow a deeper investigation into the role of $[Ca^{2+}]_m$ on epidermal homeostasis. The method employed here was initially used in HEK293 cells to assess the efficacy. Following the development of methods to extract genomic DNA, complete protein deletion was confirmed using Western blotting. In HaCaT keratinocytes, the same method led to, again confirmed by Western blotting, the deletion of the MCU protein. This method for deleting the MCU protein has previously been successful used in breast cancer cell lines (Tosatto et al., 2016), however this is the first time in an epidermal cell line.

It was observed in this chapter that increases in mitochondrial Ca^{2+} followed the addition of 1 mM $[Ca^{2+}]_o$. These transient increases in $[Ca^{2+}]_m$ were more pronounced in low Ca^{2+} cultured HaCaT keratinocytes than high Ca^{2+} cultured. In addition, in basal culture conditions, following the acute increase in Ca^{2+}, the $[Ca^{2+}]_m$ did not return to the same baseline as seen in differentiating HaCaT keratinocytes.

Work has previously established that in vitro, an increase in $[Ca^{2+}]_o$ leads to transient increases in cytosolic (Bikle et al., 1996, Hennings et al., 1989) and ER Ca^{2+} in keratinocytes (Beck et al., 2008) and this increase is an early initiator of differentiation (Sharpe et al., 1989). The rise in agonist-induced intracellular Ca^{2+} has been observed to be increased in low Ca^{2+} cultured cells (Kruszewski et al., 1991, Hennings et al., 1989). In addition, although direct $[Ca^{2+}]_m$ increases have not been shown in keratinocytes, mitochondrial depolarisation occurs following $[Ca^{2+}]_o$

addition. This depolarisation is more pronounced in low Ca^{2+} cultured HaCaT keratinocytes (Savignan et al., 2004),. These data suggest that mitochondria play a role in the handling of Ca^{2+} in keratinocytes and are sensitive to stimuli that modulate proliferation and differentiation.

The recently identified MCU is required for Ca^{2+} influx into mitochondria, the transient increase in $[Ca^{2+}]_m$ observed here following $[Ca^{2+}]_o$ increase was more pronounced in low Ca^{2+} HaCaTs. Interestingly, this increase in transient peak was accompanied by a decrease (~10 %) in MICU2 RNA. This is consistent with the notion that the MICU family fine-tune the Ca^{2+} influx mediated by MCU (Patron et al., 2014).

Studies have identified a role of MICU2 as a bonafide inhibitor of MCU open probability (Patron et al., 2014). Knockdown of MICU2 leads to a significant increase in agonist-induced Ca^{2+} influx to mitochondria (Matesanz-Isabel et al., 2016). Matesanz-Isabel *et al* (2016) confirmed that silencing of MICU2 increases agonist-evoked $[Ca^{2+}]_m$ uptake. This $[Ca^{2+}]_m$ uptake this was followed by an increased flow of $[Ca^{2+}]_{er}$ into the cytoplasm.

It was hypothesised that the ability of mitochondria to uptake more Ca^{2+} led to a reduction in the negative feedback of $[Ca^{2+}]_c$ on $[Ca^{2+}]_{er}$ release (Matesanz-Isabel et al., 2016). Here, it was observed that the agonist-evoked increase in $[Ca^{2+}]_m$ was more pronounced in proliferating cells. Despite these maintaining a lower resting $[Ca^{2+}]_{er}$ (Beck et al., 2008), it is plausible that following the 'Ca^{2+} switch', more $[Ca^{2+}]_{er}$ is released into the cytoplasm in proliferating than differentiating cells.

Growing HaCaT keratinocytes in low Ca^{2+} medium (0.03 mM) or high Ca^{2+} medium (< 0.1 mM) has an effect on their proliferation rate (Deyrieux and Wilson, 2007). With low Ca^{2+} medium lending towards a proliferative phenotype and high Ca^{2+} medium inducing differentiation. Using a proliferation assay, this variation in proliferation state was confirmed, with basal HaCaT keratinocytes proliferating ~ 20 % more than the differentiating cells. When HaCaT keratinocyte MCU -/- cells are grown in high Ca^{2+} conditions, the proliferation rate is vastly decreased whereas those grown in low Ca^{2+}, although still slower than the wild type proliferating cells, proliferate much quicker. Overall this alludes to an important role for mitochondrial Ca^{2+} in differentiating HaCaT keratincoytes.

In addition to a change in proliferation state, HaCaT keratinocytes grown in low Ca^{2+} medium (0.03 mM) or high Ca^{2+} medium (< 0.1 mM) show a variation in morphology (Deyrieux and Wilson, 2007). Here, following > 3 weeks culture in their respective media, the morphology of HaCaT keratinocytes changed to reflect their proliferation state. HaCaTs in high Ca^{2+} were cuboidal with a granular-like appearance. However, those grown in low Ca^{2+} had a more spindle-like morphology This change in morphology to match proliferation state is well documented (Deyrieux and Wilson, 2007). Beginning at around 72 hours with the loss of tight junctions, the complete loss of the differentiating marker K1 is observed at around 3 weeks (Deyrieux and Wilson, 2007).

A change in morphology is secondary to the change in the proteomic profile and therefore proliferative state of HaCaT keratinocytes. Interestingly, MCU -/- cells grown in high Ca^{2+} did not have the same morphology as high Ca^{2+} wild type HaCaTs. Some heterogeneity was seen in the MCU-/- clone, with some cells

appearing similar, others were characterised by greatly enlarged cytoplasm. Interestingly, MCU -/- HaCaTs grown in low Ca^{2+} mimic the morphology of wild type HaCaTs in the same conditions. Therefore, the knockout of MCU appears to only have a significant impact on HaCaT keratinocytes when they are in differentiating conditions.

Silencing of MCU in HeLa cells is able to attenuate Ca^{2+} uptake proportionate to the level of knockdown (Baughman et al., 2011). Oxygen consumption rate (OCR), an indicator or respiration is a common assay to assess of mitochondria's functionality and therefore health. Interestingly, silencing of MCU has no effect on OCR or membrane potential, however, it does inhibit the action of the TCA cycle (Baughman et al., 2011, Tosatto et al., 2016), as expected due to the presence of Ca^{2+} activated dehydrogenases (Denton et al., 1980). The attenuation of TCA cycle would not only reduce ROS production as seen previously (Tosatto et al., 2016) but would also attenuate ATP production in the mitochondria (Denton et al., 1980). ROS has previously been identified as a key rate limiting step for epidermal differentiation (Hamanaka et al., 2013). In addition, a lower TCA cycle activity would lead to a reduction in cellular ATP is known to play a role in cell senescence through the activation of AMPK (Wang et al., 2003), which is characterised by an increase in cell size.

5.6 Conclusion

This work has, for the first time, begun to elucidate the role that the mitochondrial Ca^{2+} uniporter has on epidermal homeostasis. Previous studies have identified that mitochondrial changes such as depolarisation and increased ROS production directly impact HaCaT keratinocyte differentiation, however to date, there are no studies that have investigated the direct effect of the MCU complex and Ca^{2+} influx on HaCaT keratinocytes.

5.7 Further work

Following on from this preliminary work is imperative to understanding more of the role of MCU and mitochondrial Ca^{2+} on epidermal homeostasis. Early experiments would make use of genetically encoded Ca^{2+} sensors, like G-CEPIA3mt, G-CEPIA4mt, and mito-Aeq as well as Ca^{2+} dyes that are sequestered into mitochondria, such as X-Rhod. These probes/dyes would elucidate whether mitochondrial Ca^{2+} uptake in keratinocytes is attenuated following loss of MCU. Once this has been established, cytosolic dyes such as Fura-2 and Fluo-4 would identify if, as seen in HeLa cells, loss of MCU does not affect cytoplasmic Ca^{2+} levels.

As ROS have been reported to play a direct role in epidermal differentiation and a loss of mitochondrial Ca^{2+} would lead to a reduction in ROS through attenuation of TCA cycle, using ROS reporters such as CellRox (ThermoFisher #C10422) would confirm the decrease in ROS expected and reported, from an MCU KO cell line. In addition to ROS production, Ca^{2+} signalling has a direct impact on mitochondrial respiration, seahorse experiments would assess the cells ability to respire. Outside of

Ca^{2+} handling, as Ca^{2+} is a driver of epidermal differentiation, further quantitative PCR and western blotting to assess relative expression of differentiation factors and other MCU components between high and low cultured HaCaTs and high and low cultured MCU -/- HaCaTs would assess the change in differentiation status and also any compensatory increases in MCU cofactors in order to try and recover mitochondrial Ca^{2+} uptake.

As a change in HaCaT keratinocyte cell morphology has already been observed here, further investigation into mitochondrial structure, morphology, and rates of mitophagy would be essential in determining mitochondrial handling in these cells at various differentiation states and in different culture conditions.

With this information in mind, the generation of 3D pseudo-skins using MCU -/- HaCaT keratinocytes would identify any modifications to the normal epidermal homeostasis.

6 Discussion

This thesis has focused on developing molecular tools that will aid the furthering of the investigaion into the role of Ca^{2+} in keratinocyte and in turn, epidermal homeostasis. The direct conclusions of the results have already been discussed, therefore this chapter will attempt to discuss the broader implications of the work and also provide an updated model of the role of Ca^{2+} on keratinocyte proliferation state.

6.1 Real time quantification of $[Ca^{2+}]_e$, the missing link?

A wealth of evidence suggests that increases in $[Ca^{2+}]_o$ lead to the initiation of keratinocyte differentiation both *in vitro* and *in vivo* (Section 1.4). In addition, both PIXE and FLIM studies have identified a gradient in extracellular $[Ca^{2+}]$, with the $[Ca^{2+}]_o$ increasing as cells progress further towards terminal differentiation. Following wounding, a marked decrease in $[Ca^{2+}]_o$ is observed however mathematical studies hypothesised that an increase in $[Ca^{2+}]_o$ would be required in order to restore the permeability barrier. These studies taken together, highlight the lack of concrete evidence regarding the changes to $[Ca^{2+}]_o$ in the epidermis.

In Chapter 4, a genetically-encoded Ca^{2+} sensor was generated that, following further testing, would allow the investigation into the temporal and spatial effect $[Ca^{2+}]_o$ has on keratinocyte differentiation and barrier homeostasis. In addition to homeostasis, the CEPIA1pm could become an invaluable tool to investigate disease states. Darier's disease (DD) and Hailey-Hailey disease (HHD) are caused by inactivating mutations in ATP2A2 and ATP2C1, genes that encode the sarco/endoplasmic reticulum Ca^{2+}-ATPase 2 (SERCA2) and the SPCA1, respectively (Foggia and Hovnanian, 2004). In HHD, the epidermal Ca^{2+} gradient is markedly different, with a

general decrease in total $[Ca^{2+}]$. However, the $[Ca^{2+}]_i$ in basal cells is similar to that of the control *in vivo* but reduced *in vitro* (Hu et al., 2000). This variation in $[Ca^{2+}]_i$ handling could be mirrored, or caused by variations in $[Ca^{2+}]_o$, therefore the use of the CEPIA1pm probe would allow the *in vitro* and *in vivo* investigations into $[Ca^{2+}]_o$ changes.

There are a number of other systems whereby an Ca^{2}+ sensor measuring variations to the $[Ca^{2+}]_o$ could prove useful. The plasma membrane Ca^{2+}-ATPase (PMCA) is an ATP-driven pump that is essential for maintaining low $[Ca^{2+}]_c$. Naturally, defects in the PMCA would lead to an increased $[Ca^{2+}]_c$ and therefore the activation of cell death mechanisms. On the other hand, overexpression of some PMCA isoforms has been indicated in breast cancer (reviewed in Bruce, 2018). An extracellular Ca^{2+} sensor, sensitive to Ca^{2+} efflux, would enable the investigation into the activity of plasma membrane Ca^{2+} channels such as PMCA and allow further investigation into the role of Ca^{2+} influx and efflux on cell fate. In addition, the role of Ca^{2+} in the tumour microenvironment may be of great interest.

6.2 Mitochondria, a regulator of keratinocyte differentiation?

There is very little information regarding the role of mitochondria as a pivotal regulator of keratinocyte differentiation. As dicussed in Section 1.5, two independent studies identified that mitochondrial ROS and depolarisation are necessary for differentiation. Despite this, little work has continued on from these studies. Both mitochondrial ROS and depolarisation have been observed to stem from an increase in $[Ca^{2+}]_m$ which is often secondary to an agonist-evoked increase in $[Ca^{2+}]_c$. In Chapter 5, a modification of $[Ca^{2+}]_m$ handling was observed when HaCaT keratinocytes were grown in proliferating or differentiating conditions. Although studies have identified that $[Ca^{2+}]_{er}$ release is greater in basal keratinocytes and would therefore lend to the idea that mitochondrial uptake would be greater following ER depletion, there is also a decrease in the MCU inhibitor, MICU2. This genotypic modification, brought on by growth conditions, would allow the hypothesis that an increased $[Ca^{2+}]_m$ uptake is both expected and necessary. In addition, it has previously been observed that with mitochondria acting as a buffer rather than a store, following stimulation and $[Ca^{2+}]_m$ transient increases, $[Ca^{2+}]_m$ returns to a resting level. Interestingly, HaCaT keratinocytes grown in low Ca^{2+} conditions, following an agonist-evoked transient increase in $[Ca^{2+}]_m$, the $[Ca^{2+}]_m$ remains slightly elevated. This indicates a continued uptake of $[Ca^{2+}]_m$ following agonist stimulation in proliferating HaCaT keratinocytes compared to those undergoing differentiation.

Work has identified that resting $[Ca^{2+}]_c$ levels are increased in keratinocytes that mimic the hyperproliferative skin disorder Hailey-Hailey disease (Foggia et al.,

2006). As discussed in Chapter 1, increased levels of $[Ca^{2+}]_c$ can lead to cell death mechanisms. Here, following the deletion of MCU protein, HaCaTs struggle to proliferate in high Ca^{2+} conditions however the proliferation rate is rescued in low Ca^{2+} growth conditions. This indicates that the deletion of MCU has a pronounced detrimental effect on HaCaT keratinocytes during differentiation. The effect of MCU -/- on mitochondrial Ca^{2+} needs to be verified, however impaired ROS generation in mitochondria can lead to an inhibition of epidermal differentiation.

Overall, this thesis suggeststhat a reduction in $[Ca^{2+}]_m$ due to an ablation of MCU, leads to a defect within the Ca^{2+} handling of HaCaT keratinocytes and suggests a role for $[Ca^{2+}]_m$ in epidermal homeostasis *in vivo.*

6.3 Model

Using the information discussed in Chapter 1 and the results obtained in this thesis, a new model has been proposed, indicating $[Ca^{2+}]_m$ as playing an important role in keratinocyte differentiation. This model will be explained below.

Basal keratinocytes are maintained in low $[Ca^{2+}]_o$ for proliferation in the basal layer with these cells containing lower relative organelle Ca^{2+}. As cells divide, they are forced upwards away from the basememnt membrane encountering higher $[Ca^{2+}]_o$. This increase in $[Ca^{2+}]_o$ leads to the activation of the CaR on the cell membrane. This in turn, leads to an IP_3-mediated Ca^{2+} response, releasing Ca^{2+} from the ER, which is taken up by mitochondria, inducing a transient increase in $[Ca^{2+}]_m$. This large increase in $[Ca^{2+}]_m$ leads to depolarisation of the membrane and an increase in ROS production, both of which necessary for keratinocyte differentiation (Hamanaka et al., 2013, Savignan et al., 2004). In addition, this release in ER Ca^{2+} would activate XBP1,as hypothesised by Celli *et al* (2011). Mitochondria maintain a higher resting Ca^{2+}, allowing contined activiation of Ca^{2+} dependant processes. In addition, the delayed mitochondrial release and inhibition of $[Ca^{2+}]_c$ negative feedback on $[Ca^{2+}]_{er}$ release, maintains the $[Ca^{2+}]_c$ increase for a longer duration, allowing Ca^{2+} sensitive processes such as transcription and protein activation to take place. As the $[Ca^{2+}]_c$ continues to rise, it is maintained by an increased Ca^{2+} flow into the cell via non-specific cation channels and voltage-gated Ca^{2+} channels. An upregulation of the SERCA pump and calreticulin is needed in order to sequester the rising $[Ca^{2+}]_c$, protecting from cell death. Along with this, an increase in the MCU inhibitor MICU2 limits mitochondrial overloading and early apoptosis. This model is depicted in Figure 6.1.

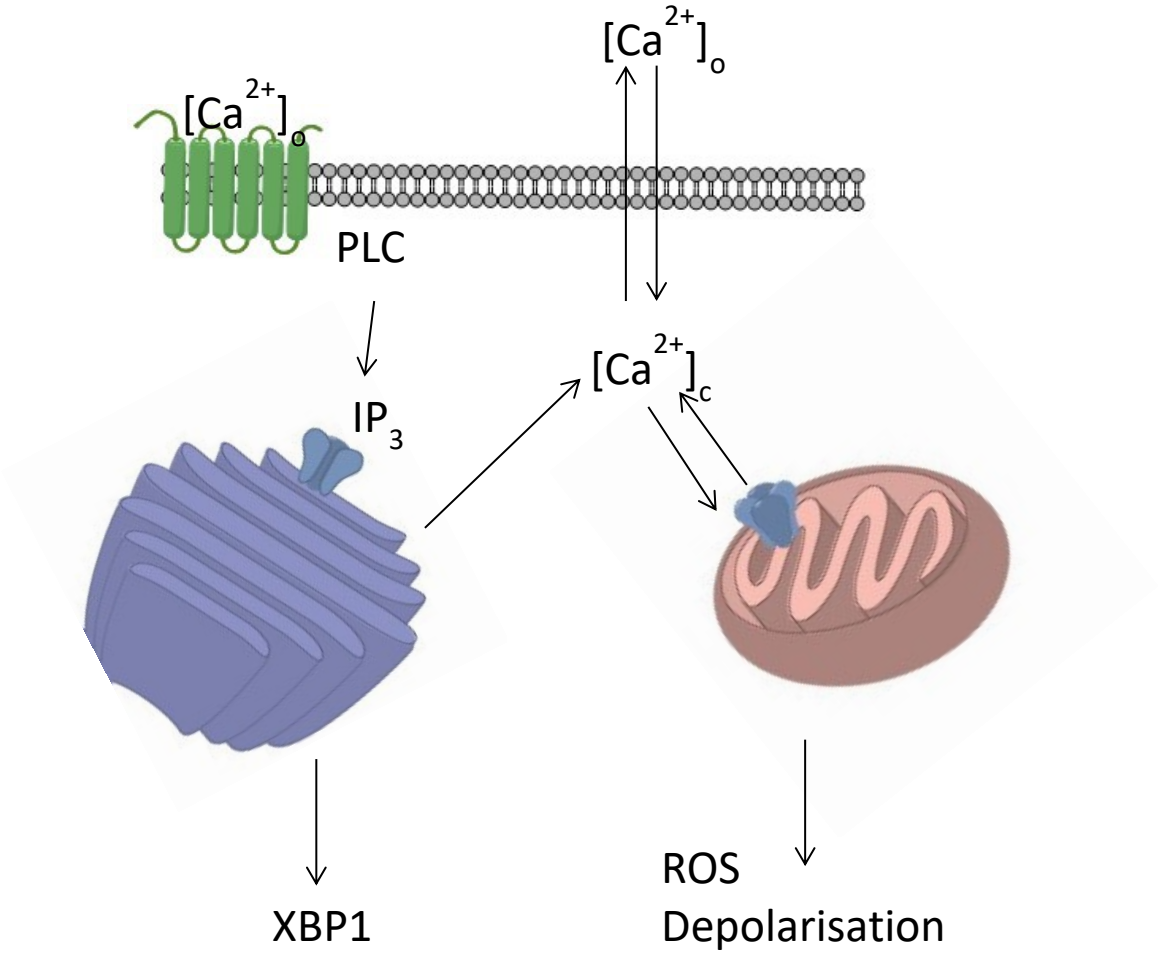

Figure 6.1. Model depicting the role of mitochondria in keratinocyte differentiation.

7 Bibliography

Acosta-Alvear, D., Zhou, Y., Blais, A., Tsikitis, M., Lents, N. H., Arias, C., Lennon, C. J., Kluger, Y. and Dynlacht, B. D. (2007) 'XBP1 controls diverse cell type- and condition-specific transcriptional regulatory networks', *Mol Cell,* 27(1), pp. 53-66.

Adams, J. C. and Watt, F. M. (1990) 'Changes in keratinocyte adhesion during terminal differentiation: reduction in fibronectin binding precedes alpha 5 beta 1 integrin loss from the cell surface', *Cell,* 63(2), pp. 425-35.

Adams, M. P., Mallet, D. G. and Pettet, G. J. (2015) 'Towards a Quantitative Theory of Epidermal Calcium Profile Formation in Unwounded Skin', *PLOS ONE,* 10(1), pp. e0116751.

Allombert-Blaise, C., Tamiji, S., Mortier, L., Fauvel, H., Tual, M., Delaporte, E., Piette, F., DeLassale, E. M., Formstecher, P., Marchetti, P. and Polakowska, R. (2003) 'Terminal differentiation of human epidermal keratinocytes involves mitochondria- and caspase-dependent cell death pathway', *Cell Death And Differentiation,* 10, pp. 850.

Almers, W. and Neher, E. (1985) 'The Ca signal from fura-2 loaded mast cells depends strongly on the method of dye-loading', *FEBS Lett,* 192(1), pp. 13-8.

Alvarez, J. and Montero, M. (2002) 'Measuring [Ca2+] in the endoplasmic reticulum with aequorin', *Cell Calcium,* 32(5-6), pp. 251-60.

Ando, H., Niki, Y., Ito, M., Akiyama, K., Matsui, M. S., Yarosh, D. B. and Ichihashi, M. (2012) 'Melanosomes are transferred from melanocytes to keratinocytes through the processes of packaging, release, uptake, and dispersion', *J Invest Dermatol,* 132(4), pp. 1222-9.

Anesti, V. and Scorrano, L. (2006) 'The relationship between mitochondrial shape and function and the cytoskeleton', *Biochim Biophys Acta,* 1757(5-6), pp. 692-9.

Arnaudeau, S., Kelley, W. L., Walsh, J. V., Jr. and Demaurex, N. (2001) 'Mitochondria recycle Ca(2+) to the endoplasmic reticulum and prevent the depletion of neighboring endoplasmic reticulum regions', *J Biol Chem,* 276(31), pp. 29430-9.

Babu, Y. S., Bugg, C. E. and Cook, W. J. (1988) 'Structure of calmodulin refined at 2.2 A resolution', *J Mol Biol,* 204(1), pp. 191-204.

Baird, G. S., Zacharias, D. A. and Tsien, R. Y. (1999) 'Circular permutation and receptor insertion within green fluorescent proteins', *Proceedings of the National Academy of Sciences of the United States of America,* 96(20), pp. 11241-11246.

Banks-Schlegel, S. and Green, H. (1980) 'Formation of epidermis by serially cultivated human epidermal cells transplanted as an epithelium to athymic mice', *Transplantation,* 29(4), pp. 308-13.

Baughman, J. M., Perocchi, F., Girgis, H. S., Plovanich, M., Belcher-Timme, C. A., Sancak, Y., Bao, X. R., Strittmatter, L., Goldberger, O., Bogorad, R. L., Koteliansky, V. and Mootha, V. K. (2011) 'Integrative genomics identifies MCU as an essential component of the mitochondrial calcium uniporter', *Nature,* 476(7360), pp. 341-345.

Beck, B., Lehen'kyi, V., Roudbaraki, M., Flourakis, M., Charveron, M., Bordat, P., Polakowska, R., Prevarskaya, N. and Skryma, R. (2008) 'TRPC channels determine human keratinocyte differentiation: new insight into basal cell carcinoma', *Cell Calcium,* 43(5), pp. 492-505.

Behne, M. J., Sanchez, S., Barry, N. P., Kirschner, N., Meyer, W., Mauro, T. M., Moll, I. and Gratton, E. (2011) 'Major translocation of calcium upon epidermal barrier insult: imaging and quantification via FLIM/Fourier vector analysis', *Arch Dermatol Res,* 303(2), pp. 103-15.

Bence, N. F., Sampat, R. M. and Kopito, R. R. (2001) 'Impairment of the ubiquitin-proteasome system by protein aggregation', *Science,* 292(5521), pp. 1552-5.

Bennetzen, J. L. and Hall, B. D. (1982) 'Codon selection in yeast', *J Biol Chem,* 257(6), pp. 3026-31.

Berridge, M. J., Bootman, M. D. and Roderick, H. L. (2003) 'Calcium signalling: dynamics, homeostasis and remodelling', *Nat Rev Mol Cell Biol,* 4(7), pp. 517-29.

Berridge, M. J., Lipp, P. and Bootman, M. D. (2000) 'The versatility and universality of calcium signalling', *Nat Rev Mol Cell Biol,* 1(1), pp. 11-21.

Bertolotti, A., Zhang, Y., Hendershot, L. M., Harding, H. P. and Ron, D. (2000) 'Dynamic interaction of BiP and ER stress transducers in the unfolded-protein response', *Nat Cell Biol,* 2(6), pp. 326-32.

Bidaux, G., Borowiec, A. S., Gordienko, D., Beck, B., Shapovalov, G. G., Lemonnier, L., Flourakis, M., Vandenberghe, M., Slomianny, C., Dewailly, E., Delcourt, P., Desruelles, E., Ritaine, A., Polakowska, R., Lesage, J., Chami, M., Skryma, R. and Prevarskaya, N. (2015) 'Epidermal TRPM8 channel isoform controls the balance between keratinocyte proliferation and differentiation in a cold-dependent manner', *Proc Natl Acad Sci U S A,* 112(26), pp. E3345-54.

Bikle, D. D., Ratnam, A., Mauro, T., Harris, J. and Pillai, S. (1996) 'Changes in calcium responsiveness and handling during keratinocyte differentiation. Potential role of the calcium receptor', *J Clin Invest,* 97(4), pp. 1085-93.

Blanpain, C. and Fuchs, E. (2006) 'Epidermal Stem Cells of the Skin', *Annual review of cell and developmental biology,* 22, pp. 339-373.

Bloomquist, E. and Curtis, B. A. (1972) 'The Action of Serotonin on Calcium-45 Efflux from the Anterior Byssal Retractor Muscle of Mytilus edulis', *The Journal of General Physiology,* 59(4), pp. 476-485.

Bolotin, A., Quinquis, B., Sorokin, A. and Ehrlich, S. D. (2005) 'Clustered regularly interspaced short palindrome repeats (CRISPRs) have spacers of extrachromosomal origin', *Microbiology,* 151(Pt 8), pp. 2551-61.

Borowiec, A. S., Bidaux, G., Pigat, N., Goffin, V., Bernichtein, S. and Capiod, T. (2014) 'Calcium channels, external calcium concentration and cell proliferation', *Eur J Pharmacol,* 739, pp. 19-25.

Breitwieser, G. E. and Gama, L. (2001) 'Calcium-sensing receptor activation induces intracellular calcium oscillations', *Am J Physiol Cell Physiol,* 280(6), pp. C1412-21.

Brini, M., Murgia, M., Pasti, L., Picard, D., Pozzan, T. and Rizzuto, R. (1993) 'Nuclear Ca2+ concentration measured with specifically targeted recombinant aequorin', *The EMBO Journal,* 12(12), pp. 4813-4819.

Bruce, J. I. E. (2018) 'Metabolic regulation of the PMCA: Role in cell death and survival', *Cell Calcium,* 69, pp. 28-36.

Burgoyne, R. D. and Morgan, A. (2003) 'Secretory granule exocytosis', *Physiol Rev,* 83(2), pp. 581-632.

Campisi, J. and d'Adda di Fagagna, F. (2007) 'Cellular senescence: when bad things happen to good cells', *Nat Rev Mol Cell Biol,* 8(9), pp. 729-40.

Cannell, M. B., Berlin, J. R. and Lederer, W. J. (1987) 'Effect of membrane potential changes on the calcium transient in single rat cardiac muscle cells', *Science,* 238(4832), pp. 1419-23.

Carafoli, E. (1979) 'The calcium cycle of mitochondria', *FEBS Lett,* 104(1), pp. 1-5.

Celli, A., Sanchez, S., Behne, M., Hazlett, T., Gratton, E. and Mauro, T. (2010) 'The epidermal Ca(2+) gradient: Measurement using the phasor representation of fluorescent lifetime imaging', *Biophys J,* 98(5), pp. 911-21.

Cheng, X., Jin, J., Hu, L., Shen, D., Dong, X. P., Samie, M. A., Knoff, J., Eisinger, B., Liu, M. L., Huang, S. M., Caterina, M. J., Dempsey, P., Michael, L. E., Dlugosz, A. A., Andrews, N. C., Clapham, D. E. and Xu, H. (2010) 'TRP channel regulates EGFR signaling in hair morphogenesis and skin barrier formation', *Cell,* 141(2), pp. 331-43.

Chomiczewska, D., Trznadel-Budzko, E., Kaczorowska, A. and Rotsztejn, H. (2009) '[The role of Langerhans cells in the skin immune system]', *Pol Merkur Lekarski,* 26(153), pp. 173-7.

Cichorek, M., Wachulska, M., Stasiewicz, A. and Tymińska, A. (2013) 'Skin melanocytes: biology and development', *Advances in Dermatology and Allergology/Postępy Dermatologii I Alergologii,* 30(1), pp. 30-41.

Cieri, D., Vicario, M., Giacomello, M., Vallese, F., Filadi, R., Wagner, T., Pozzan, T., Pizzo, P., Scorrano, L., Brini, M. and Calì, T. (2017) 'SPLICS: a split green fluorescent protein-based contact site sensor for narrow and wide heterotypic organelle juxtaposition', *Cell Death & Differentiation*.

Clayton, E., Doupé, D. P., Klein, A. M., Winton, D. J., Simons, B. D. and Jones, P. H. (2007) 'A single type of progenitor cell maintains normal epidermis', *Nature,* 446(7132), pp. 185-9.

Cobbold, P. H. and Rink, T. J. (1987) 'Fluorescence and bioluminescence measurement of cytoplasmic free calcium', *Biochem J,* 248(2), pp. 313-28.

Cong, L., Ran, F. A., Cox, D., Lin, S., Barretto, R., Habib, N., Hsu, P. D., Wu, X., Jiang, W., Marraffini, L. A. and Zhang, F. (2013) 'Multiplex genome engineering using CRISPR/Cas systems', *Science,* 339(6121), pp. 819-23.

Cornejo, V. H., Pihán, P., Vidal, R. L. and Hetz, C. (2013) 'Role of the unfolded protein response in organ physiology: lessons from mouse models', *IUBMB Life,* 65(12), pp. 962-75.

Csordás, G., Golenár, T., Seifert, E. L., Kamer, K. J., Sancak, Y., Perocchi, F., Moffat, C., Weaver, D., Perez, S. d. l. F., Bogorad, R., Koteliansky, V., Adijanto, J., Mootha, V. K. and Hajnóczky, G. (2013) 'MICU1 controls both the threshold and cooperative activation of the mitochondrial Ca(2+) uniporter', *Cell metabolism,* 17(6), pp. 976-987.

Csordás, G., Thomas, A. P. and Hajnóczky, G. (1999) 'Quasi-synaptic calcium signal transmission between endoplasmic reticulum and mitochondria', *The EMBO Journal,* 18(1), pp. 96-108.

Danial, N. N. and Korsmeyer, S. J. (2004) 'Cell death: critical control points', *Cell,* 116(2), pp. 205-19.

Dantuma, N. P., Lindsten, K., Glas, R., Jellne, M. and Masucci, M. G. (2000) 'Short-lived green fluorescent proteins for quantifying ubiquitin/proteasome-dependent proteolysis in living cells', *Nat Biotechnol,* 18(5), pp. 538-43.

de la Fuente, S., Matesanz-Isabel, J., Fonteriz, R. I., Montero, M. and Alvarez, J. (2014) 'Dynamics of mitochondrial Ca2+ uptake in MICU1-knockdown cells', *Biochem J,* 458(1), pp. 33-40.

De Stefani, D., Raffaello, A., Teardo, E., Szabò, I. and Rizzuto, R. (2011) 'A 40 kDa protein of the inner membrane is the mitochondrial calcium uniporter', *Nature,* 476(7360), pp. 336-340.

Deltcheva, E., Chylinski, K., Sharma, C. M., Gonzales, K., Chao, Y., Pirzada, Z. A., Eckert, M. R., Vogel, J. and Charpentier, E. (2011) 'CRISPR RNA maturation by trans-encoded small RNA and host factor RNase III', *Nature,* 471(7340), pp. 602-7.

Deluca, H. F. and Engstrom, G. W. (1961) 'Calcium uptake by rat kidney mitochondria', *Proc Natl Acad Sci U S A,* 47, pp. 1744-50.

Denda, M., Fujiwara, S. and Hibino, T. (2006) 'Expression of voltage-gated calcium channel subunit alpha1C in epidermal keratinocytes and effects of agonist and antagonists of the channel on skin barrier homeostasis', *Exp Dermatol,* 15(6), pp. 455-60.

Denda, S., Kumamoto, J., Takei, K., Tsutsumi, M., Aoki, H. and Denda, M. (2012) 'Ryanodine receptors are expressed in epidermal keratinocytes and associated with keratinocyte differentiation and epidermal permeability barrier homeostasis', *J Invest Dermatol,* 132(1), pp. 69-75.

Denton, R. M., McCormack, J. G. and Edgell, N. J. (1980) 'Role of calcium ions in the regulation of intramitochondrial metabolism. Effects of Na+, Mg2+ and ruthenium red on the Ca2+-stimulated oxidation of oxoglutarate and on pyruvate dehydrogenase activity in intact rat heart mitochondria', *Biochem J,* 190(1), pp. 107-17.

Deyrieux, A. F. and Wilson, V. G. (2007) 'In vitro culture conditions to study keratinocyte differentiation using the HaCaT cell line', *Cytotechnology,* 54(2), pp. 77-83.

Drago, I., De Stefani, D., Rizzuto, R. and Pozzan, T. (2012) 'Mitochondrial Ca(2+) uptake contributes to buffering cytoplasmic Ca(2+) peaks in cardiomyocytes', *Proceedings of the National Academy of Sciences of the United States of America,* 109(32), pp. 12986-12991.

Drahota, Z., Carafoli, E., Rossi, C. S., Gamble, R. L. and Lehninger, A. L. (1965) 'The steady state maintenance of accumulated Ca2+ in rat liver mitochondria', *J Biol Chem,* 240, pp. 2712-20.

Dykes, P. J., Jenner, L. A. and Marks, R. (1982) 'The effect of calcium on the initiation and growth of human epidermal cells', *Arch Dermatol Res,* 273(3-4), pp. 225-31.

Eckert, R. L. (1989) 'Structure, function, and differentiation of the keratinocyte', *Physiol Rev,* 69(4), pp. 1316-46.

Engler, C. and Marillonnet, S. (2013) 'Combinatorial DNA assembly using Golden Gate cloning', *Methods Mol Biol,* 1073, pp. 141-56.

Feingold, K. R. (2007) 'Thematic review series: skin lipids. The role of epidermal lipids in cutaneous permeability barrier homeostasis', *J Lipid Res,* 48(12), pp. 2531-46.

Feingold, K. R., Man, M. Q., Menon, G. K., Cho, S. S., Brown, B. E. and Elias, P. M. (1990) 'Cholesterol synthesis is required for cutaneous barrier function in mice', *J Clin Invest,* 86(5), pp. 1738-45.

Foggia, L., Aronchik, I., Aberg, K., Brown, B., Hovnanian, A. and Mauro, T. M. (2006) 'Activity of the hSPCA1 Golgi Ca2+ pump is essential for Ca2+-

mediated Ca2+ response and cell viability in Darier disease', *J Cell Sci,* 119(Pt 4), pp. 671-9.

Foggia, L. and Hovnanian, A. (2004) 'Calcium pump disorders of the skin', *Am J Med Genet C Semin Med Genet,* 131c(1), pp. 20-31.

Fogh-Andersen, N., Altura, B. M., Altura, B. T. and Siggaard-Andersen, O. (1995) 'Composition of interstitial fluid', *Clin Chem,* 41(10), pp. 1522-5.

Fonteriz, R. I., de la Fuente, S., Moreno, A., Lobatón, C. D., Montero, M. and Alvarez, J. (2010) 'Monitoring mitochondrial [Ca2+] dynamics with rhod-2, ratiometric pericam and aequorin', *Cell Calcium,* 48(1), pp. 61-69.

Fraser, R. D., Macrae, T. P. and Miller, A. (1964) 'THE COILED-COIL MODEL OF ALPHA-KERATIN STRUCTURE', *J Mol Biol,* 10, pp. 147-56.

Freinkel, R. K. and Traczyk, T. N. (1985) 'Lipid composition and acid hydrolase content of lamellar granules of fetal rat epidermis', *J Invest Dermatol,* 85(4), pp. 295-8.

Freund, A., Laberge, R.-M., Demaria, M. and Campisi, J. (2012) 'Lamin B1 loss is a senescence-associated biomarker', *Molecular Biology of the Cell,* 23(11), pp. 2066-2075.

Friedman, J. R., Lackner, L. L., West, M., DiBenedetto, J. R., Nunnari, J. and Voeltz, G. K. (2011) 'ER tubules mark sites of mitochondrial division', *Science,* 334(6054), pp. 358-62.

Fuchs, E. and Green, H. (1980) 'Changes in keratin gene expression during terminal differentiation of the keratinocyte', *Cell,* 19(4), pp. 1033-42.

Geertsma, E. R., Groeneveld, M., Slotboom, D.-J. and Poolman, B. (2008) 'Quality control of overexpressed membrane proteins', *Proceedings of the National Academy of Sciences,* 105(15), pp. 5722-5727.

Golstein, P. and Kroemer, G. (2007) 'Cell death by necrosis: towards a molecular definition', *Trends Biochem Sci,* 32(1), pp. 37-43.

Gomes, L. C., Di Benedetto, G. and Scorrano, L. (2011) 'During autophagy mitochondria elongate, are spared from degradation and sustain cell viability', *Nat Cell Biol,* 13(5), pp. 589-98.

Gouy, M. and Gautier, C. (1982) 'Codon usage in bacteria: correlation with gene expressivity', *Nucleic Acids Res,* 10(22), pp. 7055-74.

Grayson, S., Johnson-Winegar, A. G., Wintroub, B. U., Isseroff, R. R., Epstein, E. H. and Elias, P. M. (1985) 'Lamellar body-enriched fractions from neonatal mice: preparative techniques and partial characterization', *J Invest Dermatol,* 85(4), pp. 289-94.

Grubauer, G., Feingold, K. R. and Elias, P. M. (1987) 'Relationship of epidermal lipogenesis to cutaneous barrier function', *J Lipid Res,* 28(6), pp. 746-52.

Grynkiewicz, G., Poenie, M. and Tsien, R. Y. (1985) 'A new generation of Ca2+ indicators with greatly improved fluorescence properties', *J Biol Chem,* 260(6), pp. 3440-50.

Haake, A., Scott, G. and Holbrook, K. (2001) 'Structure and function of the skin: overview of the epidermis and dermis', in Frienkel, R. & Woodley, D. (eds.) *The Biology of the Skin*.

Hamanaka, R. B., Glasauer, A., Hoover, P., Yang, S., Blatt, H., Mullen, A. R., Getsios, S., Gottardi, C. J., DeBerardinis, R. J., Lavker, R. M. and Chandel, N. S. (2013) 'Mitochondrial reactive oxygen species promote epidermal differentiation and hair follicle development', *Sci Signal,* 6(261), pp. ra8.

Harding, H. P., Zhang, Y. and Ron, D. (1999) 'Protein translation and folding are coupled by an endoplasmic-reticulum-resident kinase', *Nature,* 397(6716), pp. 271-4.

Harding, H. P., Zhang, Y., Zeng, H., Novoa, I., Lu, P. D., Calfon, M., Sadri, N., Yun, C., Popko, B., Paules, R., Stojdl, D. F., Bell, J. C., Hettmann, T., Leiden, J. M. and Ron, D. (2003) 'An integrated stress response regulates amino acid metabolism and resistance to oxidative stress', *Mol Cell,* 11(3), pp. 619-33.

Hayflick, L. and Moorhead, P. S. (1961) 'The serial cultivation of human diploid cell strains', *Exp Cell Res,* 25, pp. 585-621.

Haze, K., Yoshida, H., Yanagi, H., Yura, T. and Mori, K. (1999) 'Mammalian transcription factor ATF6 is synthesized as a transmembrane protein and activated by proteolysis in response to endoplasmic reticulum stress', *Mol Biol Cell,* 10(11), pp. 3787-99.

Heilbrunn, L. V. and Wiercinski, F. J. (1947) 'The action of various cations on muscle protoplasm', *J Cell Comp Physiol,* 29(1), pp. 15-32.

Heim, R. and Tsien, R. Y. (1996) 'Engineering green fluorescent protein for improved brightness, longer wavelengths and fluorescence resonance energy transfer', *Curr Biol,* 6(2), pp. 178-82.

Hennings, H., Kruszewski, F. H., Yuspa, S. H. and Tucker, R. W. (1989) 'Intracellular calcium alterations in response to increased external calcium in normal and neoplastic keratinocytes', *Carcinogenesis,* 10(4), pp. 777-80.

Hennings, H., Michael, D., Cheng, C., Steinert, P., Holbrook, K. and Yuspa, S. H. (1980) 'Calcium regulation of growth and differentiation of mouse epidermal cells in culture', *Cell,* 19(1), pp. 245-54.

Hennings, H., Steinert, P. and Buxman, M. M. (1981) 'Calcium induction of transglutaminase and the formation of epsilon(gamma-glutamyl) lysine cross-links in cultured mouse epidermal cells', *Biochem Biophys Res Commun,* 102(2), pp. 739-45.

Hetz, C., Chevet, E. and Oakes, S. A. (2015) 'Proteostasis control by the unfolded protein response', *Nat Cell Biol,* 17(7), pp. 829-38.

Hetz, C., Martinon, F., Rodriguez, D. and Glimcher, L. H. (2011) 'The unfolded protein response: integrating stress signals through the stress sensor IRE1α', *Physiol Rev,* 91(4), pp. 1219-43.

Hofer, A. M. and Machen, T. E. (1993) 'Technique for in situ measurement of calcium in intracellular inositol 1,4,5-trisphosphate-sensitive stores using the fluorescent indicator mag-fura-2', *Proc Natl Acad Sci U S A,* 90(7), pp. 2598-602.

Hofer, A. M. and Schulz, I. (1996) 'Quantification of intraluminal free [Ca] in the agonist-sensitive internal calcium store using compartmentalized fluorescent indicators: some considerations', *Cell Calcium,* 20(3), pp. 235-42.

Holleran, W. M., Man, M. Q., Gao, W. N., Menon, G. K., Elias, P. M. and Feingold, K. R. (1991) 'Sphingolipids are required for mammalian epidermal barrier function. Inhibition of sphingolipid synthesis delays barrier recovery after acute perturbation', *J Clin Invest,* 88(4), pp. 1338-45.

Horvath, P. and Barrangou, R. (2010) 'CRISPR/Cas, the immune system of bacteria and archaea', *Science,* 327(5962), pp. 167-70.

Hsiung, N., Warrick, H., deRiel, J. K., Tuan, D., Forget, B. G., Skoultchi, A. and Kucherlapati, R. (1980) 'Cotransfer of circular and linear prokaryotic and

eukaryotic DNA sequences into mouse cells', *Proc Natl Acad Sci U S A,* 77(8), pp. 4852-6.

Hu, Z., Bonifas, J. M., Beech, J., Bench, G., Shigihara, T., Ogawa, H., Ikeda, S., Mauro, T. and Epstein Jr, E. H. (2000) 'Mutations in ATP2C1, encoding a calcium pump, cause Hailey-Hailey disease', *Nature Genetics,* 24, pp. 61.

Huddart, H. and West, M. (1975) 'Quinine stimulation of Ca-45 efflux from arthropod skeletal muscle in relation to quinine effects on fibre calcium translocation and binding', *Experientia,* 31(6), pp. 665-7.

Hung, V., Zou, P., Rhee, H.-W., Udeshi, N. D., Cracan, V., Svinkina, T., Carr, S. A., Mootha, V. K. and Ting, A. Y. (2014) 'Proteomic mapping of the human mitochondrial intermembrane space in live cells via ratiometric APEX tagging', *Molecular cell,* 55(2), pp. 332-341.

Ingolia, N. T., Ghaemmaghami, S., Newman, J. R. and Weissman, J. S. (2009) 'Genome-wide analysis in vivo of translation with nucleotide resolution using ribosome profiling', *Science,* 324(5924), pp. 218-23.

Ivics, Z., Hackett, P. B., Plasterk, R. H. and Izsvak, Z. (1997) 'Molecular reconstruction of Sleeping Beauty, a Tc1-like transposon from fish, and its transposition in human cells', *Cell,* 91(4), pp. 501-10.

Jeyapalan, J. C., Ferreira, M., Sedivy, J. M. and Herbig, U. (2007) 'Accumulation of senescent cells in mitotic tissue of aging primates', *Mech Ageing Dev,* 128(1), pp. 36-44.

Jinek, M., Chylinski, K., Fonfara, I., Hauer, M., Doudna, J. A. and Charpentier, E. (2012) 'A programmable dual-RNA-guided DNA endonuclease in adaptive bacterial immunity', *Science,* 337(6096), pp. 816-21.

Joiner, M.-l. A., Koval, O. M., Jingdong, L., He, B. J., Allamargot, C., Gao, Z., Luczak, E. D., Hall, D. D., Fink, B. D., Chen, B., Yang, J., Moore, S. A., Scholz, T. D., Strack, S., Mohler, P. J., Sivitz, W. I., Song, L.-S. and Anderson, M. E. (2012) 'CaMKII determines mitochondrial stress responses in heart', *Nature,* 491(7423), pp. 269-273.

Jones, P. H., Harper, S. and Watt, F. M. (1995) 'Stem cell patterning and fate in human epidermis', *Cell,* 80(1), pp. 83-93.

Jones, P. H. and Watt, F. M. (1993) 'Separation of human epidermal stem cells from transit amplifying cells on the basis of differences in integrin function and expression', *Cell,* 73(4), pp. 713-24.

Jouaville, L. S., Pinton, P., Bastianutto, C., Rutter, G. A. and Rizzuto, R. (1999) 'Regulation of mitochondrial ATP synthesis by calcium: evidence for a long-term metabolic priming', *Proc Natl Acad Sci U S A,* 96(24), pp. 13807-12.

Kendall, J. M., Dormer, R. L. and Campbell, A. K. (1992) 'Targeting aequorin to the endoplasmic reticulum of living cells', *Biochem Biophys Res Commun,* 189(2), pp. 1008-16.

Kennedy, L. H., Sutter, C. H., Leon Carrion, S., Tran, Q. T., Bodreddigari, S., Kensicki, E., Mohney, R. P. and Sutter, T. R. (2013) '2,3,7,8-Tetrachlorodibenzo-p-dioxin-mediated production of reactive oxygen species is an essential step in the mechanism of action to accelerate human keratinocyte differentiation', *Toxicol Sci,* 132(1), pp. 235-49.

Kerr, J. F., Wyllie, A. H. and Currie, A. R. (1972) 'Apoptosis: a basic biological phenomenon with wide-ranging implications in tissue kinetics', *Br J Cancer,* 26(4), pp. 239-57.

Kobayashi, Y., Sawabu, Y., Kitahata, H., Denda, M. and Nagayama, M. (2016) 'Mathematical model for calcium-assisted epidermal homeostasis', *J Theor Biol,* 397, pp. 52-60.

Komuves, L., Oda, Y., Tu, C. L., Chang, W. H., Ho-Pao, C. L., Mauro, T. and Bikle, D. D. (2002) 'Epidermal expression of the full-length extracellular calcium-sensing receptor is required for normal keratinocyte differentiation', *J Cell Physiol,* 192(1), pp. 45-54.

Krieger, C. and Duchen, M. R. (2002) 'Mitochondria, Ca2+ and neurodegenerative disease', *Eur J Pharmacol,* 447(2-3), pp. 177-88.

Kruszewski, F. H., Hennings, H., Yuspa, S. H. and Tucker, R. W. (1991) 'Regulation of intracellular free calcium in normal murine keratinocytes', *Am J Physiol,* 261(5 Pt 1), pp. C767-73.

Krähling, H., Mally, S., Eble, J. A., Noël, J., Schwab, A. and Stock, C. (2009) 'The glycocalyx maintains a cell surface pH nanoenvironment crucial for integrin-mediated migration of human melanoma cells', *Pflugers Arch,* 458(6), pp. 1069-83.

Kumamoto, J., Goto, M., Nagayama, M. and Denda, M. (2017) 'Real-time imaging of human epidermal calcium dynamics in response to point laser stimulation', *Journal of Dermatological Science,* 86(1), pp. 13-20.

Källberg, M., Wang, H., Wang, S., Peng, J., Wang, Z., Lu, H. and Xu, J. (2012) 'Template-based protein structure modeling using the RaptorX web server', *Nat Protoc,* 7(8), pp. 1511-22.

Lam, S. S., Martell, J. D., Kamer, K. J., Deerinck, T. J., Ellisman, M. H., Mootha, V. K. and Ting, A. Y. (2015) 'Directed evolution of APEX2 for electron microscopy and proteomics', *Nature methods,* 12(1), pp. 51-54.

Lane, N. and Martin, W. (2010) 'The energetics of genome complexity', *Nature,* 467(7318), pp. 929-34.

Lavker, R. M. and Sun, T. T. (1982) 'Heterogeneity in epidermal basal keratinocytes: morphological and functional correlations', *Science,* 215(4537), pp. 1239-41.

Lechler, T. and Fuchs, E. (2005) 'Asymmetric cell divisions promote stratification and differentiation of mammalian skin', *Nature,* 437(7056), pp. 275-280.

Lee, A. H., Iwakoshi, N. N. and Glimcher, L. H. (2003) 'XBP-1 regulates a subset of endoplasmic reticulum resident chaperone genes in the unfolded protein response', *Mol Cell Biol,* 23(21), pp. 7448-59.

Lee, S. H., Elias, P. M., Proksch, E., Menon, G. K., Mao-Quiang, M. and Feingold, K. R. (1992) 'Calcium and potassium are important regulators of barrier homeostasis in murine epidermis', *J Clin Invest,* 89(2), pp. 530-8.

Lin, Y.-C., Boone, M., Meuris, L., Lemmens, I., Van Roy, N., Soete, A., Reumers, J., Moisse, M., Plaisance, S., Drmanac, R., Chen, J., Speleman, F., Lambrechts, D., Van de Peer, Y., Tavernier, J. and Callewaert, N. (2014) 'Genome dynamics of the human embryonic kidney 293 lineage in response to cell biology manipulations', *Nature Communications,* 5, pp. 4767.

Mackenzie, I. C. (1970) 'Relationship between mitosis and the ordered structure of the stratum corneum in mouse epidermis', *Nature,* 226(5246), pp. 653-5.

Mallilankaraman, K., Doonan, P., Cárdenas, C., Chandramoorthy, H. C., Muller, M., Miller, R., Hoffman, N. E., Gandhirajan, R., Molgó, J., Birnbaum, M. J., Rothberg, B., Mak, D.-O. D., Foskett, J. K. and Madesh, M. (2012) 'MICU1 is an Essential Gatekeeper for MCU-Mediated Mitochondrial Ca(2+) Uptake That Regulates Cell Survival', *Cell,* 151(3), pp. 630-644.

Marciniak, S. J., Yun, C. Y., Oyadomari, S., Novoa, I., Zhang, Y., Jungreis, R., Nagata, K., Harding, H. P. and Ron, D. (2004) 'CHOP induces death by promoting protein synthesis and oxidation in the stressed endoplasmic reticulum', *Genes Dev,* 18(24), pp. 3066-77.

Matesanz-Isabel, J., Arias-del-Val, J., Alvarez-Illera, P., Fonteriz, R. I., Montero, M. and Alvarez, J. (2016) 'Functional roles of MICU1 and MICU2 in mitochondrial Ca2 + uptake', *Biochimica et Biophysica Acta (BBA) - Biomembranes,* 1858(6), pp. 1110-1117.

Matoltsy, A. G. and Matoltsy, M. N. (1970) 'THE CHEMICAL NATURE OF KERATOHYALIN GRANULES OF THE EPIDERMIS', *The Journal of Cell Biology,* 47(3), pp. 593-603.

Mauro, T., Bench, G., Sidderas-Haddad, E., Feingold, K., Elias, P. and Cullander, C. (1998) 'Acute barrier perturbation abolishes the Ca2+ and K+ gradients in murine epidermis: quantitative measurement using PIXE', *J Invest Dermatol,* 111(6), pp. 1198-201.

McCormack, J. G., Bromidge, E. S. and Dawes, N. J. (1988) 'Characterization of the effects of Ca2+ on the intramitochondrial Ca2+-sensitive dehydrogenases within intact rat-kidney mitochondria', *Biochim Biophys Acta,* 934(3), pp. 282-92.

McCullough, K. D., Martindale, J. L., Klotz, L. O., Aw, T. Y. and Holbrook, N. J. (2001) 'Gadd153 sensitizes cells to endoplasmic reticulum stress by down-regulating Bcl2 and perturbing the cellular redox state', *Mol Cell Biol,* 21(4), pp. 1249-59.

Menon, G. K., Elias, P. M., Lee, S. H. and Feingold, K. R. (1992) 'Localization of calcium in murine epidermis following disruption and repair of the permeability barrier', *Cell Tissue Res,* 270(3), pp. 503-12.

Menon, G. K., Grayson, S. and Elias, P. M. (1985) 'Ionic calcium reservoirs in mammalian epidermis: ultrastructural localization by ion-capture cytochemistry', *J Invest Dermatol,* 84(6), pp. 508-12.

Miyawaki, A., Llopis, J., Heim, R., McCaffery, J. M., Adams, J. A., Ikura, M. and Tsien, R. Y. (1997) 'Fluorescent indicators for Ca2+ based on green fluorescent proteins and calmodulin', *Nature,* 388(6645), pp. 882-7.

Mojica, F. J., Díez-Villaseñor, C., García-Martínez, J. and Soria, E. (2005) 'Intervening sequences of regularly spaced prokaryotic repeats derive from foreign genetic elements', *J Mol Evol,* 60(2), pp. 174-82.

Moll, I., Roessler, M., Brandner, J. M., Eispert, A. C., Houdek, P. and Moll, R. (2005) 'Human Merkel cells--aspects of cell biology, distribution and functions', *Eur J Cell Biol,* 84(2-3), pp. 259-71.

Montero, M., Brini, M., Marsault, R., Alvarez, J., Sitia, R., Pozzan, T. and Rizzuto, R. (1995) 'Monitoring dynamic changes in free Ca2+ concentration in the endoplasmic reticulum of intact cells', *EMBO J,* 14(22), pp. 5467-75.

Moore, C. L. (1971) 'Specific inhibition of mitochondrial Ca++ transport by ruthenium red', *Biochem Biophys Res Commun,* 42(2), pp. 298-305.

Mukherjee, S., Chiu, R., Leung, S. M. and Shields, D. (2007) 'Fragmentation of the Golgi apparatus: an early apoptotic event independent of the cytoskeleton', *Traffic,* 8(4), pp. 369-78.

Mátés, L., Chuah, M. K., Belay, E., Jerchow, B., Manoj, N., Acosta-Sanchez, A., Grzela, D. P., Schmitt, A., Becker, K., Matrai, J., Ma, L., Samara-Kuko, E.,

Gysemans, C., Pryputniewicz, D., Miskey, C., Fletcher, B., VandenDriessche, T., Ivics, Z. and Izsvák, Z. (2009) 'Molecular evolution of a novel hyperactive Sleeping Beauty transposase enables robust stable gene transfer in vertebrates', *Nat Genet,* 41(6), pp. 753-61.

Mátés, L., Izsvák, Z. and Ivics, Z. (2007) 'Technology transfer from worms and flies to vertebrates: transposition-based genome manipulations and their future perspectives', *Genome Biol,* 8 Suppl 1, pp. S1.

Nabauer, M., Callewaert, G., Cleemann, L. and Morad, M. (1989) 'Regulation of Calcium Release Is Gated by Calcium Current, Not Gating Charge, in Cardiac Myocytes', *Science,* 244(4906), pp. 800-803.

Nakai, J., Ohkura, M. and Imoto, K. (2001) 'A high signal-to-noise Ca(2+) probe composed of a single green fluorescent protein', *Nat Biotechnol,* 19(2), pp. 137-41.

Nishimasu, H., Ran, F. A., Hsu, P. D., Konermann, S., Shehata, S. I., Dohmae, N., Ishitani, R., Zhang, F. and Nureki, O. (2014) 'Crystal structure of Cas9 in complex with guide RNA and target DNA', *Cell,* 156(5), pp. 935-49.

Numaga-Tomita, T. and Putney, J. W. (2013) 'Role of STIM1- and Orai1-mediated Ca(2+) entry in Ca(2+)-induced epidermal keratinocyte differentiation', *Journal of Cell Science,* 126(2), pp. 605-612.

Oda, Y., Tu, C. L., Chang, W., Crumrine, D., Komuves, L., Mauro, T., Elias, P. M. and Bikle, D. D. (2000) 'The calcium sensing receptor and its alternatively spliced form in murine epidermal differentiation', *J Biol Chem,* 275(2), pp. 1183-90.

Palmer, A. E., Giacomello, M., Kortemme, T., Hires, S. A., Lev-Ram, V., Baker, D. and Tsien, R. Y. (2006) 'Ca2+ Indicators Based on Computationally

Redesigned Calmodulin-Peptide Pairs', *Chemistry & Biology,* 13(5), pp. 521-530.

Pan, X., Liu, J., Nguyen, T., Liu, C., Sun, J., Teng, Y., Fergusson, M. M., Rovira, I. I., Allen, M., Springer, D. A., Aponte, A. M., Gucek, M., Balaban, R. S., Murphy, E. and Finkel, T. (2013) 'The physiological role of mitochondrial calcium revealed by mice lacking the mitochondrial calcium uniporter (MCU)', *Nature cell biology,* 15(12), pp. 1464-1472.

Passos, J. F., von Zglinicki, T. and Kirkwood, T. B. (2007) 'Mitochondria and ageing: winning and losing in the numbers game', *Bioessays,* 29(9), pp. 908-17.

Patron, M., Checchetto, V., Raffaello, A., Teardo, E., Vecellio Reane, D., Mantoan, M., Granatiero, V., Szabò, I., De Stefani, D. and Rizzuto, R. (2014) 'MICU1 and MICU2 Finely Tune the Mitochondrial Ca(2+) Uniporter by Exerting Opposite Effects on MCU Activity', *Molecular Cell,* 53(5), pp. 726-737.

Pellegatti, P., Falzoni, S., Pinton, P., Rizzuto, R. and Di Virgilio, F. (2005) 'A Novel Recombinant Plasma Membrane-targeted Luciferase Reveals a New Pathway for ATP Secretion', *Molecular Biology of the Cell,* 16(8), pp. 3659-3665.

Perocchi, F., Gohil, V. M., Girgis, H. S., Bao, X. R., McCombs, J. E., Palmer, A. E. and Mootha, V. K. (2010) 'MICU1 encodes a mitochondrial EF hand protein required for Ca(2+) uptake', *Nature,* 467(7313), pp. 291-296.

Pillai, S., Menon, G. K., Bikle, D. D. and Elias, P. M. (1993) 'Localization and quantitation of calcium pools and calcium binding sites in cultured human keratinocytes', *J Cell Physiol,* 154(1), pp. 101-12.

Plovanich, M., Bogorad, R. L., Sancak, Y., Kamer, K. J., Strittmatter, L., Li, A. A., Girgis, H. S., Kuchimanchi, S., De Groot, J., Speciner, L., Taneja, N., Oshea,

J., Koteliansky, V. and Mootha, V. K. (2013) 'MICU2, a Paralog of MICU1, Resides within the Mitochondrial Uniporter Complex to Regulate Calcium Handling', *PLoS ONE,* 8(2), pp. e55785.

Potten, C. S. (1974) 'The epidermal proliferative unit: the possible role of the central basal cell', *Cell Tissue Kinet,* 7(1), pp. 77-88.

Potten, C. S. (1981) 'Cell replacement in epidermis (keratopoiesis) via discrete units of proliferation', *Int Rev Cytol,* 69, pp. 271-318.

Powell, J. R. and Moriyama, E. N. (1997) 'Evolution of codon usage bias in Drosophila', *Proc Natl Acad Sci U S A,* 94(15), pp. 7784-90.

Prasher, D. C., Eckenrode, V. K., Ward, W. W., Prendergast, F. G. and Cormier, M. J. (1992) 'Primary structure of the Aequorea victoria green-fluorescent protein', *Gene,* 111(2), pp. 229-33.

Qian, W., Yang, J. R., Pearson, N. M., Maclean, C. and Zhang, J. (2012) 'Balanced codon usage optimizes eukaryotic translational efficiency', *PLoS Genet,* 8(3), pp. e1002603.

Qiu, J., Tan, Y.-W., Hagenston, A. M., Martel, M.-A., Kneisel, N., Skehel, P. A., Wyllie, D. J. A., Bading, H. and Hardingham, G. E. (2013) 'Mitochondrial calcium uniporter Mcu controls excitotoxicity and is transcriptionally repressed by neuroprotective nuclear calcium signals', *Nature Communications,* 4, pp. 2034.

Quevedo, W. C., Fitzpatrick, T. B., Pathak, M. A. and Jimbow, K. (1975) 'Role of light in human skin color viariation', *Am J Phys Anthropol,* 43(3), pp. 393-408.

Raffaello, A., De Stefani, D., Sabbadin, D., Teardo, E., Merli, G., Picard, A., Checchetto, V., Moro, S., Szabò, I. and Rizzuto, R. (2013) 'The

mitochondrial calcium uniporter is a multimer that can include a dominant-negative pore-forming subunit', *The EMBO Journal,* 32(17), pp. 2362-2376.

Raine, A. E., Bedford, L., Simpson, A. W., Ashley, C. C., Brown, R., Woodhead, J. S. and Ledingham, J. G. (1993) 'Hyperparathyroidism, platelet intracellular free calcium and hypertension in chronic renal failure', *Kidney Int,* 43(3), pp. 700-5.

Rasola, A. and Bernardi, P. (2011) 'Mitochondrial permeability transition in Ca(2+)-dependent apoptosis and necrosis', *Cell Calcium,* 50(3), pp. 222-33.

Rey, O., Young, S. H., Jacamo, R., Moyer, M. P. and Rozengurt, E. (2010) 'Extracellular calcium sensing receptor stimulation in human colonic epithelial cells induces intracellular calcium oscillations and proliferation inhibition', *J Cell Physiol,* 225(1), pp. 73-83.

Rice, R. H. and Green, H. (1978) 'Relation of protein synthesis and transglutaminase activity to formation of the cross-linked envelope during terminal differentiation of the cultured human epidermal keratinocyte', *J Cell Biol,* 76(3), pp. 705-11.

Ridgway, E. B. and Ashley, C. C. (1967) 'Calcium transients in single muscle fibers', *Biochemical and Biophysical Research Communications,* 29(2), pp. 229-234.

Ringer, S. (1883) 'A further Contribution regarding the influence of the different Constituents of the Blood on the Contraction of the Heart', *J Physiol,* 4(1), pp. 29-42.3.

Rink, T. J. and Tsien, R. Y. (1982) 'Cytoplasmic free [Ca2+] in very small intact cells', *Biochemical Society Transactions,* 10(4), pp. 209.

Rizzuto, R., Brini, M., Murgia, M. and Pozzan, T. (1993) 'Microdomains with high Ca2+ close to IP3-sensitive channels that are sensed by neighboring mitochondria', *Science,* 262(5134), pp. 744-7.

Rizzuto, R., Pinton, P., Carrington, W., Fay, F. S., Fogarty, K. E., Lifshitz, L. M., Tuft, R. A. and Pozzan, T. (1998) 'Close contacts with the endoplasmic reticulum as determinants of mitochondrial Ca2+ responses', *Science,* 280(5370), pp. 1763-6.

Rizzuto, R., Simpson, A. W., Brini, M. and Pozzan, T. (1992) 'Rapid changes of mitochondrial Ca2+ revealed by specifically targeted recombinant aequorin', *Nature,* 358(6384), pp. 325-7.

Rodier, F., Coppe, J. P., Patil, C. K., Hoeijmakers, W. A., Munoz, D. P., Raza, S. R., Freund, A., Campeau, E., Davalos, A. R. and Campisi, J. (2009) 'Persistent DNA damage signalling triggers senescence-associated inflammatory cytokine secretion', *Nat Cell Biol,* 11(8), pp. 973-9.

Roe, M. W., Lemasters, J. J. and Herman, B. (1990) 'Assessment of Fura-2 for measurements of cytosolic free calcium', *Cell Calcium,* 11(2-3), pp. 63-73.

Ron, D. and Walter, P. (2007) 'Signal integration in the endoplasmic reticulum unfolded protein response', *Nat Rev Mol Cell Biol,* 8(7), pp. 519-29.

Rossi, C. S. and Lehninger, A. L. (1964) 'Stoichiometry of respiratory stimulation, accumulation of Ca++ and phosphate, and oxidative phosphorylation in rat liver mitochondria,' *J Biol Chem,* 239, pp. 3971-80.

Rutkowski, D. T., Arnold, S. M., Miller, C. N., Wu, J., Li, J., Gunnison, K. M., Mori, K., Sadighi Akha, A. A., Raden, D. and Kaufman, R. J. (2006) 'Adaptation to ER stress is mediated by differential stabilities of pro-survival and pro-apoptotic mRNAs and proteins', *PLoS Biol,* 4(11), pp. e374.

Sancak, Y., Markhard, A. L., Kitami, T., Kovács-Bogdán, E., Kamer, K. J., Udeshi, N. D., Carr, S. A., Chaudhuri, D., Clapham, D. E., Li, A. A., Calvo, S. E., Goldberger, O. and Mootha, V. K. (2013) 'EMRE is an essential component of the mitochondrial calcium uniporter complex', *Science (New York, N.Y.),* 342(6164), pp. 1379-1382.

Santos, M., Paramio, J. M., Bravo, A., Ramirez, A. and Jorcano, J. L. (2002) 'The expression of keratin k10 in the basal layer of the epidermis inhibits cell proliferation and prevents skin tumorigenesis', *J Biol Chem,* 277(21), pp. 19122-30.

Savignan, F., Ballion, B., Odessa, M. F., Charveron, M., Bordat, P. and Dufy, B. (2004) 'Mitochondrial membrane potential (DeltaPsi) and Ca2+-induced differentiation in HaCaT keratinocytes', *Journal of Biomedical Science,* 11(5), pp. 671-682.

Schieber, M. and Chandel, N. S. (2014) 'ROS Function in Redox Signaling and Oxidative Stress', *Current biology : CB,* 24(10), pp. R453-R462.

Sharp, P. M. and Li, W. H. (1987) 'The codon Adaptation Index--a measure of directional synonymous codon usage bias, and its potential applications', *Nucleic Acids Res,* 15(3), pp. 1281-95.

Sharpe, G. R., Gillespie, J. I. and Greenwell, J. R. (1989) 'An increase in intracellular free calcium is an early event during differentiation of cultured human keratinocytes', *FEBS Lett,* 254(1-2), pp. 25-8.

Shen, J., Chen, X., Hendershot, L. and Prywes, R. (2002) 'ER stress regulation of ATF6 localization by dissociation of BiP/GRP78 binding and unmasking of Golgi localization signals', *Dev Cell,* 3(1), pp. 99-111.

Shimomura, O. (1979) 'Structure of the chromophore of Aequorea green fluorescent protein', *FEBS Letters,* 104(2), pp. 220-222.

Shimomura, O. and Johnson, F. H. (1978) 'Peroxidized coelenterazine, the active group in the photoprotein aequorin', *Proc Natl Acad Sci U S A,* 75(6), pp. 2611-5.

Shimomura, O., Johnson, F. H. and Saiga, Y. (1962) 'Extraction, purification and properties of aequorin, a bioluminescent protein from the luminous hydromedusan, Aequorea', *J Cell Comp Physiol,* 59, pp. 223-39.

Shimomura, O., Musicki, B. and Kishi, Y. (1989) 'Semi-synthetic aequorins with improved sensitivity to Ca2+ ions', *Biochemical Journal,* 261(3), pp. 913-920.

Shore, G. C., Papa, F. R. and Oakes, S. A. (2011) 'Signaling cell death from the endoplasmic reticulum stress response', *Curr Opin Cell Biol,* 23(2), pp. 143-9.

Stanley, J. R. and Yuspa, S. H. (1983) 'Specific epidermal protein markers are modulated during calcium-induced terminal differentiation', *J Cell Biol,* 96(6), pp. 1809-14.

Steinberg, S. F., Bilezikian, J. P. and Al-Awqati, Q. (1987) 'Fura-2 fluorescence is localized to mitochondria in endothelial cells', *Am J Physiol,* 253(5 Pt 1), pp. C744-7.

Sternberg, S. H., Redding, S., Jinek, M., Greene, E. C. and Doudna, J. A. (2014) 'DNA interrogation by the CRISPR RNA-guided endonuclease Cas9', *Nature,* 507(7490), pp. 62-7.

Sugiura, K., Muro, Y., Futamura, K., Matsumoto, K., Hashimoto, N., Nishizawa, Y., Nagasaka, T., Saito, H., Tomita, Y. and Usukura, J. (2009) 'The unfolded

protein response is activated in differentiating epidermal keratinocytes', *J Invest Dermatol,* 129(9), pp. 2126-35.

Suzuki, J., Kanemaru, K., Ishii, K., Ohkura, M., Okubo, Y. and Iino, M. (2014) 'Imaging intraorganellar Ca2+ at subcellular resolution using CEPIA', *Nat Commun,* 5, pp. 4153.

Swarts, D. C., Mosterd, C., van Passel, M. W. and Brouns, S. J. (2012) 'CRISPR interference directs strand specific spacer acquisition', *PLoS One,* 7(4), pp. e35888.

Tabas, I. and Ron, D. (2011) 'Integrating the mechanisms of apoptosis induced by endoplasmic reticulum stress', *Nat Cell Biol,* 13(3), pp. 184-90.

Takahashi, A., Camacho, P., Lechleiter, J. D. and Herman, B. (1999) 'Measurement of intracellular calcium', *Physiol Rev,* 79(4), pp. 1089-125.

Tarasov, A. I., Semplici, F., Ravier, M. A., Bellomo, E. A., Pullen, T. J., Gilon, P., Sekler, I., Rizzuto, R. and Rutter, G. A. (2012) 'The Mitochondrial Ca(2+) Uniporter MCU Is Essential for Glucose-Induced ATP Increases in Pancreatic β-Cells', *PLoS ONE,* 7(7), pp. e39722.

Tavadia, S., Authi, K. S., Hodgins, M. B. and Munro, C. S. (2004) 'Expression of the sarco/endoplasmic reticulum calcium ATPase type 2 and 3 isoforms in normal skin and Darier's disease', *British Journal of Dermatology,* 151(2), pp. 440-445.

Tepikin, A. V., Llopis, J., Snitsarev, V. A., Gallacher, D. V. and Petersen, O. H. (1994) 'The droplet technique: measurement of calcium extrusion from single isolated mammalian cells', *Pflügers Archiv,* 428(5), pp. 664-670.

Thacher, S. M. and Rice, R. H. (1985) 'Keratinocyte-specific transglutaminase of cultured human epidermal cells: relation to cross-linked envelope formation and terminal differentiation', *Cell,* 40(3), pp. 685-95.

Thanaraj, T. A. and Argos, P. (1996) 'Protein secondary structural types are differentially coded on messenger RNA', *Protein Sci,* 5(10), pp. 1973-83.

Tirasophon, W., Welihinda, A. A. and Kaufman, R. J. (1998) 'A stress response pathway from the endoplasmic reticulum to the nucleus requires a novel bifunctional protein kinase/endoribonuclease (Ire1p) in mammalian cells', *Genes Dev,* 12(12), pp. 1812-24.

Tosatto, A., Sommaggio, R., Kummerow, C., Bentham, R. B., Blacker, T. S., Berecz, T., Duchen, M. R., Rosato, A., Bogeski, I., Szabadkai, G., Rizzuto, R. and Mammucari, C. (2016) 'The mitochondrial calcium uniporter regulates breast cancer progression via HIF-1alpha', *EMBO Mol Med,* 8(5), pp. 569-85.

Tsien, R. and Pozzan, T. (1989) 'Measurement of cytosolic free Ca2+ with quin2', *Methods Enzymol,* 172, pp. 230-62.

Tsien, R. Y. (1980) 'New calcium indicators and buffers with high selectivity against magnesium and protons: design, synthesis, and properties of prototype structures', *Biochemistry,* 19(11), pp. 2396-404.

Tsien, R. Y. (1981) 'A non-disruptive technique for loading calcium buffers and indicators into cells', *Nature,* 290(5806), pp. 527-8.

Tsien, R. Y., Pozzan, T. and Rink, T. J. (1982) 'Calcium homeostasis in intact lymphocytes: cytoplasmic free calcium monitored with a new, intracellularly trapped fluorescent indicator', *J Cell Biol,* 94(2), pp. 325-34.

Tu, C. L., Chang, W. and Bikle, D. D. (2007) 'The role of the calcium sensing receptor in regulating intracellular calcium handling in human epidermal keratinocytes', *J Invest Dermatol,* 127(5), pp. 1074-83.

Tuller, T., Carmi, A., Vestsigian, K., Navon, S., Dorfan, Y., Zaborske, J., Pan, T., Dahan, O., Furman, I. and Pilpel, Y. (2010) 'An evolutionarily conserved mechanism for controlling the efficiency of protein translation', *Cell,* 141(2), pp. 344-54.

Wang, Q., Shui, B., Kotlikoff, M. I. and Sondermann, H. (2008) 'Structural basis for calcium sensing by GCaMP2', *Structure,* 16(12), pp. 1817-27.

Wang, S. and Kaufman, R. J. (2012) 'The impact of the unfolded protein response on human disease', *J Cell Biol,* 197(7), pp. 857-67.

Wang, W., Yang, X., Lopez de Silanes, I., Carling, D. and Gorospe, M. (2003) 'Increased AMP:ATP ratio and AMP-activated protein kinase activity during cellular senescence linked to reduced HuR function', *J Biol Chem,* 278(29), pp. 27016-23.

Watt, F. M. (1987) 'Influence of cell shape and adhesiveness on stratification and terminal differentiation of human keratinocytes in culture', *J Cell Sci Suppl,* 8, pp. 313-26.

Werth, J. L. and Thayer, S. A. (1994) 'Mitochondria buffer physiological calcium loads in cultured rat dorsal root ganglion neurons', *J Neurosci,* 14(1), pp. 348-56.

Wertz, P. W., Downing, D. T., Freinkel, R. K. and Traczyk, T. N. (1984) 'Sphingolipids of the stratum corneum and lamellar granules of fetal rat epidermis', *J Invest Dermatol,* 83(3), pp. 193-5.

Wikipedia (2018) *Epidermis*. Available at: https://en.wikipedia.org/wiki/Epidermis 2018).

Wilson, M. H., Coates, C. J. and George, A. L. (2007) 'PiggyBac Transposon-mediated Gene Transfer in Human Cells', *Mol Ther,* 15(1), pp. 139-145.

Yamamoto, K., Sato, T., Matsui, T., Sato, M., Okada, T., Yoshida, H., Harada, A. and Mori, K. (2007) 'Transcriptional induction of mammalian ER quality control proteins is mediated by single or combined action of ATF6alpha and XBP1', *Dev Cell,* 13(3), pp. 365-76.

Yant, S. R., Wu, X., Huang, Y., Garrison, B., Burgess, S. M. and Kay, M. A. (2005) 'High-Resolution Genome-Wide Mapping of Transposon Integration in Mammals', *Molecular and Cellular Biology,* 25(6), pp. 2085-2094.

Ye, J. and Koumenis, C. (2009) 'ATF4, an ER stress and hypoxia-inducible transcription factor and its potential role in hypoxia tolerance and tumorigenesis', *Curr Mol Med,* 9(4), pp. 411-6.

Yoon, Y. S., Yoon, D. S., Lim, I. K., Yoon, S. H., Chung, H. Y., Rojo, M., Malka, F., Jou, M. J., Martinou, J. C. and Yoon, G. (2006) 'Formation of elongated giant mitochondria in DFO-induced cellular senescence: involvement of enhanced fusion process through modulation of Fis1', *J Cell Physiol,* 209(2), pp. 468-80.

Yoshiki, K., Azuma, H., Yoshioka, K., Hashimoto, M. and Araki, T. (2005) 'Finding of Optimal Calcium Ion Probes for Fluorescence Lifetime Measurement', *Optical Review,* 12(5), pp. 415-419.

Zolle, O., Lawrie, A. M. and Simpson, A. W. (2000) 'Activation of the particulate and not the soluble guanylate cyclase leads to the inhibition of Ca2+

extrusion through localized elevation of cGMP', *J Biol Chem,* 275(34), pp. 25892-9.

Zou, J., Hofer, A. M., Lurtz, M. M., Gadda, G., Ellis, A. L., Chen, N., Huang, Y., Holder, A., Ye, Y., Louis, C. F., Welshhans, K., Rehder, V. and Yang, J. J. (2007) 'Developing sensors for real-time measurement of high Ca2+ concentrations', *Biochemistry,* 46(43), pp. 12275-88.